Finite Element Analysis of the fatigue strength of a big-end bolt

Master Thesis in Energy Technology

Thermal Machines

Jan Harald Langeland

Faculty of Mathematics and Natural Sciences

University of Bergen

1. June 2017

University of Bergen

Western Norway University of Applied Sciences

Rapport title: **Finite Element Analysis of the fatigue strength of a big-end bolt**	Date: **01.06.2017** Rapport number: **1**
Author: **Jan Harald Langeland**	Number of pages without attachment: **87** Number of pages attachment: **38**
Specializations: ***Master in Energy Technology*** ***Thermal machines***	
Supervisor in the field of study: **Prof Richard J. Grant** **Associate professor Lars Magne Nerheim**	Grading: No

A*ssigner*: Western Norway University of Applied Sciences	
Contact person: Richard J. Grant	*Phone:* 55 58 78 15

Summary:

FE-analysis on fatigue strength of big-end bolt using Abaqus simulation software. Simulations shows stress increase around first thread due to notch effect. Further work includes refined mesh around notch and improved thread stress distribution.

Western Norway University of Applied Sciences *Department of Engineering and Economics* *Mailing address: Post-box 7030, 5020 Bergen* *Tlf. 55 58 77 90, Fax: 55 58 77 90*	*Address*: Inndalsveien 28, Bergen *Email: post@hvl.no* *Homepage*: www.hvl.no

Keywords: FEM, FEA, Finite Element Method, Abaqus, Fatigue, Big-end Bolt

Table of Contents

Table of Figures

Table of Tables

Table of Equations

ABSTRACT

This thesis investigates, with the use of finite element method, the stress formation in a big-end bolt during the power stroke in an IC piston engine. The method used is quasi-static analysis of the lower part of the connection rod (big-end) assembly for different time intervals during the stroke.

Two big end configurations is analyzed with the aim of finding regions in the bolt with stress concentrating feature that could induce fatigue. The simulation is, performed with Abaqus FEA software. The results is, compared with previous performed studies, industrial reports and hand calculations.

Supported by literature, the results shows that the combination of reduced area due to thread curvature, and forces through bolt from power stroke creates high stresses. The weakest part of the bolt is the first thread, as this carries most of the load.

Future work will include improving the FE model and performing FE analysis on other configurations. This could include investigating different bolt configurations and more complex and realistic bolt geometry.

PREFACE

Firstly, I would like to thank my supervisor at HVL, Professor Richard John Grant and Lars Magne Nerheim for academic guidance, valuable input, encouragement and assistance from preparation to completion of this thesis.

Secondly, I would like to express my appreciation to the group of master students, who have worked with me at the university office, consisting of: Nelu Munteanu, Christoffer Stenerud, Jarle Tingstad and Erlend Nygård. Their moral support and valuable discussions has given me increased motivation throughout the thesis work.

I would also like to thank OneSubsea Processing AS with Øyvind Teige for giving me a position as mechanical engineer. They are allowing me a flexible schedule enabling me to deliver the thesis on time.

Finally, yet importantly, I would like to thank my family and friends for their support and motivation throughout the period of my master's studies.

1 INTRODUCTION

The world today has an increasing demand for energy [1]. To transform the energy from energy resources to usable energy, machines are needed, e.g. thermal engines, wind turbines and water turbines. Machines under operation are exposed to wear, tear and fatigue. It is important to understand how these mechanisms works in order to improve the machines.

In internal combustion engines, the connection rod, piston and crankshaft are some of the components, which have to withstand most movement hence fluctuating forces. The connection rod is split in order to be assembled around the crankpin, and is held together by pre-tensioned big-end bolts. The same arrangement is found in all crank mechanisms from engines to pump-units. All the forces from the piston, either from a pumping or firing pressure goes through the crankshaft and the big end bolts holding it together.

Due to the rotational movement and different running conditions, these bolts experience high fluctuation in stress over time. There are examples of big-end bolts failing leading to total engine failure. This may leave the engine impossible to repair. Replacing an engine or pump is expensive both with regards to purchase and downtime.

1.1 Issue

This master thesis investigates how firing pressure and inertia forces effects the stress in the big-end part of the connection and big-end bolts. Different configurations of the design might have and impact on the big-end bolt's fatigue life. The FE-simulation software Abaqus will be used for simulating and analyzing the results.

1.2 Aims

The aim of this study is to analyze the stress in the big-end bolts during the stroke and use the information for design change propositions, improving bolt fatigue life.

1.3 Objectives

This master thesis is divided into objectives or milestones for better mapping project progress.

1. Survey current literature on fatigue and IC reciprocating design.
2. Become familiar with Abaqus FEA software.
3. Contact various engine manufacturers, to collect data on design, test results, and fatigue life.

4. Create FEA models for simulating physical features such as, bolt pre-tension, contact mechanics and bearing loads.
5. Verify that the simulating methods for the point above (4) are appropriate and accurate
6. Create a simplified model to simulate the big-end assembly.
7. Verify the simplified model
8. Create a realistic model of big-end assembly and verify the results with and industrial example
9. Suggest design changes for improved fatigue-life.
10. Delivery of the project 1 June 2017.

1.4 Motivation

Motivation for the master thesis is to highlight changes in the design of big-end assembly, which improves the fatigue life of the big-end bolts. This is important for avoiding engine failure. Clever design and methods for preventing fatigue in these bolts can improve service life and reduce the lifetime cost of the application.

1.5 Hypothesis

In aerospace and automotive engineering typical joining methods for aluminum plates is by usage of rivets. Aluminum is not easy to weld, which is one of the reasons that rivets are used for joining. A typical design feature is to use many small rivets instead of a few large ones when joining aluminum and composites [2].

The same can be seen in wood-constructed buildings where wood beams are fastened using numerous of screws/studs rather than only one or two larger ones. Using smaller screws in wood is better as the wooden fiber does not split as easy. To use large bolts would easily split the wood, where pre-boring the material would have to be applied for prevention, this is time consuming [3].

Engine designer and previously R&D discipline leader Lars Magne Nerheim, had experienced that large big-end bolts failed due to fatigue. This was reported as surprising as the bolts had very good material properties against fatigue, and designed with dimensions so large that fatigue should not be an issue. The hypothesis on the failure is that the bolt was so large and coarse that “it lived it’s own life”. The use of coarse threaded bolts instead of fine threaded bolts could have an impact, as there is less material in the coarse threaded ones.

1.6 Structure of the thesis

The model consist of several mechanisms working together. As a new user to Abaqus, much time will be invested in understanding how these mechanisms work and behave in combination. The mechanisms or features, which needs to be controlled in order to build a complete model, is as follows:

- Contact mechanism between bearing and cap/connection rod
- Contact mechanism between connection rod and cap
- Contact mechanism between bottom surface bolts and cap/connection rod
- Bolt pre tensioning
- Closing of gaps and clearances when load is applied between bearing and cap/connection rod.

Learning and mastering the mechanisms or features in Abaqus is crucial for getting FE-results.

Objectives or activities

Activity Number	Activity Group	Activity Name
1	**Mechanisms**	
1.1		Contact simulation
1.2		Bolt Pre-tensioning simulation
1.3		Bearing Load simulation
1.4		Verify Contact results
1.5		Verify Bolt Pre-tensioning results
1.6		Verify Bearing Load results
2	**Simplified model (Global model)**	
2.1		Create 3D model
2.2		Create loads & constrains
2.3		Get completed simulations
2.4		Verify simplified model results
3	**Realistic model (Global model)**	
3.1		Create 3D model
3.2		Create loads & constrains
3.3		Get completed simulations
3.4		Verify realistic model results
4	**Fatigue Calculations**	

Table 1: Activity plan

Mechanisms or features are required to be created in Abaqus and simulated. The simulation result needs validation to conform that things are correctly specified. This can be performed by doing hand calculations, to verifying the stresses/strains within a ballpark estimate. Comparing the result with published work is also a good verification method.

After obtaining reasonable results on each of the mechanisms one by one, they must be combined in a simplified model. The simplified model has very simplified geometry. The aim of this model is to verify that all the mechanisms work together, as combining the mechanisms may lead to failing simulations.

The simplified model requires verification. This can be done by comparing with hand calculations and published work. After getting results from the simplified model within reasonable values, the next step is to create a model with more realistic geometry.

The realistic geometry model is comparable with a model created in the industry. The aim of the realistic model is to be a global model highlighting stress concentrating areas in the assembly. The geometry and results have been validated by a company, and been used in a production engine. The goal in this step is to try to replicate the results to be within the same range.

2 BACKGROUND

This chapter explains the basics in an engine, crank & connection rod assembly, and some fatigue theory and fracture mechanics. This is necessary background information for understanding what is going on during the power stroke.

2.1 Reciprocating engines (General applications with big-end bolts)

Reciprocating engines, also known as piston engines, are widely used for power production. The piston engine was first introduced as a steam engine in the 18th century [4] leading the way for the industrial revolution. Today the piston engine is mainly used in two types of engine, SI-engine (Spark Ignition) and CI engine (Compression Ignition).

In general, the piston engine has many similar parts for SI and CI engines. These similar parts are the piston, cylinder, cylinder cover, valves, connection rod, crankshaft, camshaft, rollers, bearings, bolt-connections. Auxiliary systems such as air-system, cooling system, oil-system, exhaust system, and fuel system are also necessary for operation; here the difference between a CI and SI engine is larger [5].

Pumps share many of the same parts as an engine, and can be compared with a reversed engine. Meaning that a pump uses energy to create higher pressure. Especially piston pumps such as axial and radial piston pumps has many of the same mechanisms as an engine, including the connection rod parts [5].

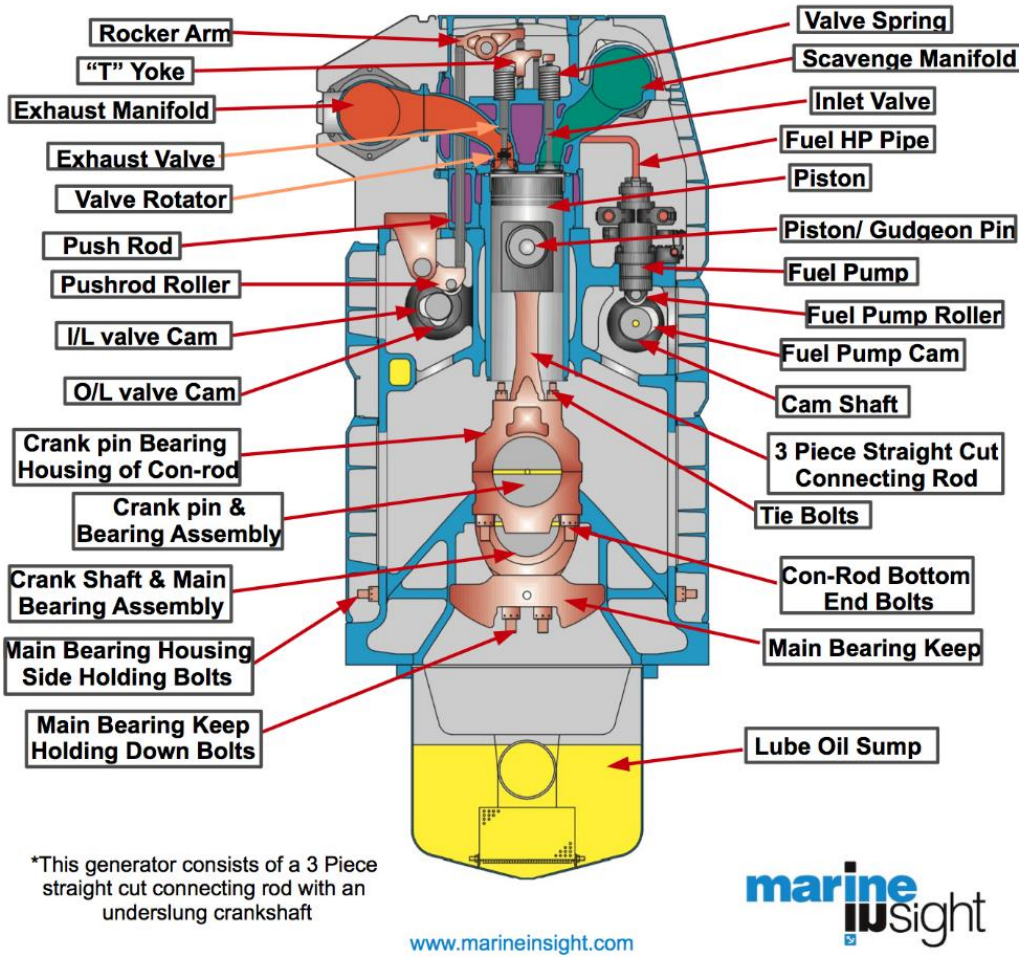

Figure 1: Marine diesel engine

Many of the parts are the same for a CI and SI engine, but they might vary in size and function depending on arrangement. The figure is from marineinsight.com a platform focusing on providing information on various aspects of the marine world.

The machine parts are exposed to many forms of wear mechanisms. The combustion room is exposed to rapidly pressure and temperature increase. The connection rod and cylinder cover is exposed to high pressure cycles. The crankshaft to pressure and torsional forces. Machine parts are sliding and rolling on each other. Parts are exposed to high pressure and temperatures, and need lubricants and cooling. Vibrational forces shakes the machinery. Proper design and maintenance is crucial for reducing the probability of failure [5].

2.2 Connection rod assembly

This thesis focuses on the connection interface between the connection-rod and crankpin, the big-end. The function of the connection rod assembly is to transform the reciprocating motion from the piston, to circular movement in the crankshaft. A typical arrangement of these parts is shown in Figure 2. The connection rod is split with the upper part “connection rod” and lower part “big-end cap”, or just cap. The bearing shells are placed between the crankpin and connection rod and cap. The assembly is locked together by cap bolts, or “big-end bolts”. The whole assembly is under cyclic movement during operation.

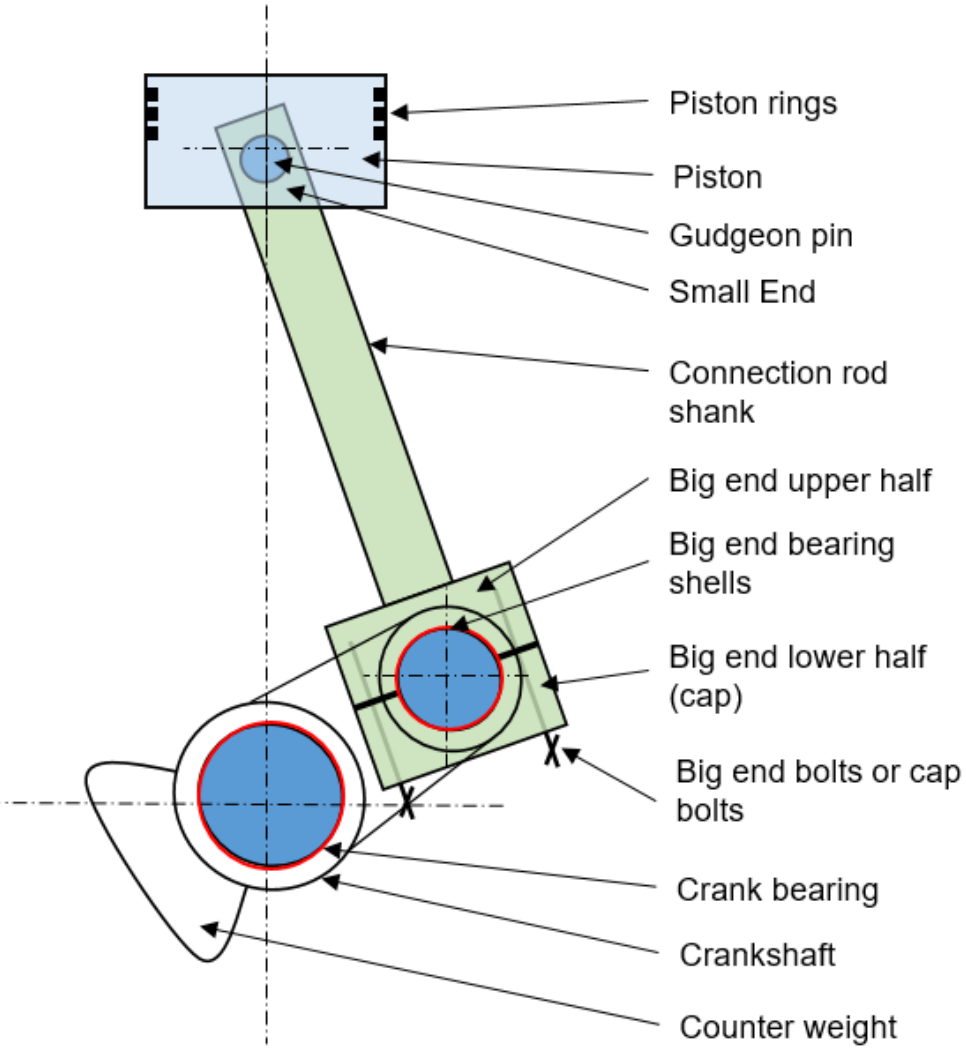

Figure 2: Typical connection rod assembly

2.2.1 Connection Rod

The function of the connection rod is to transfer the forces from the piston to the crankshaft. The upper part of the connection rod connected to the piston is the small end. The lower part, which connects to the crankshaft, is big-end. There are examples of different configurations of the connection rod and big-end interface to the crankshaft. Some are horizontal split, and other split in an angle.

Connection rods split in a horizontal plane see Figure 3 is typical for smaller engines such as cars, some commercial vehicles, motorcycles and smaller applications [6] . Note that large cross head engines may also use horizontal split connection rods [5].

One of the reason to use horizontal splitting is that the manufacturing process is cheaper and easier. An example of this is fracture splitting which is technique used for splitting powder forged connection rods from high carbon steels [6]. This performed by creating a small groove weakening the material creating a start point for fracture. The connection rod is then split by impacting a wedge formed stub through the big-end hole. The fracture split follows the grain structure and are unique for each connection rod [7]. This makes the cap end and connection end to fit perfectly together without the use of machining. This process can reduce the manufacturing cost by up to 30% [6]. For large crosshead engines, the con-rod and cap are split horizontal for avoiding the increased stress through the big-end bolts, which is typical for the angle split connection rod [8].

Figure 3: Motorcycle connection rod

Horizontal split using fracture splitting method, from a Yamaha engine. Picture found in paper [6]

Other configuration is to split the connection rod in an angle. This is typical for heavier engines such as high speed diesel engines for trucks, busses, ships and larger applications [8]. Wartsilla R32 connection rod (see Figure 4) is an example of angled split configuration. The connection rod is angle sliced for easy assembly and disassembly. [5] During maintenance and service of such engines, the angled splitting of the connection rod enables it to be pulled out of the cylinder liner directly. This enables the crankshaft bearing shells to be replaced without disassembling the piston head. The angled split places the big-end bolts in a though position as most of the forces will have to go through the bolt. Due to the bolt bore in the connection shank the structural integrity is also weakened leading to more stress through the bolt [8].

Figure 4: Wartsila R32 connection rod

Split in an angle with serrations in the connection interface between cap and rod, picture found at powerlinkmarine.com

2.2.2 Crankshaft and crankpin

The function of the crankshaft is to transfer the pressure buildup in the cylinder to oscillating motion from the pistons to rotational motion in the shaft. The rotational energy in the crankshaft rotates the flywheel and potential dampers, via couplings and gears until final application [5]. Due to the oscillating motion from the pistons, inertia from the mass and gas pressure a lot of vibration is created, some of this can be balanced by placing counterweights on the crankshaft [9].

2.2.3 Big-end Bolt

The function of the big-end bolt is to clamp the connection rod and bearings to the crankpin. When the crankshaft is rotating and pistons moving, fluctuating stresses is sent through the connection. This makes the big-end bolts exposed to tough conditions as they might be exposed to bending, compression, and tension through the stroke depending on configuration [9]. Sufficient pre-tensioning of the bolts is important during operation. The pre-tensioning force might be so high that the bolt is not re-usable after disassembly [8]. Big-end bolts are often created in high-strength steel alloys for high fatigue strength. Typically the yield strength may be between 800-1400MPa [8].

The geometry of the big-end bolts will vary from design to design, and application to application. For horizontal split connection rods bolts with threads over the hole stud area is quite common. For more heavy engines, the tread section might be only in the upper part of the stud, so called tensile bolts. This enables the bolt to be pre-tensioned more and clamping the assembly tighter together [8]. Figure 5 displays typical big-end bolt designs for different engine sizes, the picture is from Mahle book [8]. Note that the thread section is wider than the bolt. This is due to a manufacturing method rolling the threads [8]

Figure 5: Different types of big-end bolts.

2.2.4 Material for the selected parts

Depending on the application for the crank mechanism, the material will vary. For small stock car engines, typically aluminum alloys or steel alloys are used. While heavy-duty industrial engines uses, higher quality alloys [8]. Different casting and forging techniques enhance material properties and strengthens the part. Examples of this may be hot or cold rolling, shot peening, quenching and case hardening.

Cold Rolling is a technique used for creating compressible stress in the material, work hardening it. A combination of cold working and recrystallization can be performed generating special steel properties. Threads is a typical example; rolled threads are stronger than machined threads both due to work hardening but more intact grain structure [10], as illustrated in Figure 6 from [11].

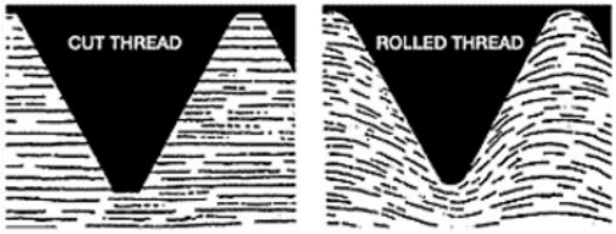

Figure 6: Cut thread vs rolled thread.

Shot Peening is a method used for creating residual compressive stress enhancing fatigue life of parts. It uses small round pieces of metal, glass or ceramics and is shot at the part with high enough impact to create small plastic deformations, changing the material properties. This method is field proven for highly stressed parts such as Formula 1 engines, and critical parts such as aero engines [12].

Case Hardening or surface hardening uses a gas rich atmosphere to create residual compressive stresses due to diffusion of atoms. Typical method are carburization, nitriding, cyaniding, flame and induction hardening. Case hardening creates a hard surface, but is softer deeper in the material [13].

2.3 Crank mechanism dynamics

The piston, connection rod and crankshaft are the main parts driving the engine. These parts can be arranged in different configurations, from inline, V-shape with different angles or boxer shape. The different configuration will have an impact on how crank drive is balanced, fluctuation movement and vibrations [14].

Periodical forces cause shaking in an engine. This is reactions from the engines torque and mass forces and mass moments. The torque reaction forces is periodically varying over the revolution of the crank. The torque tries to turn the engine, and is especially noticeable in for instance a car engine, elastically supported running on idle, as this might create resonance with the engine support frame [9]

Mass forces and mass moments is the result of the oscillating rotational movement. During one rotational cycle the forces changes direction and size, the resultant forces from these may shake the engine, but can to some extent be balanced using counterweights [9]. The engine speed (RPM) influence how large the oscillating forces is, as higher velocity means more inertia.

The gas forces from the ignition and pressure in the cylinder does not create much forces out from the engine, as most of these forces is absorbed internally in the engine [9]. Figure 7 from Lundby [9] illustrates the forces and components in a crank, connection rod, piston assembly.

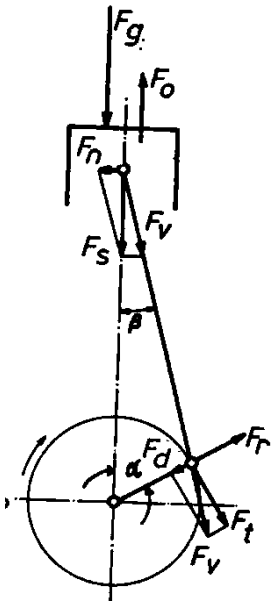

Figure 7: Crank mechanism force diagram

Where:

***Fg** is gas force from pressure in cylinder*

***Fo** is oscillating force due to inertia and mass movement of piston and connection rod*

***Fs** is piston force which is the resulting force of gas force and oscillating force*

***Fn** is a normal force a component from the piston force, in contact with cylinder lining*

***Fv** is connection rod force a component from the piston force in direction of connection rod*

***Ft** is tangential force giving torque to the crankshaft (component of connection rod force)*

***Fd** is radial force (other component of connection rod force)*

***Fr** is a rotating force from centrifugal forces from rotating masses*

MAHLE [8] illustrates the acceleration of connection rod ends through the stroke in Figure 8, with combustion chamber pressure. Note that the peak combustion pressure is displaced after TDC and only inertia forces from masses is found at TDC.

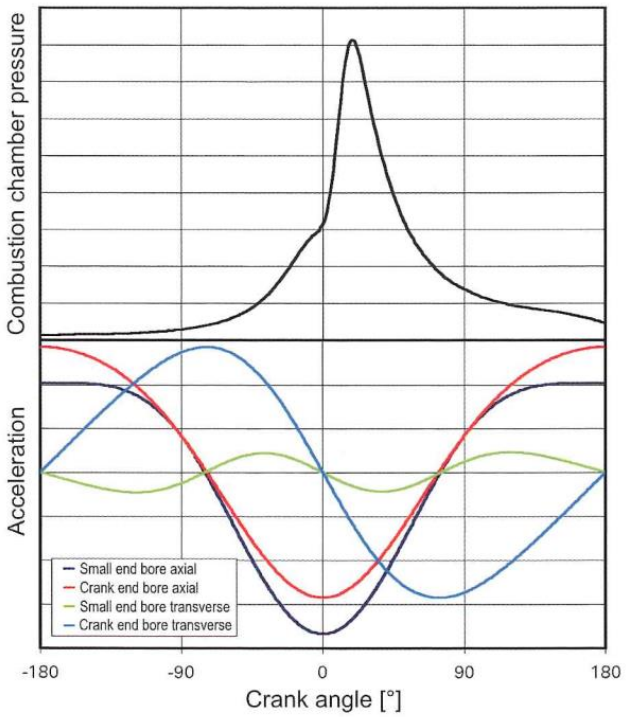

Figure 8: Gas forces and inertia forces

2.4 Threads

This thesis uses metric ISO threads from the DIN 13 [15] standard for calculations. It is assumed that the big-end bolts have rolled threads as this is typical for big-end bolts [8]. This means that the thread outer diameter is larger than the bolt rod (reduced body), as when during rolling the material is squeezed outwards. For reduced body bolts using rolled threads the bolt diameter is D2 or middle diameter, and the threads are rolled to diameter D1 and D3. For cut threads bolt the bolt diameter is D3 and threads are cut to D1 [10]. For this thesis M52 bolt is used, information on this is in the Table 2 from the DIN13 standard [15].

Metric ISO-thread DIN 13 - Nominal values

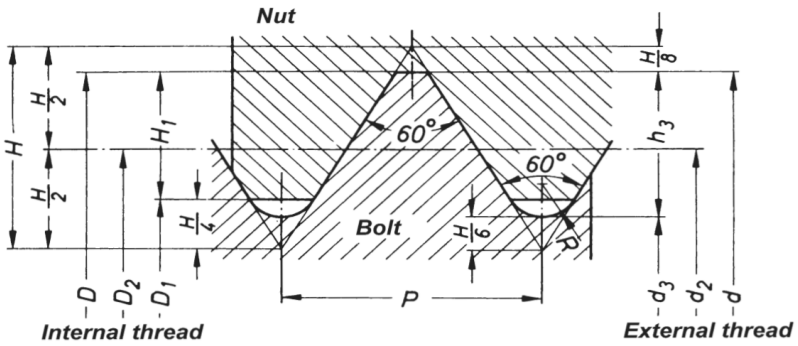

Sizes in mm

$D_1 = d - 2\,H_1$
$d_2 = D_2 = d - 0{,}64953\,P$
$d_3 = d - 1{,}22687\,P$
$H = 0{,}86603\,P$
$H_1 = 0{,}54127\,P$
$h_3 = 0{,}61343\,P$
$R = \frac{H}{6} = 0{,}14434\,P$

Nominal value of thread d = D			Pitch	Flank-⌀	Root-⌀		Depth of thread		Radius
Row 1	Row 2	Row 3	P	$d_2 = D_2$	d_3	D_1	h_3	H_1	R
M 42			4,5	39,077	36,479	37,129	2,760	2,436	0,650
	M 45		4,5	42,077	39,479	40,129	2,760	2,436	0,650
M 48			5	44,752	41,866	42,587	3,067	2,706	0,722
	M 52		5	48,752	45,866	46,587	3,067	2,706	0,722
M 56			5,5	52,428	49,252	50,046	3,374	2,977	0,794

Table 2: Metric ISO-thread DIN 13

Typical stress distribution through threads is illustrated in Figure 9 from Prof. A Leyers work on machine parts from ETH Zürich. It shows that for normal configurations the first thread holds most of the load, approx. 30% for this 6-thread configuration. By using different nut or bolt design, it is possible to make the stress distribution more evenly over the threads [16].

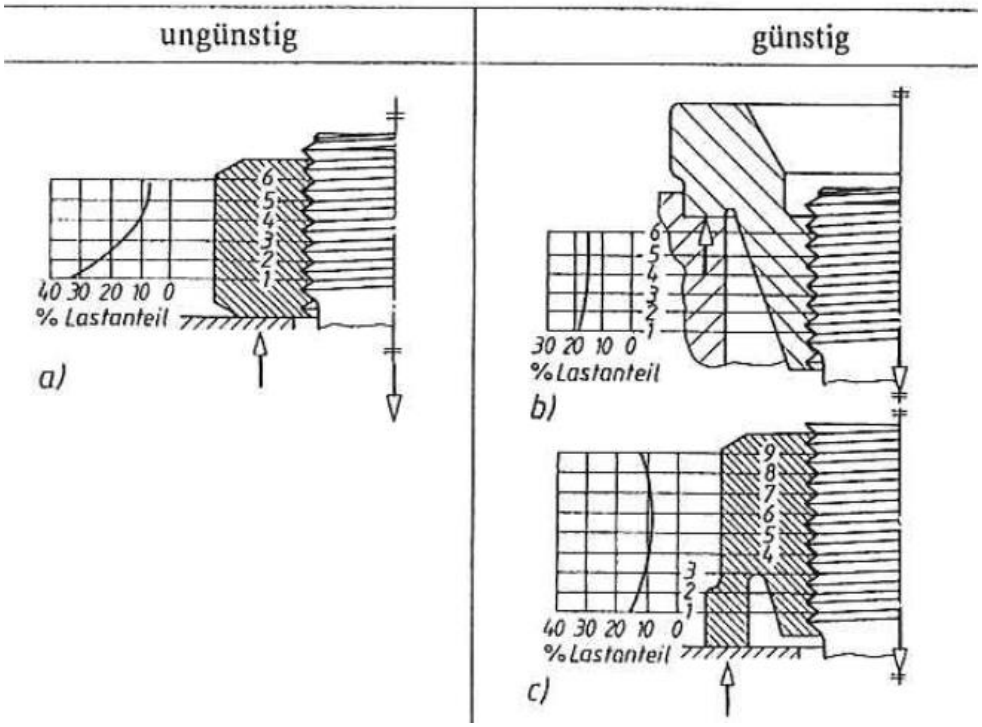

Figure 9: Thread stress distribution

2.5 Contact mechanics

Contact mechanics Is the study of solids which deforms when touching or in contact with other solids. Heinrich Hertz did a lot of work on the subject in the 1880s; his work remains as a basis for today's calculation [17].

For this thesis, the contact area between two cylinders is investigate. This geometry is typical for bearings.

The Hertz equation is collected from lecture notes based on Stachowiak and Batchelor [17]. Assumptions for calculations with Hertz equation is: frictionless contact, smooth surface, only elastic deformation, small contact area and the parts are at rest.

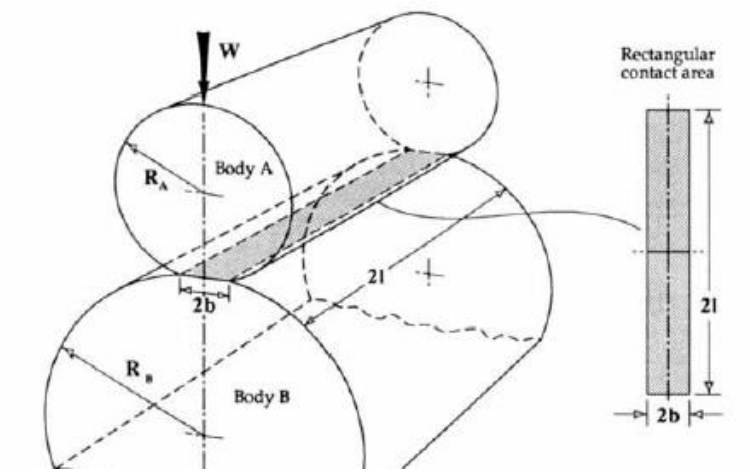

Figure 10: Geometry of contact surface.

Note that for a concave cylinder surface (bearing) the largest radius is negative

Reduced radius of curvature:

$$\frac{1}{R'} = \frac{1}{R_A} + \frac{1}{1R_B}$$

Equation 1: Reduced radius of curvature

Reduced Young's modulus

$$\frac{1}{E'} = \frac{1}{2}\left[\frac{1 - V_A^2}{E_A} + \frac{1 - V_B^2}{E_B}\right]$$

Equation 2: Reduced Young's modulus

Contact area (b):

$$b = \left(\frac{4WR'}{\pi\, l\, E'}\right)^{\frac{1}{2}}$$

Equation 3: Contact area

Average contact pressure:

$$P_{avg} = \frac{W}{\pi\, b\, l}$$

Equation 4: Average contact pressure

Maximum contact pressure:

$$P_{max} = \frac{W}{4\, b\, l}$$

Equation 5: Maximum contact pressure

$Where$:

$R_A = Radius\ of\ part\ A$

$R_B = Radius\ of\ part\ B$

$E_A = Youngs\ module\ of\ part\ A$

$E_B = Youngs\ module\ of\ part\ B$

$V_A = Poissons\ ratio\ of\ part\ A$

$V_B = Poissons\ ratio\ of\ part\ B$

$W = Force\ applied$

$l = Contact\ length$

2.6 Fatigue Theory

Repeatedly applied loads over time may cause fatigue in materials. Fatigue failure is the largest source for failure in metals. Around 90% of metallic failures are from fatigue [18]. The failure may occur very sudden and without warning often leading to catastrophic events. Unlike other failure mechanisms, fatigue is hard to detect, as for high cycle fatigue there is little plastic deformation before brittle like break.

Fatigue is categorized in two types of fatigue, high and low cycle [19]. For low cycle fatigue (LCF), the material exposed to plastic stress, giving fewer cycles before failure, e.g. opening of a sardine can. High cycle fatigue (HCF) has stress below the yield limit, typical for a connection rod in an engine. Over time, the load cycles can lead to fatigue failure. High cycle fatigue is represented in the S-N diagram or Wohler curve. Figure 11 from Ashby, Schercliff and Cebon [19] shows the relationship between high and low cycle fatigue and number of cycles.

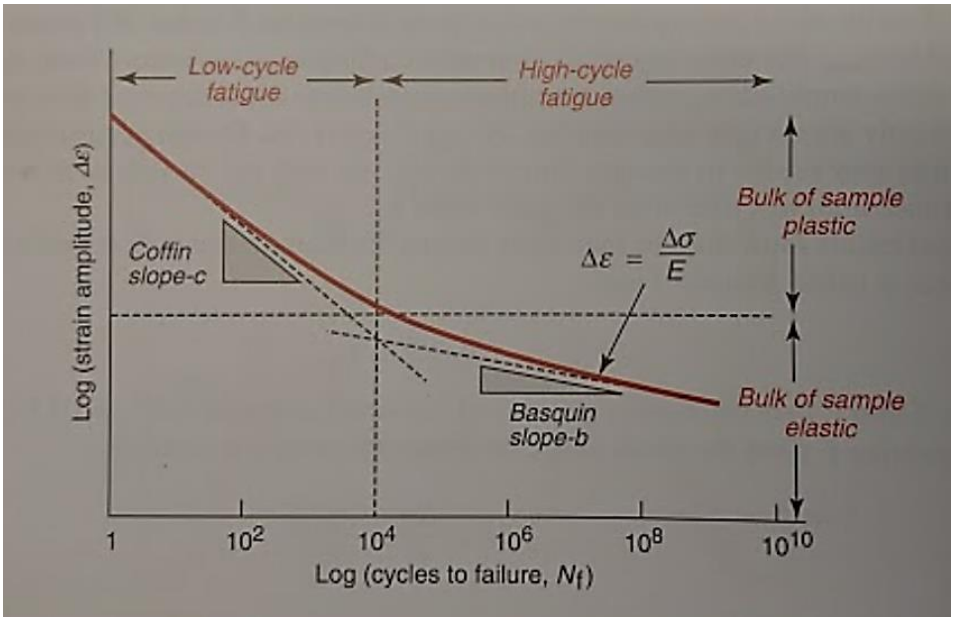

Figure 11: Low and high cylce fatigue

2.6.1 Load cycles

There are different types of load cycles that may lead to fatigue failure as illustrated in Figure 12 from Meyers and Chawla [20].

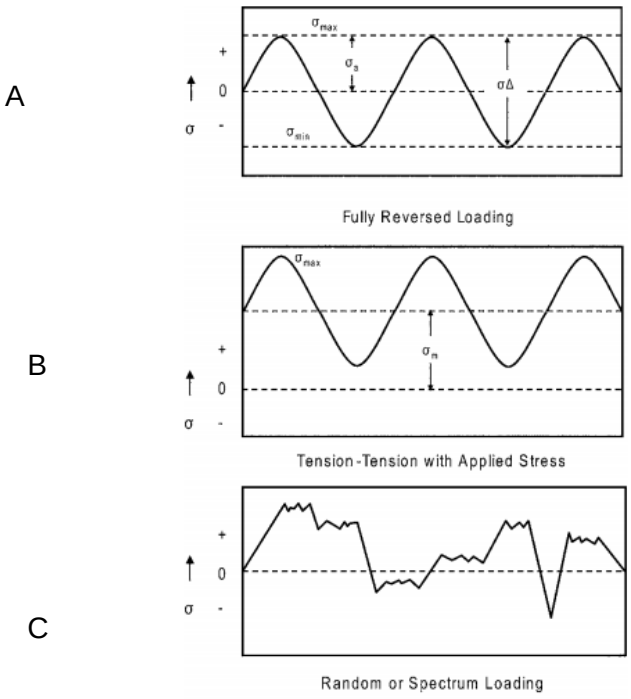

Figure 12: Different load cycles

The upper figure (A) shows that the stress is fluctuating I positive and negative direction. Meaning the material is exposed to fully reversed tension and compression. This is typical for an application with bending moment that is rotating for instance a shaft in a hoist.

The middle figure (B) has a mean stress in addition to the fluctuating stress. The material can be in tension or compression state, with fluctuating top/bottom stresses. Typical for a pre-tensioned shaft or bolt, exposed to cyclic load.

The bottom figure (C) shows a material which has random loading. Applications subjected to such loading can for instance be the suspension system in a car.

The fluctuating stress (σ_r) is made up of mean/steady stress (σ_m) and alternating/variable stress (σ_a). The stress range is the difference in max and min stress level [19].

$$\sigma_r = \sigma_{max} - \sigma_{min}$$ *Equation 6: Stress range*

Alternating/variable stress (σ_a) is half the stress range [20]

$$\sigma_a = \frac{\sigma_{max} - \sigma_{min}}{2}$$ *Equation 7: Alternating stress*

The mean stress (σ_m) is the average of the maximum and minimum stress [19].

$$\sigma_m = \frac{\sigma_{max} + \sigma_{min}}{2}$$ *Equation 8: Mean stress*

The stress ratio (R) is given by [19]:

$$R = \frac{\sigma_{min}}{\sigma_{max}}$$ *Equation 9: Stress ratio*

Amplitude ratio (A) is given by [19]:

$$A = \frac{\sigma_a}{\sigma_m} = \frac{1-R}{1+R}$$ *Equation 10: Amplitude ratio*

2.6.2 High cycle fatigue (HCF)

Occurs when the stress subjected to the material is within the elastic area. Due to lower stress, fatigue typically does not occur before after 10^5 cycles. Typical range for HCF is from 10^3 to 10^6 and even up to $5x10^8$ cycles for nonferrous metals [21]. HCF is plotted in S-N curve or Wohler curve. Both figures (Figure 13 & Figure 14) are from Meyers and Chawla [20].

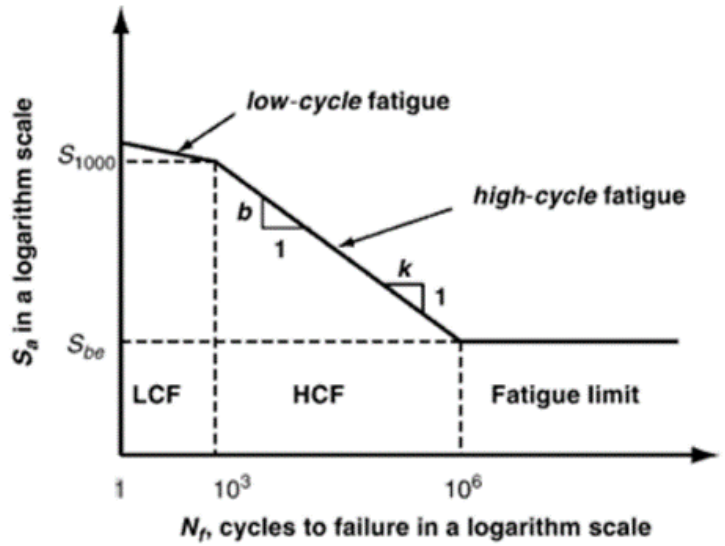

Figure 13: LCF and HCF regions in S-N curve

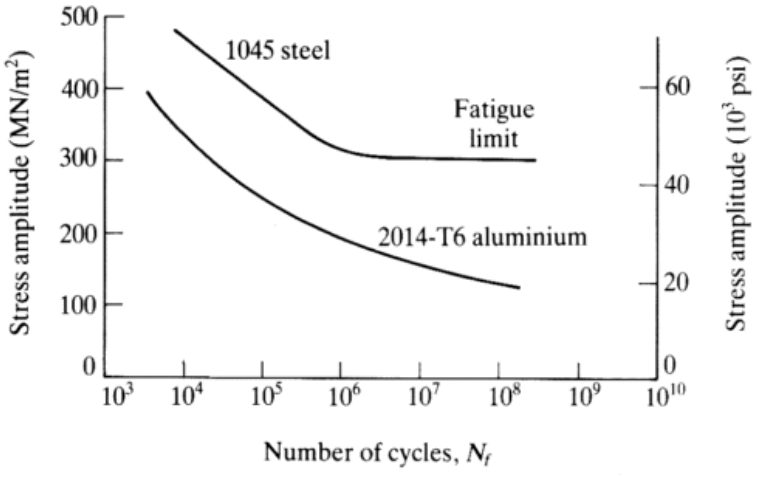

Figure 14: S-N curve for 1045 steel and 2014-T6 aluminum

The S-N curve (Figure 14) shows typical characteristics for steel and aluminum. On the x-axis the number of cycles is shown in logarithmic scale. The y-axis shows the stress amplitude for

the material. The 1045 steel has ha fatigue limit, which means that below this limit fatigue will not occur.

For many steel alloys, there is a direct correlation in increased tensile strength giving increased fatigue limit. Using high tensile strength steels is not necessary wise as these materials often are brittle and very sensitive to surface and environmental conditions [8].

2.6.3 Endurance limit

The endurance limit or fatigue limit is often defined to number of cycles above 10^8 [22]. For 12.9 grade steels, the endurance limit is given in Figure 15 from Bickford [22]. Note that the heat treatment of the bolts plays an important role in endurance limit strength. F_m is the mean load on the bolt, and $F_{0.2}$ is the yield bolt load at 0.2% elongation.

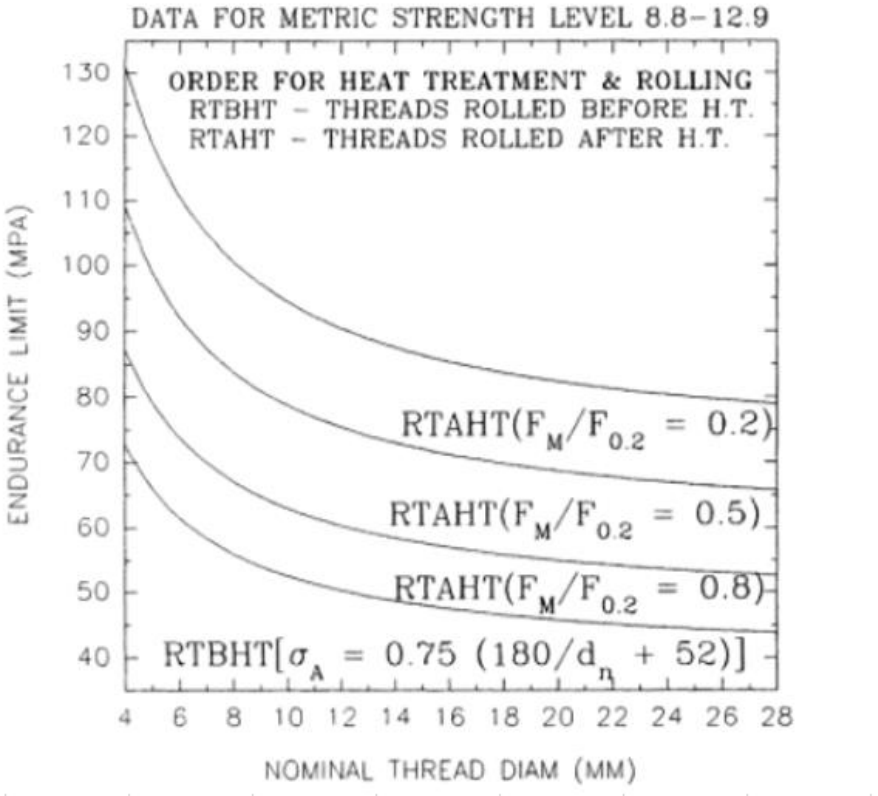

Figure 15: Endurance limit 8.8 - 12.9 grade steels

2.7 Cumulative damage

Real fatigue conditions are often different from laboratory testing. Meaning that the load cycles may vary along the lifetime of the material [19]. The palmgren-Miner rule is used for calculating this. It assumes that the fatigue follows a linear damage. This rule has limitations as the probability of fatigue failure is scattered, and that low stress cycles followed by high stress cycles does more damage than predicted [23].

$$\sum_{i=1}^{k} \frac{n_i}{N_i} = C$$

Equation 11: Palmgren-Miner rule

ni = Number of cycles accumulated at stress Si

C = The fraction of life consumed by exposure to the cycles at the different stress levels

Ni = Number of cycles until failure at the stress Si

The Palmgren-Miner rule gives the relation as described in Figure 16, from Meyers and Chawla [20].

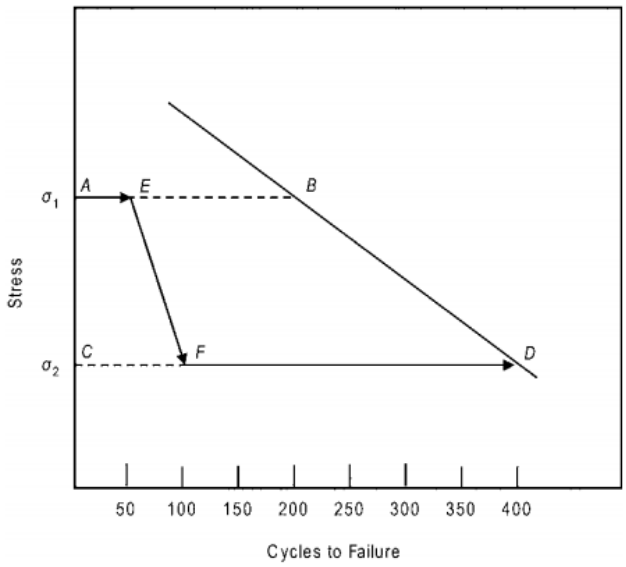

Figure 16: Cumulative damage during high-to-low loading

In point A, 0 cycles has been performed, the total number of cycles until failure is 200 (point B), this gives fatigue life of 0% consumed. After 50 cycles (Point E) the stress changes to lower σ2. Fatigue life of 25% is consumed at this point. When the cyclic stress starts with stress σ2, the

total number of cycles before failure has increased to 400, but due to 25% of consumed fatigue life, this is equivalent to a 100 cycles.

Goodman Miners rule (Equation 12) is an empirical law relating the stress range ($\Delta\sigma_{\sigma_m}$) for failure under mean stress (σ_m) with the one for zero mean stress ($\Delta\sigma_{\sigma_o}$) [19]. The zero mean stress equivalent can be used in Basquin's law for predicting number of cycles.

$$\frac{\Delta\sigma_{\sigma m}}{\left(1-\frac{\sigma m}{\sigma_{ts}}\right)} = \Delta\sigma_{\sigma_o}$$

Equation 12: Goodman

$Where$:

$\Delta\sigma_{\sigma_m} = stress\ range$

$\sigma_m = \ mean\ stress$

$\Delta\sigma_{\sigma_o} = zero\ mean\ stress$

$\sigma_{ts} = tensile\ strength$

Laboratory experiments shows relationship between stress range and high-cycle fatigue life, this is approximated in Basquin's law [19]:

$$\Delta\sigma N_f^b = C_1$$

Equation 13: Basquin's law

$Where$:

$\Delta\sigma = stress\ range$

$N_f = number\ of\ cycles$

$b = \ constant, typically\ 0.07\ and\ 0.13\ [19]$

$C_1 = constant$

2.8 Fracture Mechanics

Is the study of separations of solid bodies [20]. It investigates how cracks develops and what is driving the crack growth.

2.8.1 Fatigue crack propagation

Fatigue cracks can start at free surfaces or internal in the material typical at metallurgical imperfections creating areas with higher stress. External imperfection might be scratches from bad handling, deviation from machining, surface roughness, or a weakening due to temperature (welding)

As the material is under stress and cyclic loading the stress concentration in the weakened spot increases. The crack grows with the each cycle and expands. The crack is often documented [24] to grow normal to max principal stresses, meaning these stresses are important for this thesis. When the crack has grown large enough, the remaining cross section area is not strong enough to hold the load, resulting in final fracture. This is illustrated in Figure 17 found from Meyers and Chawla [20].

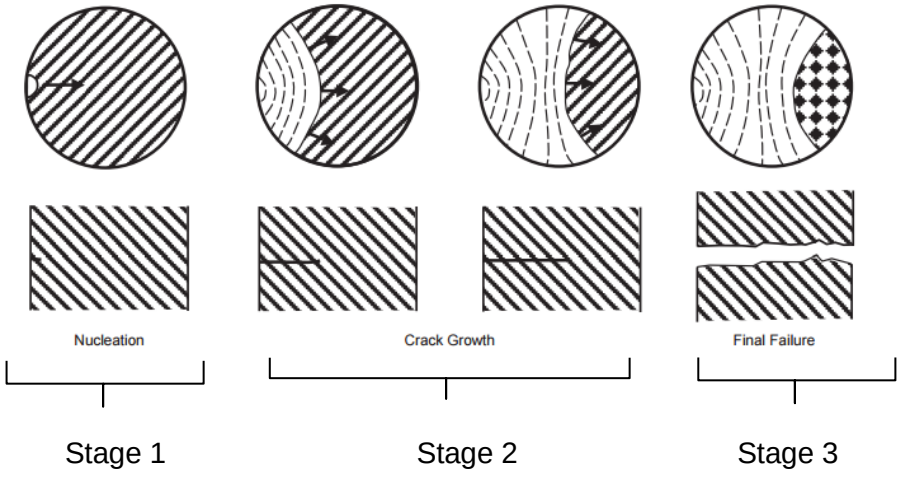

Figure 17: Typical fatigue crack propagation

Fatigue failure typically occurs as illustrated in Figure 17. It typically propagates in three steps.

1. Crack initiation. When the crack length becomes long enough for the stress field at the tip to become dominant, the crack changes direction and becomes perpendicular to the principal stress, and the crack enters stage 2

2. In the second stage the crack proceeds to grow. This process produces the typical pattern of fatigue striations and beach marks. One striation will represent one load cycle and can be viewed in a microscope. The Beach mark is the viewable for the naked eye. Each beach mark may contain thousands of striations. Beach marks are created when the stress changes, for example during starting and stopping.
3. Finale fracture occurs when the fatigue crack becomes long enough that the remaining cross section no longer can support the load. Final fracture often happens sudden and is brittle like, even for the ductile materials.

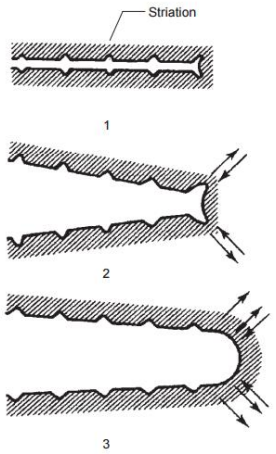

Figure 18: Striation creation in crack propagation

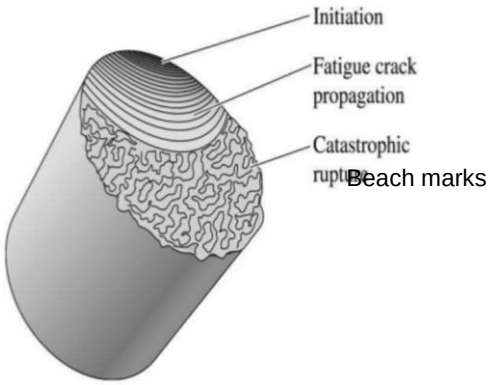

Figure 19: Typical fatigue fracture

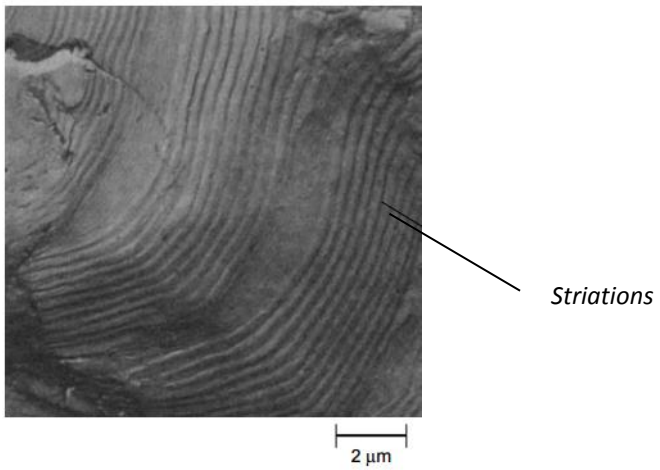

Figure 20: Striations in a crack
Taken from an electron microscope

Figure 17, Figure 18, Figure 19 and Figure 20 illustrates creation of striations and crack propagation found in Meyers and Chawla [20].

2.8.2 Paris Law

Is an empirical formula made for prediction of crack growth rate. Paris discovered that for a number of alloys the crack growth rate against stress intensity factor gave straight lines on a log-log scale, see Figure 21 from Ashby and Lebon [19]. This implies that for the area with straight line, Equation 14 is valid. This is the same area as the crack growth rate or section two, described in Figure 17.

$$\frac{dc}{dN} = C(\Delta K)^m$$ *Equation 14: Paris Law*

$Where$:
$\frac{dc}{dN} = Crack\ growth\ rate$
$\Delta K = Change\ in\ stress\ intensity\ factor$
$C = material\ property$
$m = material\ property$

$$\Delta K = K_{max} - K_{min} = \Delta\sigma Y\sqrt{\pi a}$$ *Equation 15: Change in stress*

$Where$:
$K_{max} = stress\ intensity\ factor\ max$
$K_{min} = Stress\ intensity\ factor\ min$
$\Delta\sigma = change\ in\ stress$
$a = Crack\ length$
$Y = Geometric\ factor$

When stress intensity factor (K) is larger than fracture toughness factor (K_{ic}) fracture occur, as seen in region 3, Figure 21 [19]. The fracture toughness factor is a material property and is found by laboratory experiments [19]. The stress intensity factor changes depending on crack length, as seen in Equation 15. Giving that when the crack length increases the stress intensity

increases [19]. This leads to increased crack growth rate according to Paris law. Below the threshold limit (K_{th}) the crack does not grow.

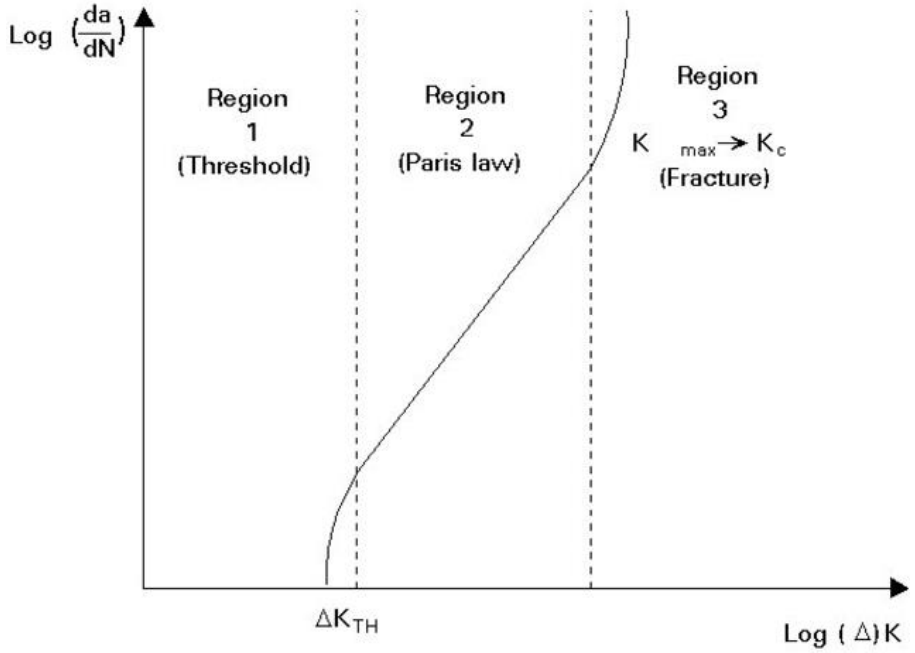

Figure 21: Crack propagation

2.9 Notch effect

Basis for calculations of stress concentration factor (SCF) is from eventure.com [25]. The stress concentration factor (K_t) is given by stress at stress notch over nominal stress, described in Equation 16.

$$K_t = \frac{\sigma_{max}}{\sigma_{ref}}$$

Equation 16: Stress concentration factor

$Where$:

$K_t = Stress\ Concentrating\ Factor$

$\sigma_{max} = Stress\ at\ Concentration\ point$

$\sigma_{ref} = Nominal\ stress, outside\ of\ concentration\ area$

The stress concentration factor is dependent on the geometry such as diameter and notch radius showed in Figure 1. For a bolt in tension, Equation 17 is a valid approximation calculation formula [26].

$$K_t = B\left(\frac{r}{d}\right)^a$$

Equation 17: Approximate Stress concentration factor

$Where$:

$a = table\ value$

$B = table\ value$

$r = filet\ radius$

$d = small\ diameter$

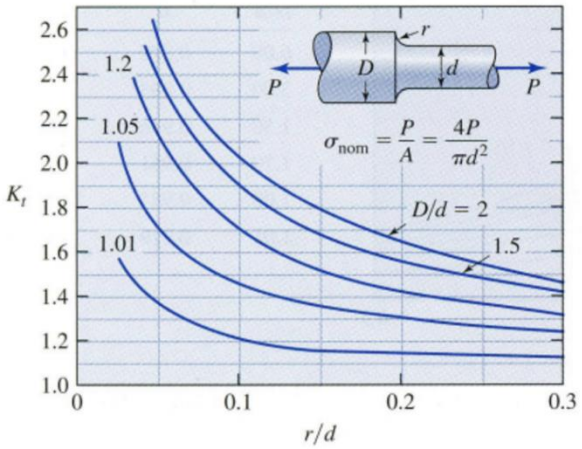

Approximate formula $K_t \approx B\left(\frac{r}{d}\right)^a$, where:

D/d	B	a
2.00	1.015	−0.300
1.50	1.000	−0.282
1.20	0.963	−0.255
1.05	1.005	−0.171
1.01	0.984	−0.105

Figure 22: Stress Concentration factor approximation formula

2.10 Introduction to Abaqus FEA software

Abaqus is a finite element system software widely used by engineers, both in research and industry. Abaqus is owned by Dassault systemes and is part of their SIMULIA packet. The software offers a complete simulation tool, and contains analysis tools for investigating linear problems and static events and low speed dynamic events (Abaqus standard/Implicit) or high dynamic events such as crash simulation, blast simulation (Abaqus Explicit). The software also contains Multiphysics such as thermal, electrical, radiation, acoustics and computational fluid dynamics (CFD) analysis [27].

For this thesis Abaqus/Standard is used, as static and quasi-static simulations has been performed. Abaqus work processes is illustrated in Figure 23 from the Abaqus user guide [28]. In the pre-processing phase, the model is created using Abaqus/CAE which also contains CAD tool set [28]. Abaqus/CAE enables the user to create parts, assemblies, materials, interactions, loads and constraints which automatically generates an input file or job file. When the job or input file is ready for simulation, Abaqus/standard takes over and uses advanced solver algorithms to solve the input file. The output file after the performed simulation is called odb file. This file can be post-prosessed in Abaqus/CAE [29].

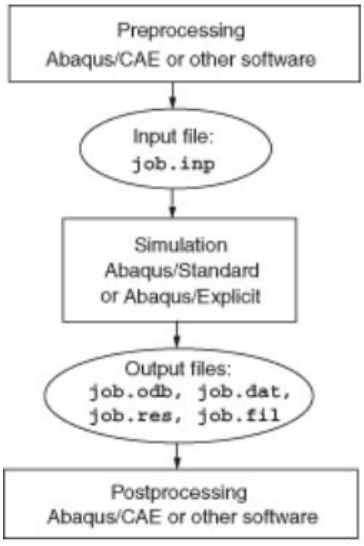

Figure 23: Abaqus analysis stages

2.11 Further Literature

Different studies and literature has been reviewed and creates a basis for this thesis. Engine manufactures has been contacted in the hope accessing information. The student has not succeeded in gaining much relevant and new information by engine manufacturers. Due to companies being concerned giving away competitive advantages. Because of this, the student has retrieved information from similar design FEA studies performed at universities, and more "general known" industrial methods or "old" technology from engine manufacturers. A few of the studies this thesis is based upon is:

R.J. Grant & B C D Flipo: A parametric study of the elastic stress distribution in pin-loaded lugs modelled in two and three dimensions and loaded in tension. [30]
Paper describing a FE study investigating effects of loading a lug with a pin. This is interesting for this thesis as loading of lug with a pin, can to some extent be related with loading a bearing to a big end hole (Bearing representing pin, and lug representing big end hole). The paper shows considerable edge effects around the end of the lugs, leading to dimensioning of wider bearing of bearing/crankpin compared to big-end hole. Furthermore, the paper shows maximum circumferential stress depending on pin clearance is around 9o'clock & 3o'clock position, when load is in 6 o'clock direction.

MAHLE GmbH, Cylinder Components, **Ed1, Wiesbaden 2010** [8]
General information from manufacturer of combustion engine components. Contains information on typical design measures for engine components such as the connection rod and big-end bolt. Explains how the stresses during power stroke effects the design of the machine component.

Connection rod FE analysis by AVL [31]
This document contains a FE analysis conducted by AVL for comparing a proposed design by an engine manufacturer with AVL experience. The report shows concern regarding the fatigue strength for the big-end bolt. Most of the stress during the power stroke is through the first threads in the big-end bolt, leading to low safety factor against fatigue. This document serves as a background for this thesis, as similar design and same load conditions is used. The document also serves as a verification document for comparing this thesis result with "industry" standard.

Leif Lundby's Forbrenningsmotorer (Combustion engines) chapter 8 Machine dynamics [9]

Leif Lunby has written a Norwegian book called "frobrenningsmotorer" or combustion engines. Chapter eight in this book explains thoroughly the forces acting in a crank assembly during the stroke. For understanding the forces in the connection rod and from where they come from this information is useful. The chapter explains with tables and figures the relation between design geometry, velocity, masses, inertia and pressure how the stress components in the crank assembly is derived. The book has previously been part of education of engineering students.

Abaqus user guide [28]

Abaqus CAE contains files for a complete user guide explaining every feature in abaqus software. This has been an important tool used by the student for creating the models and performing FEA simulations.

Technical tables and standards

Other literature has also been used for technical support, such as technical tables by Jarle Johannesen [32]. This book gives much general information on everything related to engineering from threads, friction and force calculations.

Wiley & Bosch's automotive handbook [11] is a pocket book containing information on topics related to automotive industry such as machine parts, materials, engine dynamics etc. This book serves a purpose as a quick searchable encyclopedia.

3 METHODOLOGY

This chapter highlights how the this master's thesis is performed. For doing FE analysis some elements needs to be in place, such as a geometry or part, material properties, mesh, constrains and loads. This will be explained in this chapter. For detailed step-by-step guide on building the model, please see appendix 7.1.

The main things of interest in this thesis is the forces acting in the con-rod and the bolts through the crank bearing. As these forces is fluctuating through the stroke creating stresses, bending and fretting. For being able to do calculations on input forces is needed. They can be calculated by knowing engine parameters and geometry. The parameters, which influence the stress in the assembly, is the engine speed (RPM), weight of parts and combustion pressure. However, for simplifying reasons this thesis uses bearing forces throughout the stroke, from an engine manufacturer.

This thesis consist of three simulation cases. The first case is to confirm the features in abaqus one by one, such as bolt pre-tension, contact forces and bearing force/distribution. In case two all these features are combined in a simplified connection rod assembly, to confirm that the features works in combination. The final case is to create a "realistic" connection rod based on real geometry.

For verification of the model, a combination of hand calculations and comparing with industrial simulations is used. The idea is that the simplified and realistic model should get results in the same ballpark as the industry test.

3.1 Building the model

3.1.1 CAD model

The parts in the simulation is created in Abaqus/CAE software. The software has a built in CAD tool which allows for creating 3Dmodels. Drawings of the parts is in Appendix D and E. The model consist of 3D deformable extruded parts. They can be created in the part module of Abaqus as shown in Figure 24.

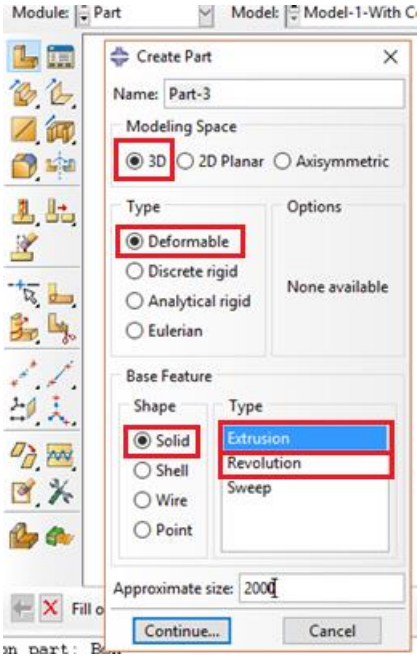

Figure 24: Create part option box

The options on the picture is used for the connection-rod, cap and bearing. The bolts is also 3D deformable solid shape, but use revolution-type for sketching. A sketch is created for the section, correct measurements is chosen and the part is extruded or revolved to correct size.

For the holes in the model, e.g. bearing hole, a datum axis is created. In the middle of the hole a reference point is placed, showed in Figure 25. This is for joining the bearing and lug together in the assembly.

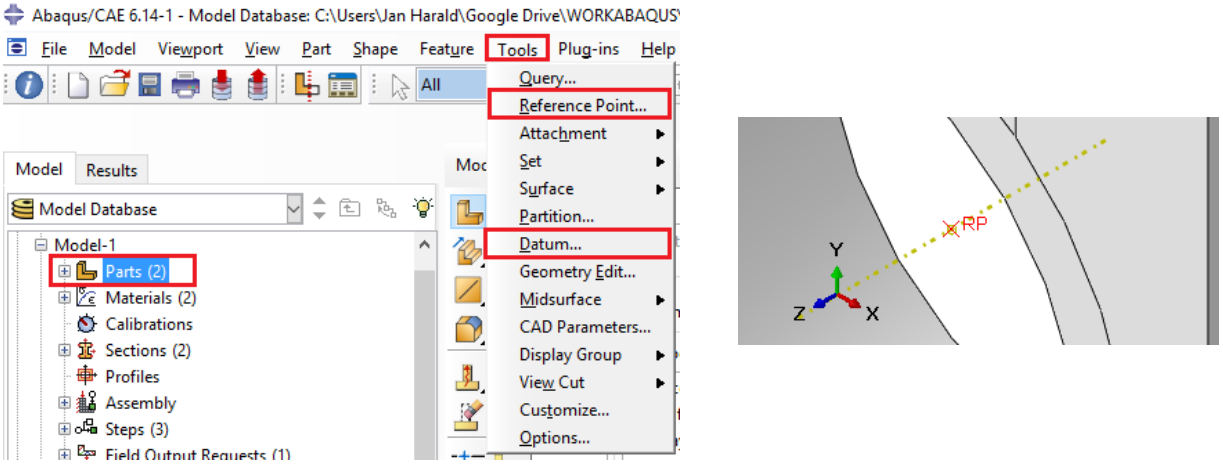

Figure 25: Creation of reference point and datum axis

3.1.2 Assembly

The assembly consists of five parts; connection rod, two bolts, bearing, and big-end cap. These parts are joined in the connection rod assembly. By sketching the parts with reference to the same coordinate system, the assembly process can be performed more effectively. This method saves time, as the parts do not have to be constrained with reference to each other.

The bolts needs to be constrained in the correct place in the assembly model. **Coaxial constraint** and **Face to Face constraint** functions are used for this. **Coincident point constraint** is used to align the bearing in the big end, as both parts has reference point at the same place. The assembling of the simplified model is illustrated in Figure 26.

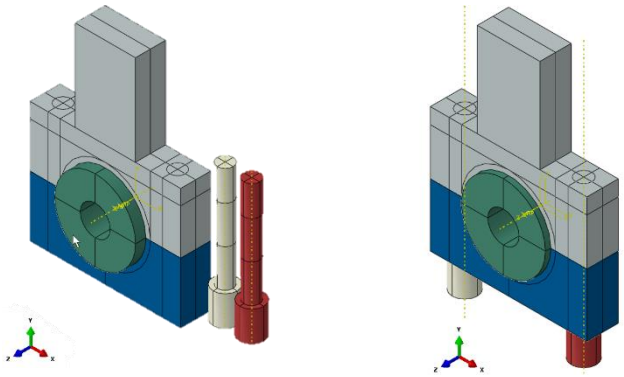

Figure 26: Simplified connection rod before (left) and after (right) assembling

3.1.3 Mesh

The simulations performed in this thesis uses C3D20R elements. This element type uses second order quadratic interpolation elements in three dimensions with reduced integration [33]. C3D20R elements gave more stable simulation results, lowering chances of failure compared to the Abaqus default element type C3D8 [33]. Both element types are illustrated in Figure 27

C3D20 element type was also tried for simulation but tests used too large calculation time. C3D20 elements has 27 integration points compared to 8 for C3D20R, resulting in approx. 3.5 times longer calculation time [33]. For contact simulations, however, the mesh density can be increased with reduced integration, leading to better contact results at the same computing capacity compared to fully integrated elements [34].

Hourglassing can be a problem for first-order, reduced-integration elements [33]. However second order reduced-integration elements does not experience the same difficulties and is recommended in cases where the result is expected to be smooth [33].

Figure 27: Linear C3D8 Element (left), Quadratic C3D20 Element (right)

Image from Abaqus Analysis User's Guide [33]

3.1.3.1 Bias meshing

Is a technique used for enhancing the mesh quality. It is done by defining local seeds for the mesh control meaning the mesh density can be controlled towards a specific area. This is a good tool for creating high-density mesh around geometry, which needs a high level of detail without increasing the mesh density for the whole model. This spares the number of elements needed for producing valid results, resulting in a more optimized model using less CPU power [28].

3.1.4 Partitioning

Is a method to cut the model making it suitable for meshing. When using quadratic brick elements the 3D model needs to be four sided enabling a good mesh. This is performed by cutting or partitioning the model, creating sections that is four sided. These sections are called cells in Abaqus. The partitioning should be symmetrical if possible. For advanced geometries, it is difficult to partition the model and use quadratic brick elements. For these cases, tetrahedron elements can be used. Note that tetrahedron elements are stiffer due to the triangular shape, meaning the mesh density must be increased getting more accurate results [33].

Figure 28 shows how the simplified model is partitioned symmetrically. It has four sided cells making it easy for creating quadratic elements. Note that the holes for the bolts creates additional needs for partitioning.

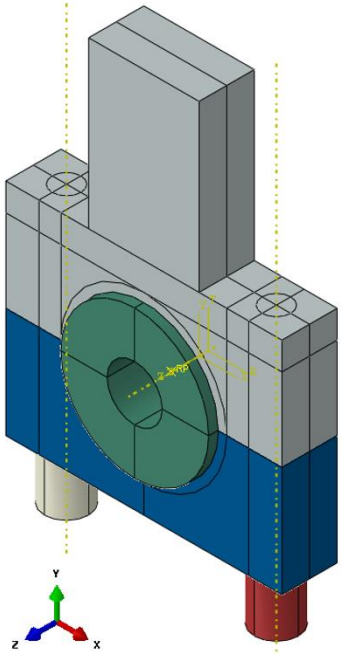

Figure 28: Partitioned simplified model assembly

3.1.5 Material Properties

For simplification, the material properties in the simulation is limited. Meaning that for the connection rod parts and bolts, general steel stiffness is used. This includes only elastic behavior with young modulus on 210E3 [MPa] and poisons ratio on 0.3. Plasticity behavior is neglected, because it is assumed that the size of the design and forces acting on it creates stress within the range of elastic deformation.

For the bearing, elastic behavior is chosen with stiffness 3 times higher compared to the connection rod. This is because that the crank pin gets low deformation or ovalization compared to the big-end hole during operation. Methods using rigid bearing was performed, but with weak results as the simulations performed unstable and with many failed attempts. The bearing has specified thermal expansion coefficient with α = [11E-6 K^{-1}] and anisotropic properties enabling the bearing to expand closing interface gaps, before load is applied, as a method for stabilizing the simulation.

Material Name	**Young-modulus [MPa]**	**Poisson ratio**	**Thermal expansion**
Material-Steel	2.10×10^5	0.3	No
Material-Stiff	6.30×10^5	0.3	Yes (11×10^{-6} K^{-1})
Selected material for parts			
Bolts	Material-Steel		
Connection rod upper	Material-Steel		
Cap	Material-Steel		
Bearing	Material-Stiff		

Table 3: Material properties for parts

3.1.6 Interaction

The interaction module in Abaqus allows the user to specify interactions in the model. This includes specifying contact mechanics, couplings, thermal interaction and constraints between regions [28].

3.1.6.1 Contact mechanics, master and slave surfaces

The parts in the assembly interacts with each other. Contact behavior between surfaces needs to be specified. Master and slave surfaces is a method Abaqus uses for specifying surfaces in contact. For simulations with two surfaces with deformable bodies, Abaqus user guide says that

the master surface should be choses of the stiffest body, or the coarsest mesh, if they have the same stiffness [28].

In simulations with rigid bodies, master surface must be chosen on the rigid surface, as this surface penetrates the slave body [28].

For creating contact surfaces Abaqus has a built in function called **Find Contact Pairs**, which automatically detects surfaces in contact or within a specified clearance [33] . An algorithm automatically detects which surface should be the master or slave. This can be manually changed. This function saves the user a lot of time, not having to manually specify all the contact areas, reducing the risk of human error. Figure 29 shows the results from the “find contact pairs” function, where the purple surfaces are slave, and red are master surfaces.

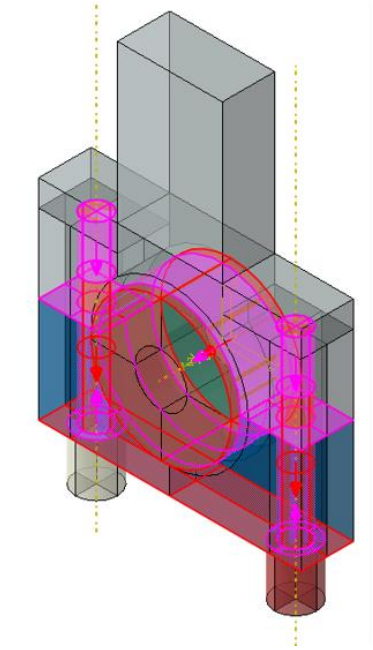

Figure 29: Contact pairs

All surfaces is steel against steel, machined surfaces, which would give static friction number of approx. 0.15 and kinetic friction number between 0.1 to 0.03 (dry to lubed) [32]. For the bolt interfaces, a friction factor of 0.18 is chosen with reference to the friction used in industrial simulation [31]. As the bolt pre tensioning feature only works when frictional behavior is turned on [33].

For the interface between the cap and connection rod **rough** interaction properties is used. This makes the parts unable to slip while in contact [28]. This is a simplification for simulating serrations.

For the interface between the bearing and big end hole frictionless behavior is turned on.

3.1.6.2 MPC-Coupling

Is a function that is used in this thesis for distributing a concentrated force over an area [28]. This is handy when attaching the bearing load, as the bearing load is defined as a force vector in the AVL report [31]. As the bearing is round, the force vector has to push over a round surface. By defining a reference point, which connects to the intended surface, the MPC-coupling is able to spread the load from the vector in the reference point, over the surface. This is done by using **MPC-coupling pin** as seen in Figure 30.

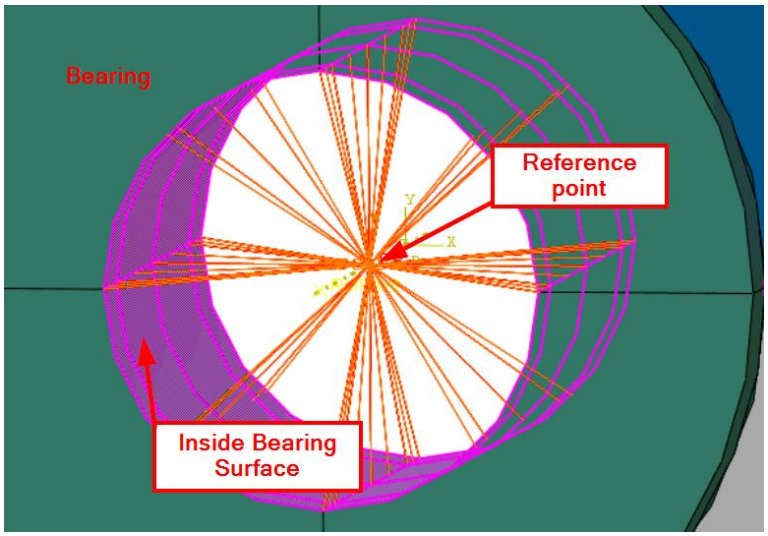

Figure 30: MPC-Coupling pin

3.1.6.3 Springs

Springs are used to hold the bearing in place during simulation. Due to the clearance between the bearing and the connection rod, the bearing needs to be connected with some sort of coupling for not creating errors in the simulation. This is done by placing a few springs with very small spring stiffness (approx. 0.01 Nm) so small that they can be neglected. This technique helps the simulation run more smoothly without errors.

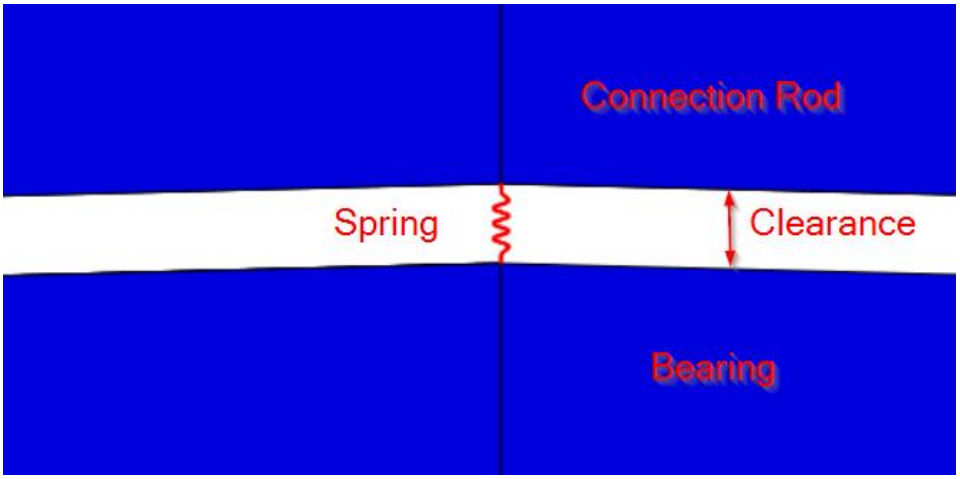

Figure 31: Using springs for stabilizing the model

3.1.7 Steps

When Abaqus perfomes simulation, steps has to be created in order to perform tasks in specific order [33]. The simulation for the models in this thesis is performed in four steps. These steps and function of them is shown in Table 4.

Step number	**Name**	**Function**
0	Initial	Initial step. Interactions is defined, such as contact mechanics, surfaces, friction and temperature.
1	Pre-tension	Bolt pre tensioning must be performed in the first step [28], this is defined by Abaqus.
2	Expand	Temperature increases. This effects only the bearing as this is the only part with material properties with defined coefficient of thermal expansion. Enables the bearing to grow, closing the gap between bearing and connection rod.
3	Apply Load	While the bearing is heated and in expanded state, the bearing force is applied with specified direction and magnitude.
4	Unexpand	Temperature decreases to initial temperature, opening the gap between the bearing and connection rod. Thermal stresses will be removed and only stresses from pre-tensioning and applied load will be present.

Table 4: Step and function

3.1.8 Loads and constrains

The connection rod is fixed or “welded” at the top (Abaqus calls this encastre). This is a simplification because in real life, the connection rod is pin connected between the crank and the piston. A more correct method could be to use dynamic explicit method, simulating the movement and forces throughout the power stroke. This is very consuming on CPU and the results collected from such a method would give more information on the stress in the connection rod arm. This thesis investigates the big-end part, which therefore legitimates the simplification fixing it at the top.

Furthermore, the bearing is constrained so that it is freely to move in two directions and rotate in three directions, but fixed in one direction. Meaning that it will not be able to fall out through the big-end hole. It will not rotate, and is limited to very little movement in the other directions as it will meet the inside of the big-end hole, and be hold in place by these walls. In real engines, the bearing shells is locked in place in the big-end by wedges [5].

The assembly is mainly exposed to two loads; bolt pre-tensioning forces and bearing forces. The bolt pre tension force is varying with the bolt material. A typical rule of thumb when pre-tensioning bolts is to pre-tension them up to 70% or 90% of yield strength for reusable or permanent connections respectively [2].

The bearing forces for the simplified connection rod and realistic connection rod is according to AVL report [31].

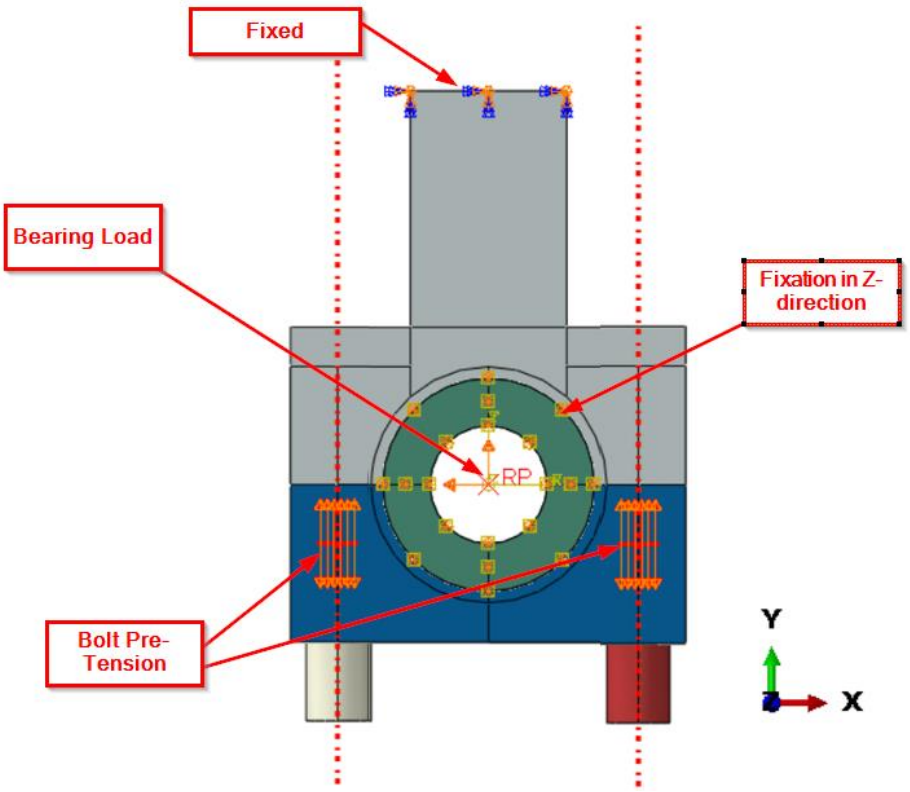

Figure 32: Loads and constrains

3.2 Verification method

A FEA-simulation of a connection rod by an engine manufacturer is the basis of the verification of this thesis, in conjunction with hand calculations and academic papers (Grant et al.). Due to intellectual property rights, details on the connection rod will not be published. If the results are within reasonable limits this will verify the robustness off the models.

To manage to build simulation model with many mechanisms working together, it is important to have tested each part mechanisms, to verify the functionality. It is easier to do one thing at a time, than trying to do everything simultaneously.

3.3 Preliminary FEA-models (exercise models)

The preliminary models are created with very simple geometry. The idea here is to verify that the different mechanisms works e.g. contact mechanisms between instances/parts, pre-tensioning of bolts, correct clearances etc. The student uses these models also for training and “getting known” to the FEA tool Abaqus.

The main models that has been used is shown in Table 5, with further explanation of the models

	Name	**Function**
1	Bolt Pre tensioning in sleeve	Bolt pre-tension feature in assembly
2	Bolt pre-tensioned in split sleeve	Bolt pre-tension feature in assembly with more parts
3	Threaded (tied) pre-tensioned bolt in hole	Bolt in threaded hole, pre-tensioned
4	Rigid shell bearing in deformable body	Simulate the bearing load through a rigid bearing to the connection rod
5	Stiff deformable bearing in deformable body	Simulate the bearing load through a stiff bearing to the connection rod (Workaround)

Table 5: Preliminary FEA-models

3.3.1 Bolt Pre-tensioning in sleeve

This exercise is to practice bolt pre-tension in sleeve. This includes creating parts, creating material properties, creating assembly, assigning contact behavior and specifying loads and constrains. Results from the exercise is showed in Figure 33 and Figure 34. Note that the FEA results (Figure 34) only purpose is to confirm that the simulation completed.

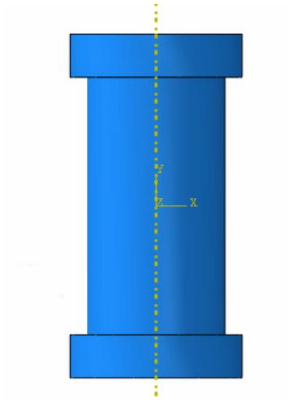

Figure 33: bolt and sleeve

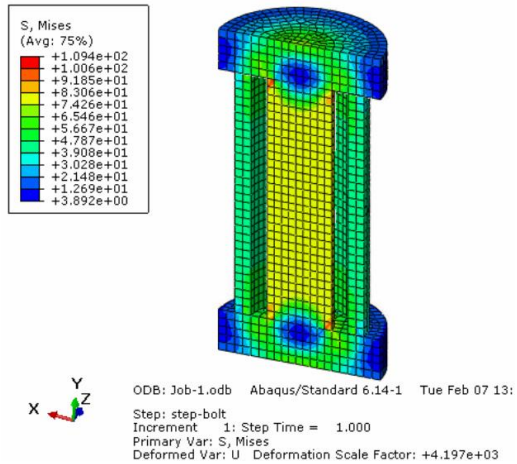

Figure 34: FEA pre-tensioned bolt results

3.3.2 Bolt pre-tensioned in split sleeve

This exercise is the same as above but with a split sleeve. This is to confirm that the pre-tension of the bolts would hold an assembly together, as it would have to do for holding the connection rod and cap together. Again, the FE is only to confirm that the simulation completed.

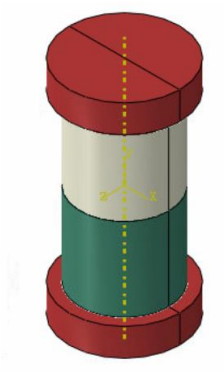

Figure 35: bolt and two sleeves

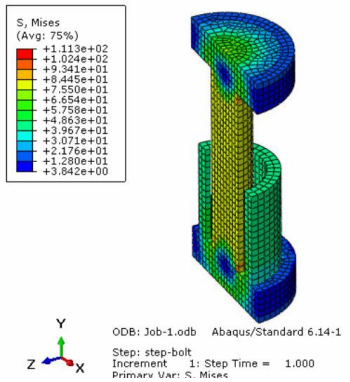

Figure 36: FEA pre-tensioned bolt results two sleeves

Upper sleeve removed for illustration

3.3.3 Threaded (bonded) pre-tensioned bolt in hole

Figure 37 sows a box with a hole, and a bolt. The exercise is to simulate fastening of a bolt with threads in a hole. A simplification is that the surfaces between the hole and bolt (thread area) is tied together. Meaning the mesh here is “welded” together, which allows for no slippage between the nodes [28].

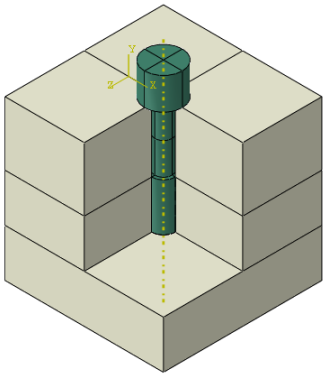

Figure 37: Bolt with threads in hole.

Note that cells has been removed for better visualization

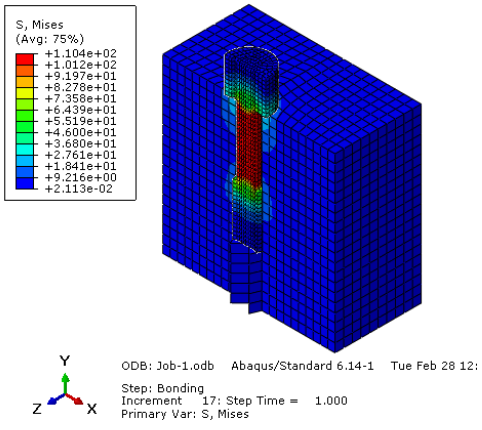

Figure 38: Thread in hole results.

Von-mises stresses after performed pre-tensioning, with cut-section view.

3.3.4 Discrete Rigid Bearing in deformable body

This method is based on creating a discrete rigid part, meaning it will not deform when exposed to forces [34]. The bearing is simulating the crank which in real life does not deform much compared to the connection rod big-end during the stroke [31].Using a discrete rigid bearing is a simplification, which reduces the calculation time [33].

After testing multiple simulations with this method, it was decided to not use the method, as the simulation was unstable resulting in many failed attempts. One of the test setup is illustrated in Figure 39. As a work around a high stiffness, deformable body method is used.

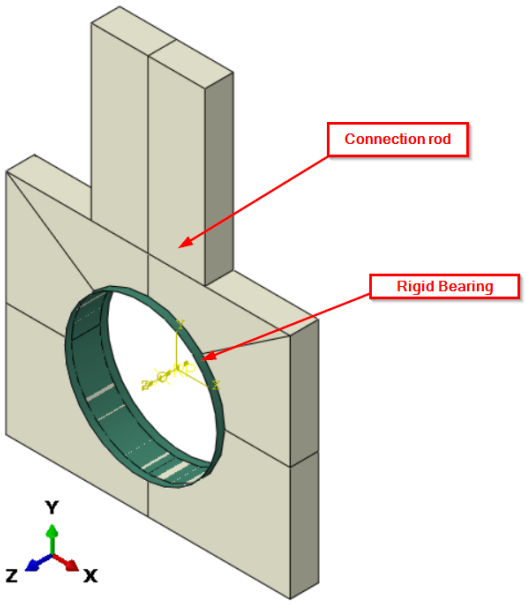

Figure 39: Rigid Bearing

3.3.5 High Stiffness bearing in deformable body

This method uses a deformable bearing instead of rigid. By having very high stiffness of the bearing material compared to the connection rod, the deformation in the bearing is so small that it can be neglected. Drawback of this method is that an extra part has to be meshed, resulting in higher calculation time. Figure 40 shows the assembly with deformable bearing.

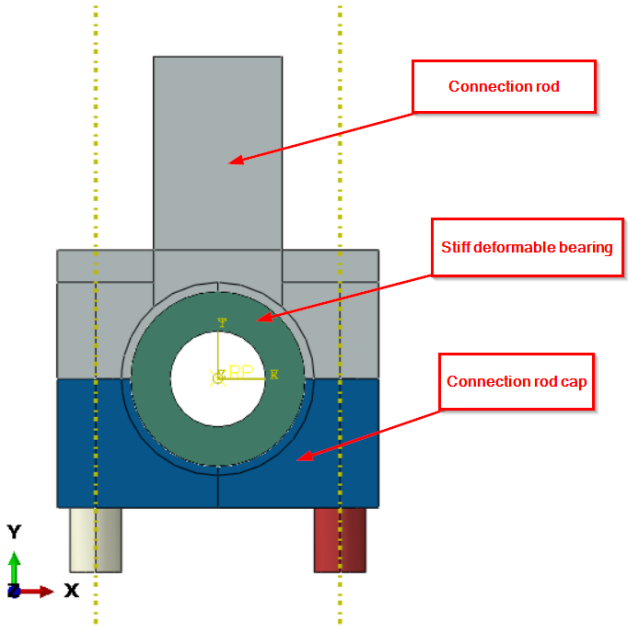

Figure 40: Stiff deformable bearing

3.4 Setup Simplified Model

Simplified model is built with symmetrical geometry enabling is easy to partitioning and meshing. The dimensions are choosed by the student and are not representing any real geometry. The overall size however is within the same ballpark as the reference industrial connection rod [31] with a big-end hole of Ø270mm.

Input parameters simplified model	
Material properties	According to Table 3: Material properties for parts
Bolt pre-tension	1.5 [MN]
Bearing Force	1362.308 [kN]
Bearing Force Direction	1.44 deg

Table 6: Input parameters simplified model

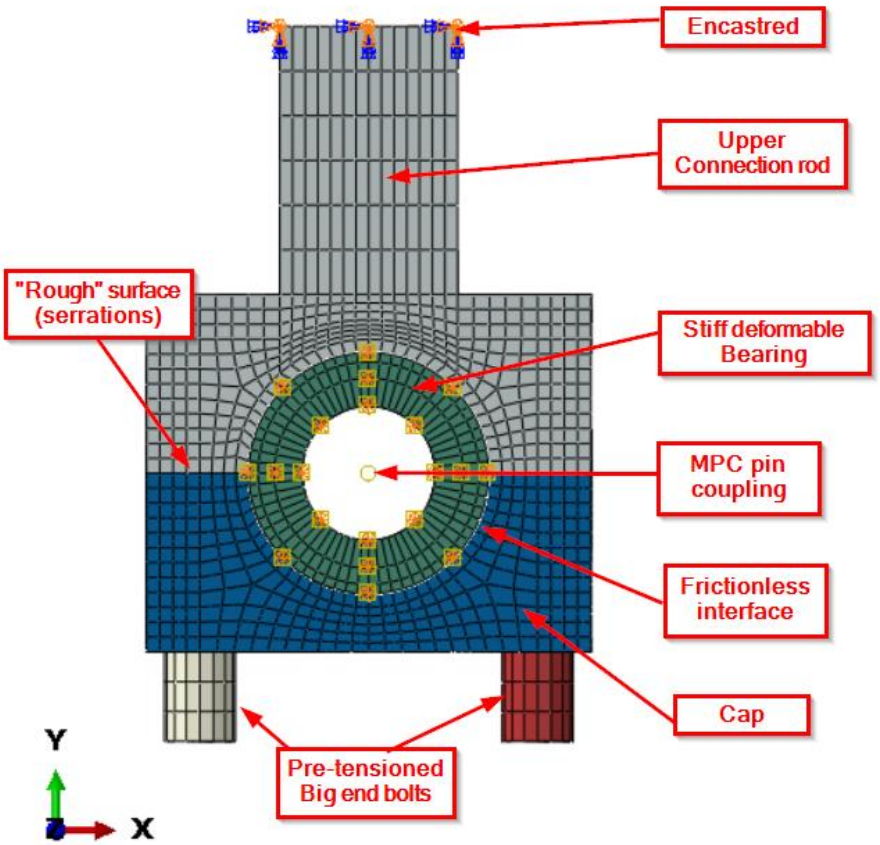

Figure 41: Simplified model setup

3.5 Setup Realistic Model

The purpose of the realistic model is to work as a global model highlighting bending, tension, shear stresses and notch effects during the power stroke. Detailed geometry for the realistic model is in Appendix D and E. Material properties for the parts is similar as for simplified model, see Table 11: Basis of calculations. Realistic model has big-end bolts with threads, fastened in the upper connection rod using technique described in chapter 3.3.3. The connection rod is encastred (welded) at top and force is acting through MPS-pin coupling on the bearing. The load cases for simulating the power stroke is described in Table 8 similar to AVL report [31]. The setup of the model is according to Figure 42 and Figure 43.

Input parameters realistic model	
Material properties	According to Table 3: Material properties for parts
Bolt pre-tension	1.529×10^6 [N]
Bearing Force	According to Table 8: Load cases for power stroke

Table 7: Input parameters realistic model

Time:	**360 deg BTDC**	**290 deg BTDC**	**180 deg BTDC**	**55deg BTDC**	**0 deg TDC**	**10 deg TDC**	**75 deg TDC**	**180 deg TDC**	**290 deg TDC**	**330 deg TDC**	**360 deg TDC**
Φ [deg]	-180	94.85	0	-73.78	0	1.44	26.85	0	-92.65	-162.75	-180
F [N]	384259	155907	343704	150276	1234854	1362308	345428	374346	155516	321957	384258

Table 8: Load cases for power stroke

Note that BTDC means number of crank degrees Before Top Dead Center. TDC indicates number of crank degrees after Top Dead Center.

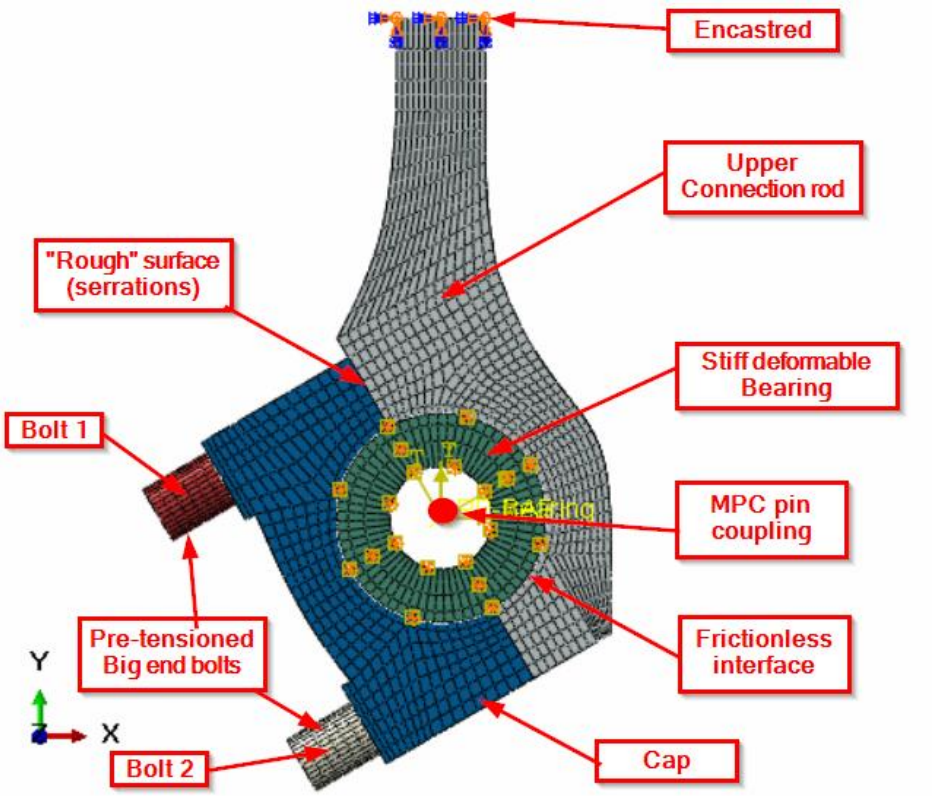

Figure 42: Realistic model setup

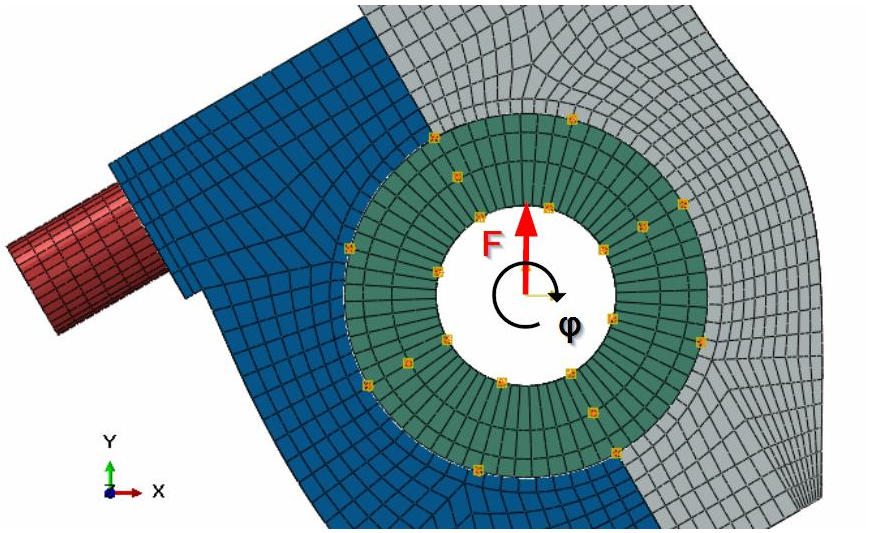

Figure 43: Load directions

4 RESULTS

4.1 Activity 1: Mechanisms Results

4.1.1 Contact Simulation Results

The contact simulation results is from FE simulation in abaqus and is illustrated in Figure 44.

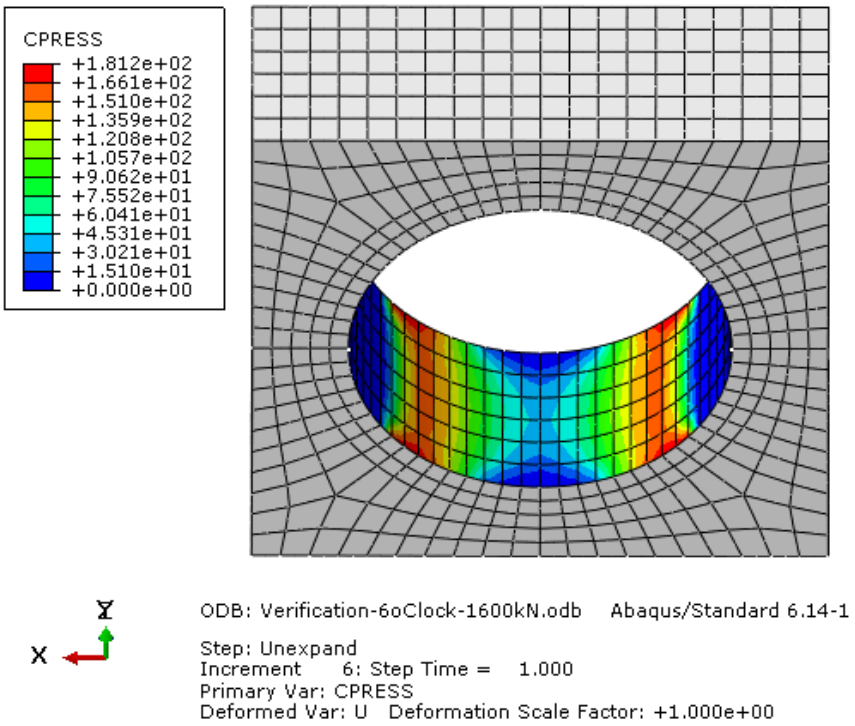

Figure 44: Contact pressure from Abaqus

This shows maximum contact pressure of approx. 180MPa. Average contact pressure is assumed to be around 120 MPa based on the colors in the middle of the lug.

4.1.1.1 Verification Contact Simulation Results

Results from hand calculations using Hertz equations in chapter 2.5

Input	
Length [mm]	100
Radius A [mm]	99
Radius B [mm]	-100
Force [N]	1.60×10^6

Young Modulus A [MPa]	2.10×10^5
Young Modulus B [MPa]	6.30×10^5
Calculations:	
E' [Mpa]	3.46×10^5
R'	9900
b contact area [mm]	34.14
Pavg [MPa]	**117.2**
Pmax [MPa]	**149.2**

Table 9: Results Hertz equations

To summarize the results from Figure 44 the max contact pressure force is approx. 180 MPa while the max hand calculated is 150 MPa. This gives a deviation of 20 %.

The average contact pressure from Figure 44 is difficult to read, but is assumed to be around 120 MPa from looking at the picture. Hand calculated average pressure is 117.2 MPa. This gives a deviation of 2.4%

4.1.2 Bolt-Pre Tension Results

Typical rule of thumb according to eFunda [26] and Johannesen [2] when applying bolt pre-tension, is to use 75 % and 90 % of the yield strength of the material for respectively reusable and permanent bolt. Bolt material grade 12.9 is choosed, giving the following results.

Bolt Pre-Tension Calculation data		
Material	**Steel**	**Units**
Material Grade	12.9	
Tensile strength	1220	MPa
Yield strength:	1098.0	MPa
Nominal diameter	52	mm
Pitch	5	mm
Bolt pitch diameter:	48.8	mm
Bolt area:	1866.7	mm2
Tension force Reusable:	1.537×10^3	kN
Tension force permanent:	1.844×10^3	kN
K correction factor:	0.3	
Torque reusable:	22.482×10^3	kNmm
Torque permanent:	26.979×10^3	kNmm
Pre-tension Stress Reusable:	824	Mpa
Pre-tension Stress Permanent:	988	MPa

Table 10: Bolt Pre-Tension Calculation data

The simulation results on the pre tensioning feature in Abaqus has given the following results as shown in Figure 45. This is based on pre-load on 1500kN.

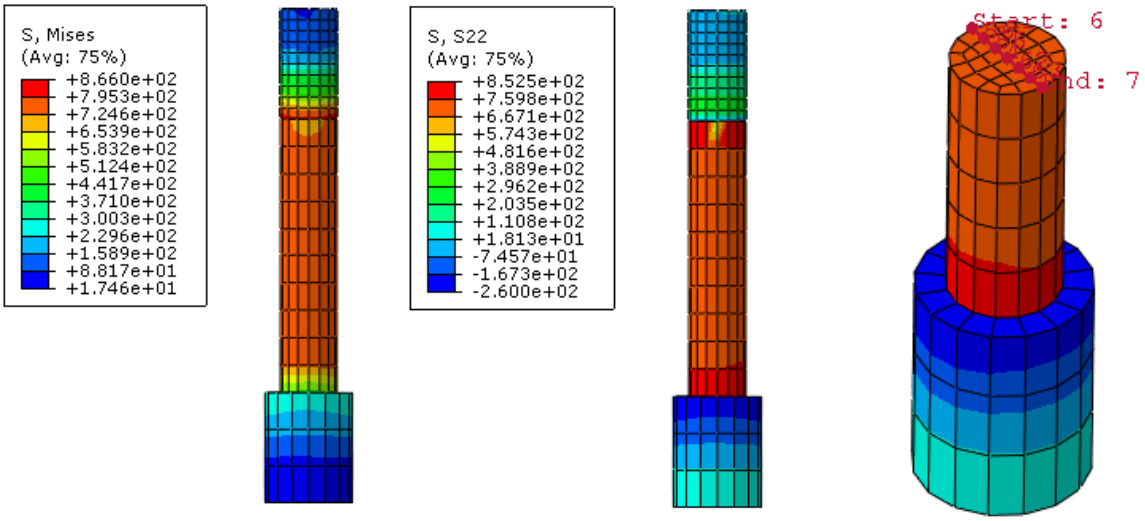

Figure 45: Mises stress, S22 stress and path

Through pre tensioned bolt, from left to right respectively

The stress along the path defined in Figure 45 is illustrated in Figure 46.

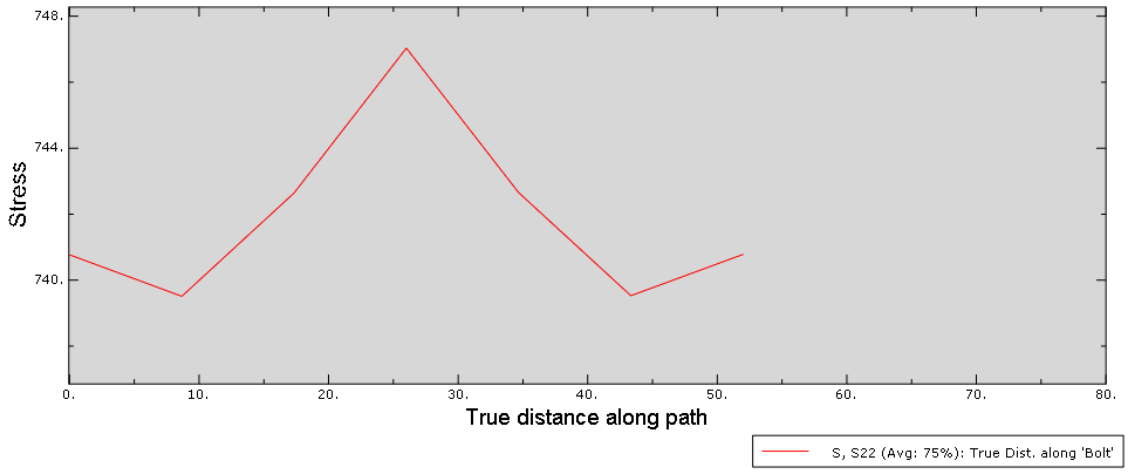

Figure 46: S22 stress along path through bolt

4.1.2.1 Verification Bolt-Pre Tension Results

The average stress from Figure 46 is approx. 743MPa. From hand calculation, the axial stress should be 823 MPa for the pre-tensioning force selected. This gives a deviation of 9.7%.

4.1.3 Bearing Load Simulation

The following results is collected from a FEM-simulation. The goal of this simulation is to have some results, which can be compared to hand calculations, verifying that the setup of the model is correct.

The basic of the calculation is a lug with a clearance fit bearing. The bearing is pressed downwards in negative Y-direction (6 o'clock), details listed in Table 11.

Material Properties				
	Part	**Young-modulus [MPa]**	**Poisson ratio**	**Thermal expansion**
Material-Steel	Lug	2.10E+05	0.3	No
Material-Stiff	Bearing	6.30E+05	0.3	Yes (0.01)
Forces				
Load Force:	1600	kN		
Direction:	180	deg	(6 o'clock)	
Boundary	Encastred at top			

Table 11: Basis of calculations

Figure 47 shows the setup of the model. This simulation contains contact mechanics between bearing and lug, not investigated in this section. The load force is illustrated with the letter F.

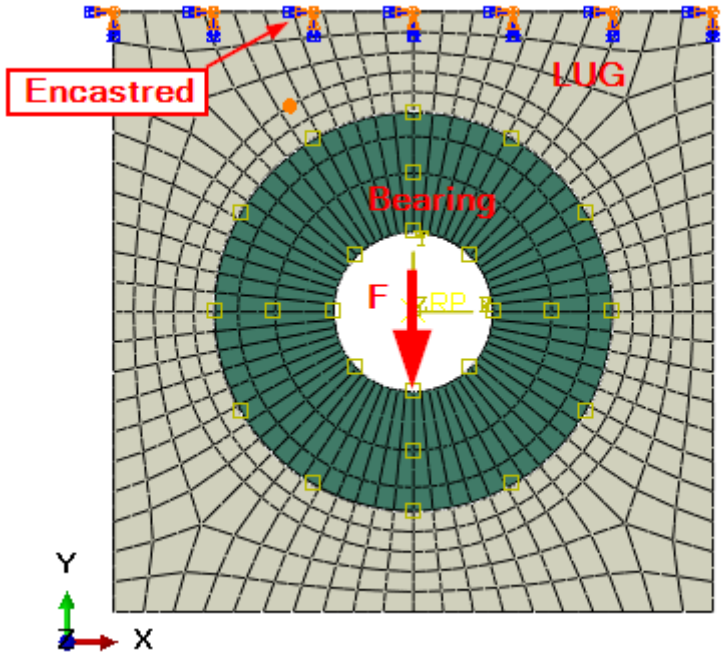

Figure 47: Bearing and lug, with boundary constraints

For this simulation the principal stresses around the middle of the lug hole, and tension forces in the lug sides has been investigated. The setup for the results has been done by using paths (Figure 48).

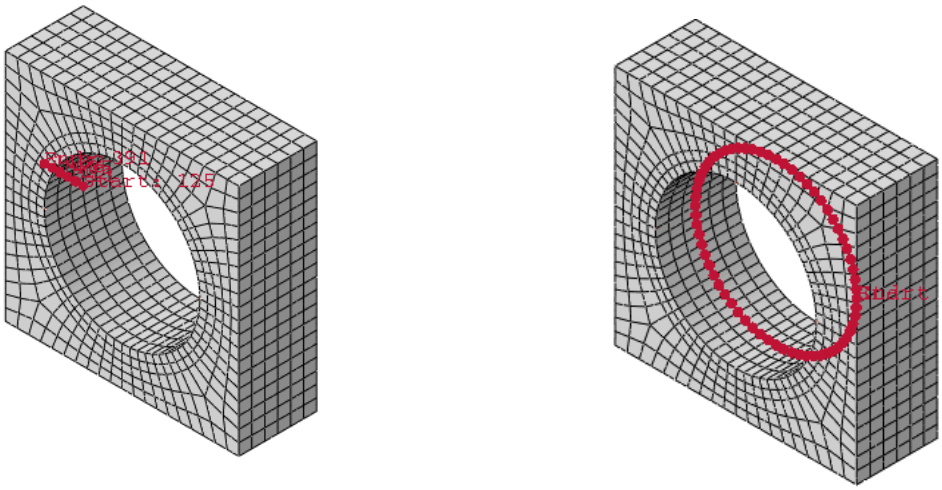

Figure 48: Path through lug wall (left) and around lug (right)

Results from lug wall

Figure 49 shows the probed values from the nodes found in the path through the lug wall. Note that the direction of probing is from the inner hole to the outside, meaning that the highest stress is closes to the lug-hole.

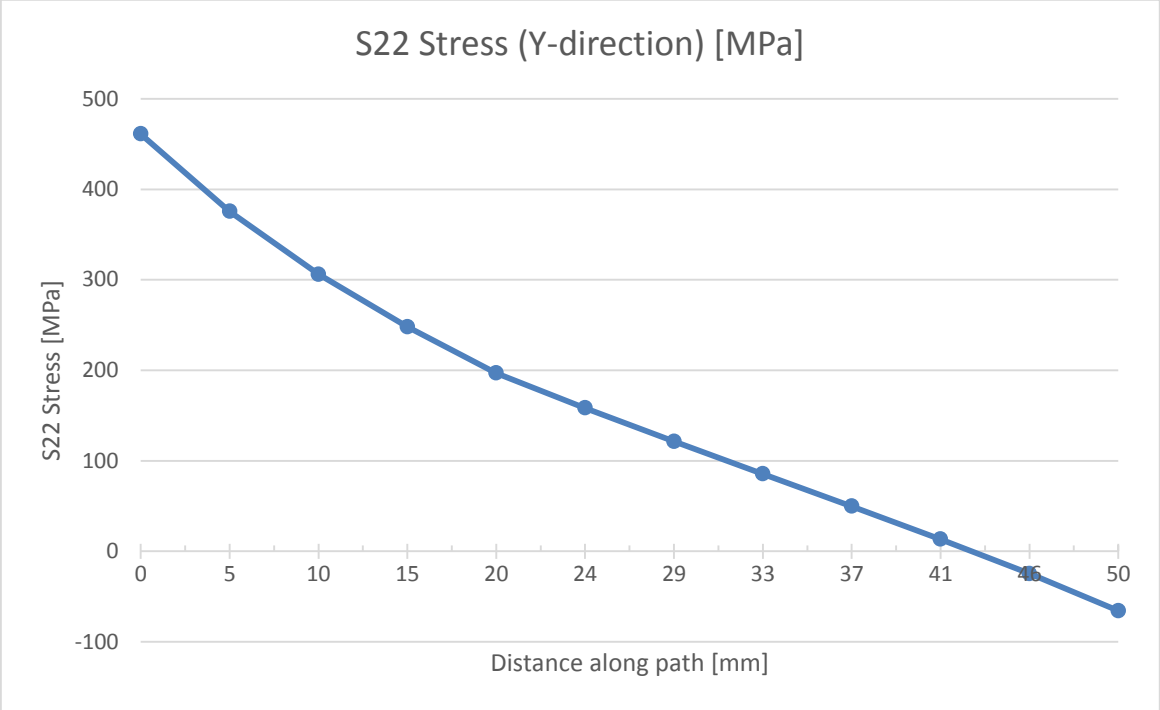

Figure 49: Probed S22 stress along path

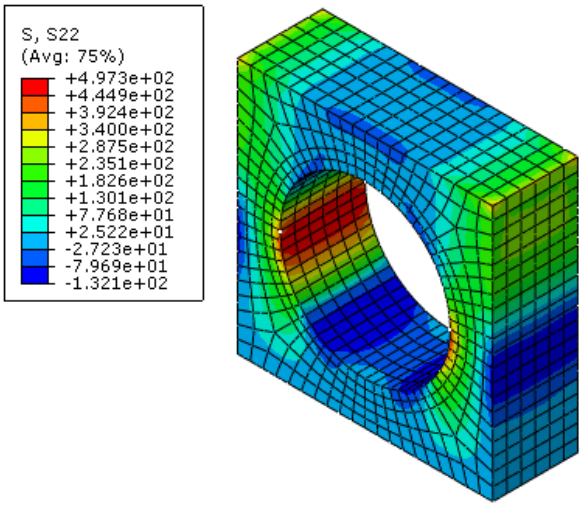

Figure 50: S22 stress of lug part

Results from lug hole

Mainly principal stresses are investigated as these can be compared with a paper from Grant et al. where a similar study was performed on lugs. The Principal stress are as follows:

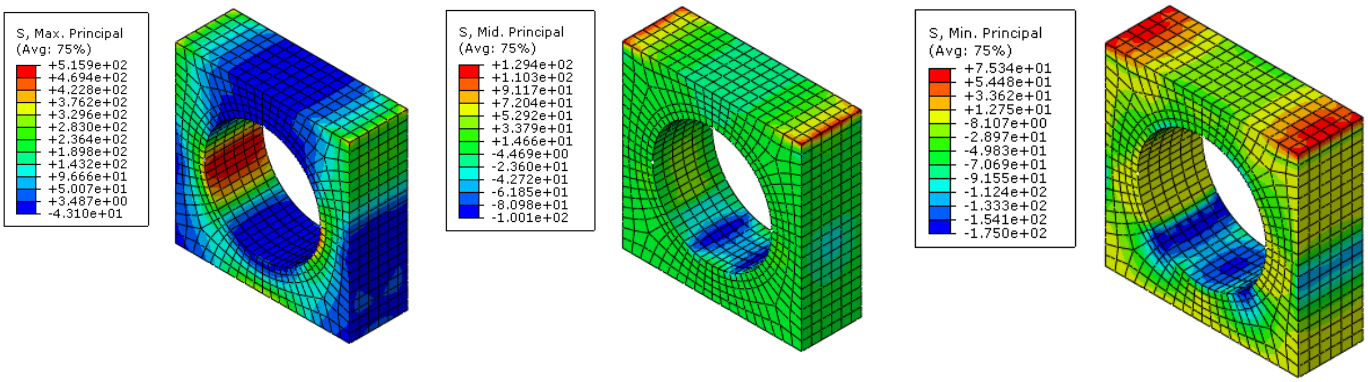

Figure 28: FE-analysis results, max-principal (left), mid-principal (middle), min-principal (right)

By combining the results along the path in the lug hole, the following graph shows the principal stresses occurs.

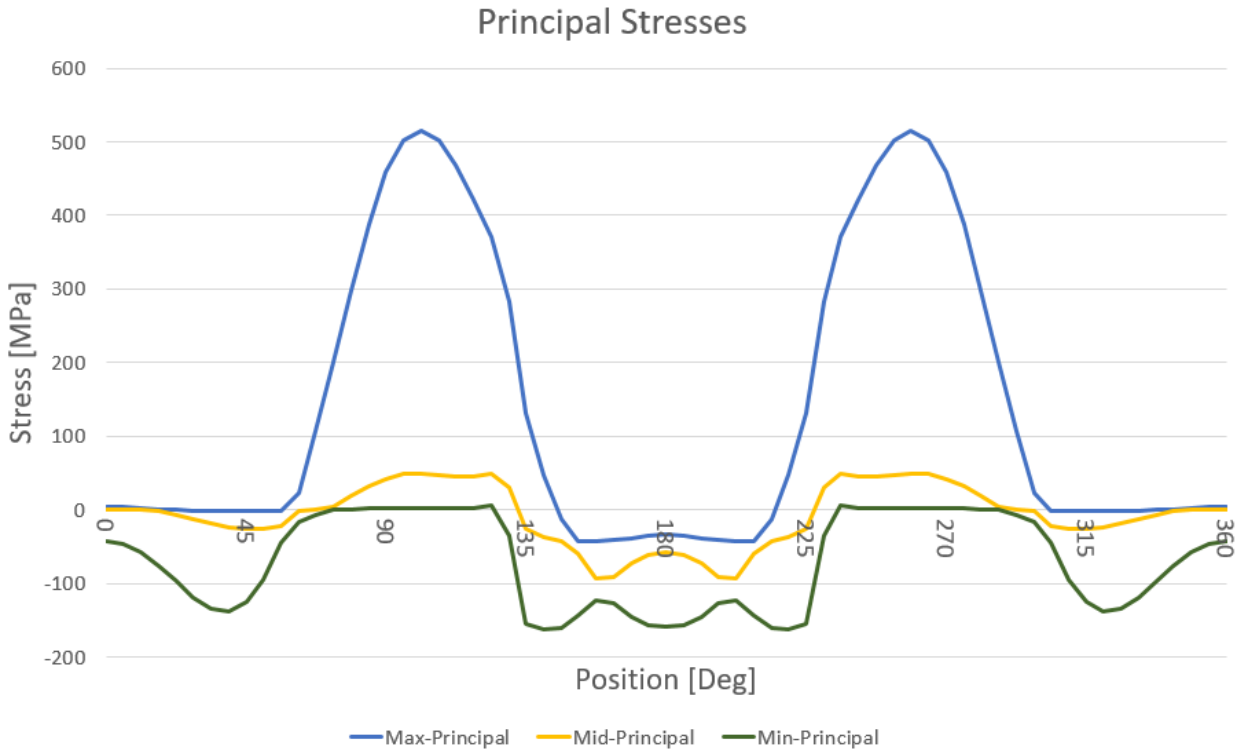

Figure 51: Principal stresses around lughole for clearance fit bearing

4.1.3.1 Verify Bearing Load Simulation

Verifying the bearing load is done by comparing the results from the FE-analysis with hand calculations and papers.

The hand calculation is simplified using formula for axial loading.

$$\sigma = \frac{F}{A}$$

Equation 18: Axial Loading

Where:

$\sigma = Axial\ Stress$

$F = Force$

$A = Area$

The geometry of the lug hole is simplified, and only the area which is left in the middle of the lug is taken into consideration, as this would give highest axial stress. The calculation gave the following results:

Hand calculations axial-stress y-direction		
Force	1.60×10^6	N
Direction	6 o'clock	
Width	50	mm
Depth	100	mm
Area	5000	mm^2
Total Area	10000	mm^2
Mean Stress (Y-direction)	**160**	**MPa**

Table 12: Results hand calculations axial stress

Results from the lug hole gave the graph as shown in Figure 49. By integrating the graph finding area under the curve the mean stress is found. For integration the slice sample method or

rectangle method is used using the midpoint approximation between each x-position point and the curve to find the area under curve

Probed Values from Abaqus		
X-position	**S22 [MPa]**	**Area (Slice sampled)**
0.0	461.1	2091.7
5.0	375.5	1704.1
10.0	306.1	1385.3
15.0	248.0	1112.4
20.0	197.0	761.3
24.3	158.3	599.1
28.6	121.3	443.0
32.9	85.5	289.8
37.1	49.8	135.3
41.4	13.4	-24.5
45.7	-24.8	-194.0
50.0	-65.7	-328.6
	Sum [N/mm]	7974.9
	Mean Stress [MPa]	**159.5**

Table 13: Probed values lug hole wall S22 (Y-direction)

The hand calculations gave a result of 160MPa for the mean stress. Average from integrated probed values gave 159.5 MPa. This is a deviation of 0.0625%.

Circumferential stress verification

Grant et al. [30] study on pin loaded lug shows that for a clearance fit pin under load the circumferential stress around the lughole is highest around position 75deg from bottom (6o'clock position) where the load is applied. This is illustrated in from the study [30].

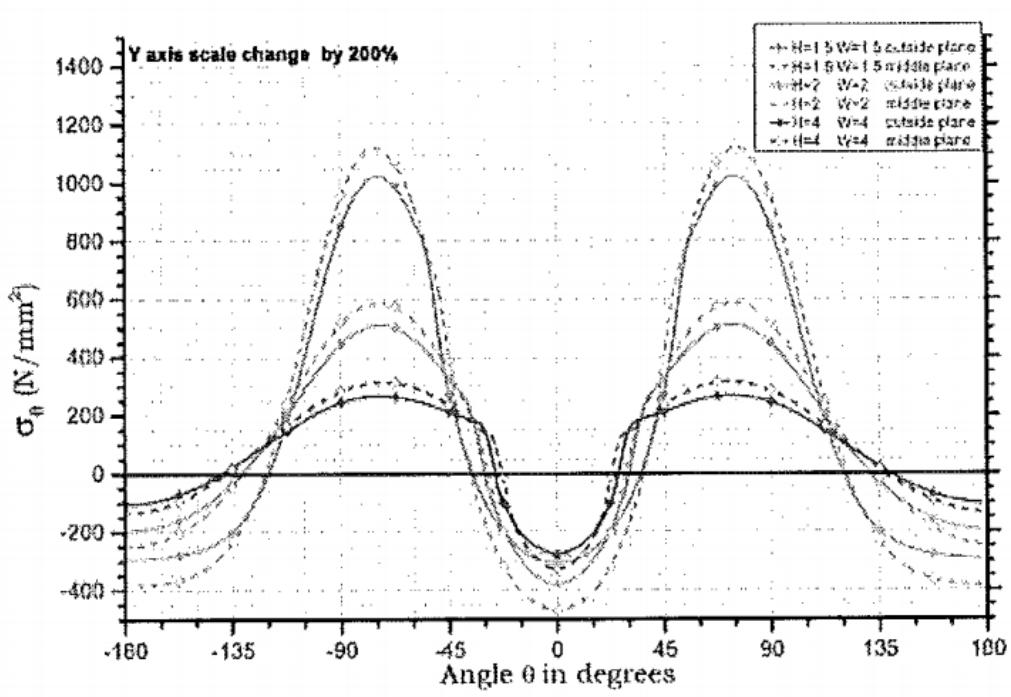

Figure 52: Grant et al. circumferential stress around clearance fit lughole

The position of highest circumferential stress on Figure 51 is in the same area as for the Grant et al. study.

4.2 Activity 2: Simplified Model Results

Simplified model results shows that all mechanisms works together without failing. Highest max principal stresses is in the bolts, with a pre tension stress of around 850 MPa according to Figure 54.

Mises stresses

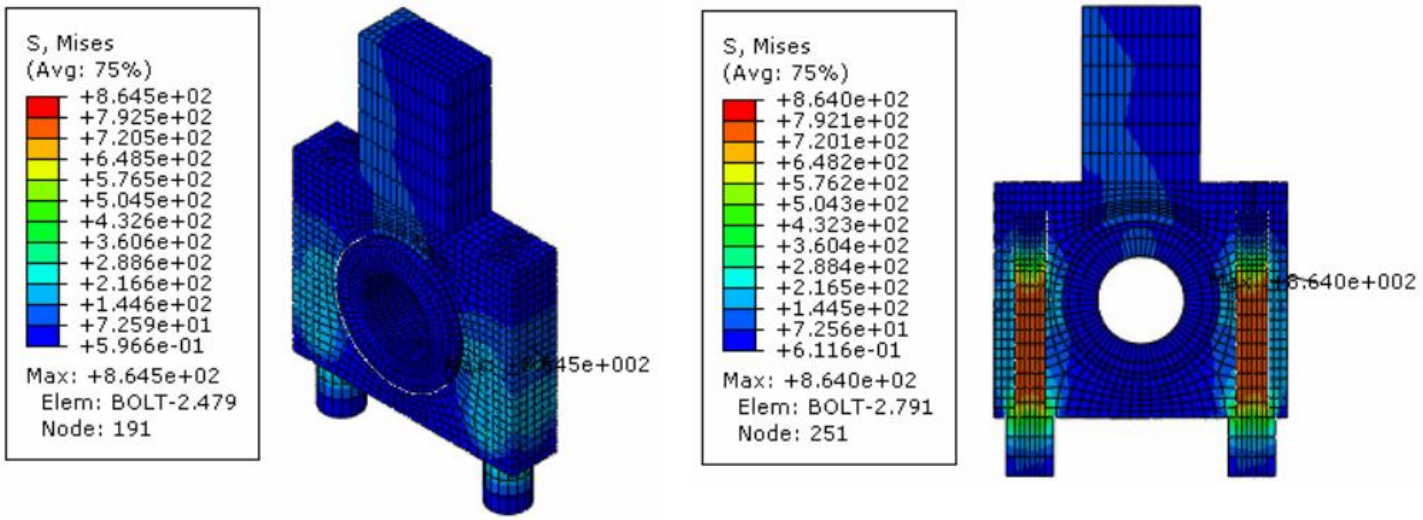

Figure 53: Simplified model mises stresses

Principal stresses

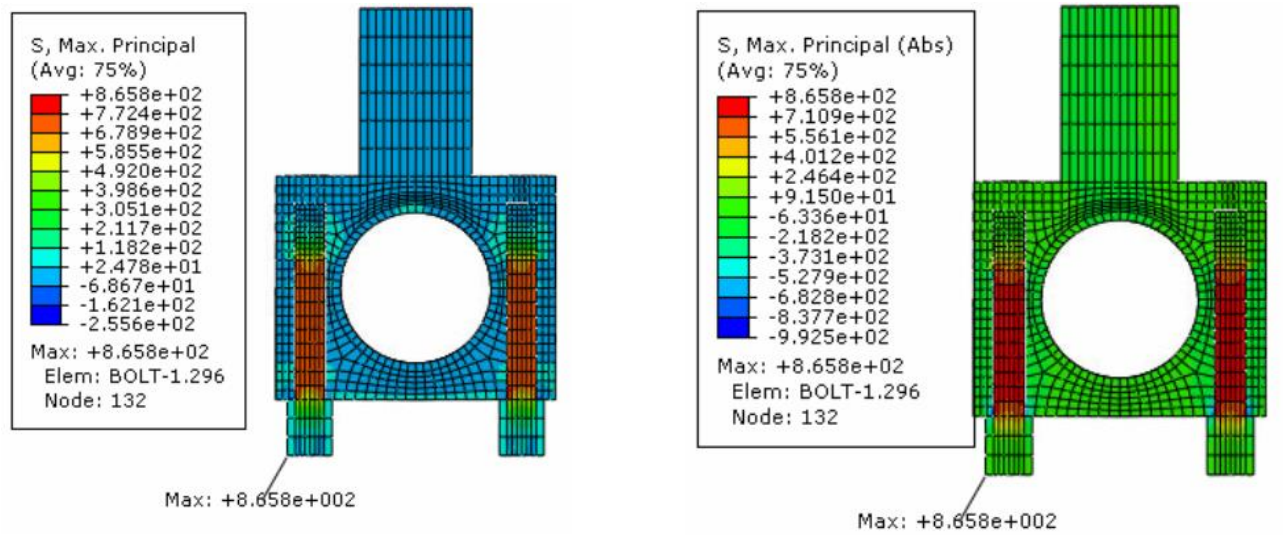

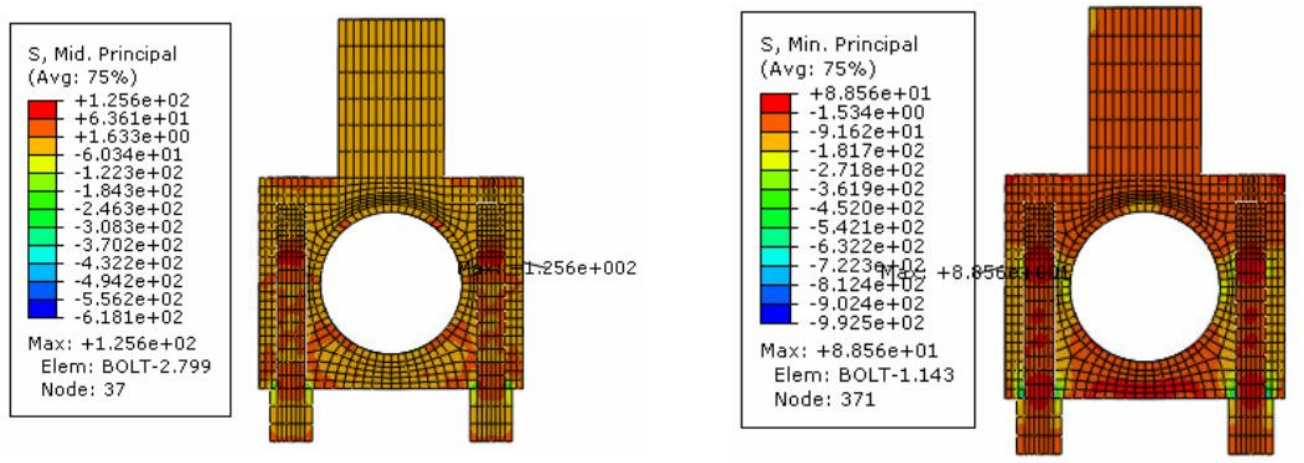

Figure 54: Simplified model, Principal stresses (4 figures)

Bearing Load Distribution

The bearing load pressure is distributed evenly in to the connection rod as seen in Figure 55. The stress is in the range of approx. 0 to 110 MPa.

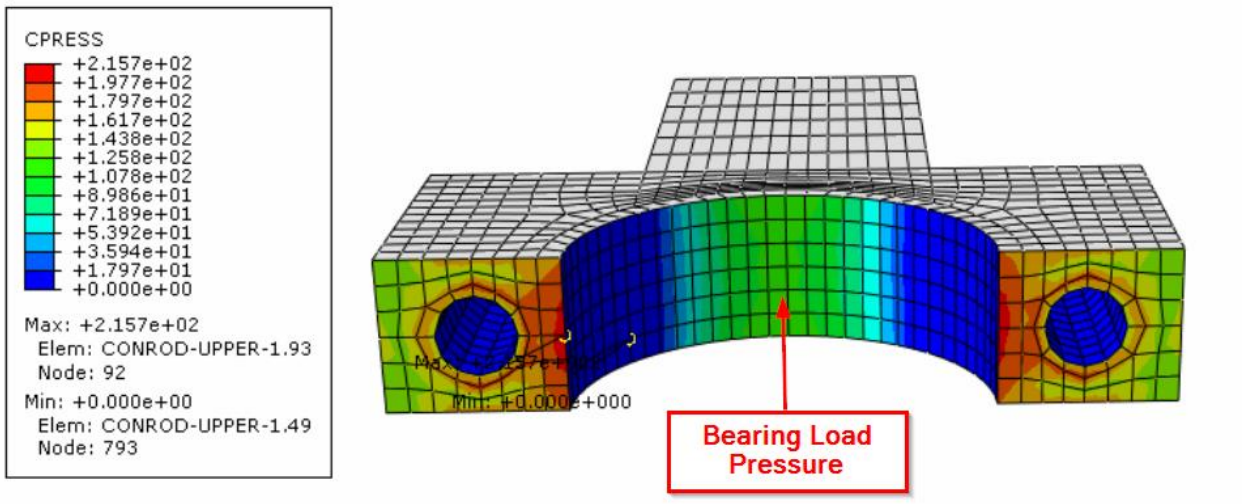

Figure 55: Bearing load pressure distribution

4.2.1 Verification Simplified Model Results

Maximum principal stress result shows stress around 850 MPa for the bolt. Hand calculations on pre-tensioned bolt strength according to Table 10 gives 820 MPa, which is within the same ballpark estimate.

The bearing load stress from Figure 55 of approx. 110 MPa is within the same range as for Figure 44 at an average of approx. 120 MPa.

4.3 Mesh Sensitivity Analysis Realistic Model

For knowing how many C3D20R elements is needed to produce valid results, a mesh sensitivity study is performed. The aim of the study is to find a mesh size which produce correct results but without using to many elements as this increase calculation time. The study uses maximum mises stress and is set up with approx. average elements size from 50mm to 2.5 mm. The results show that the curve is converging around 2100MPa for elements smaller than 5mm. This gives a mesh consisting of 21289 elements for one bolt. Due to the high number of elements and observation that the highest stresses in start of thread section, bias meshing is used for saving computer power and keeping result quality of the area.

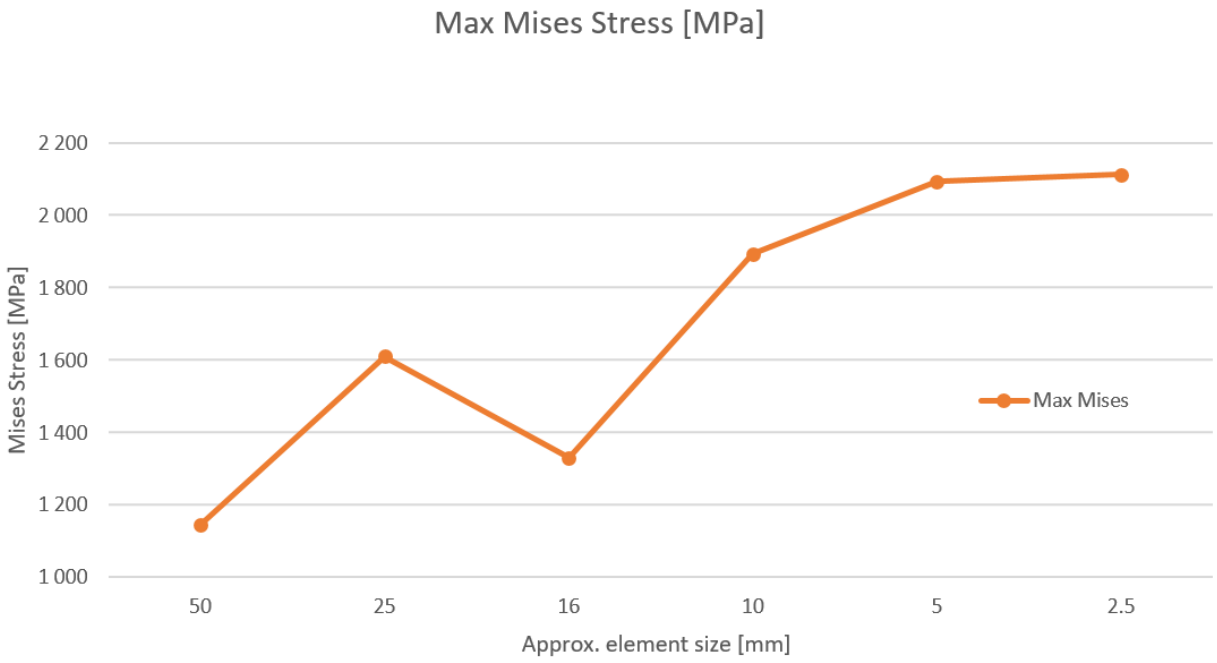

Figure 56: Max mises stress and element size

4.4 Activity 3: Realistic Model Results

Realistic model consist of 11 simulations from different snapshots during the power stroke. The realistic model is representing a global model. The 11 simulations is performed for finding the change in stress, which can be used for fatigue analysis. For finding the most vulnerable areas in the global geometry, the simulation after 10deg TDC is used as basis as this contains the highest forces.

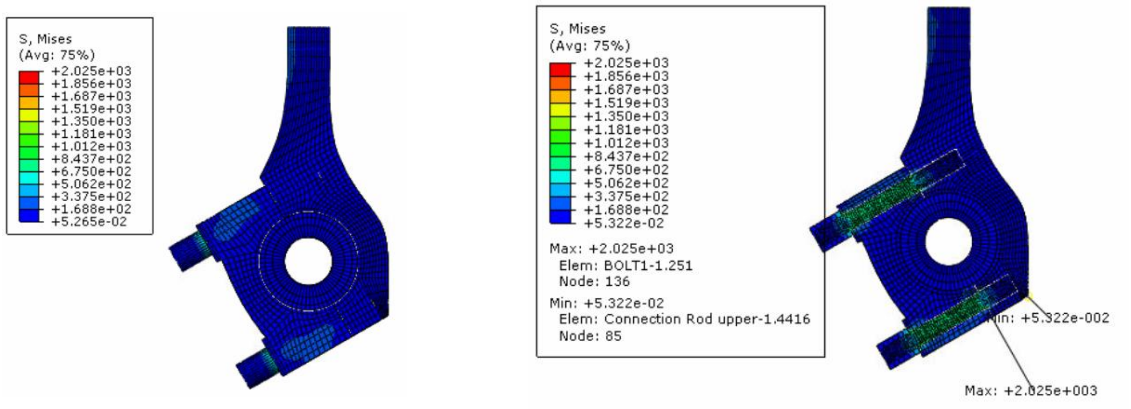

Figure 57: Realistic model, mises stress

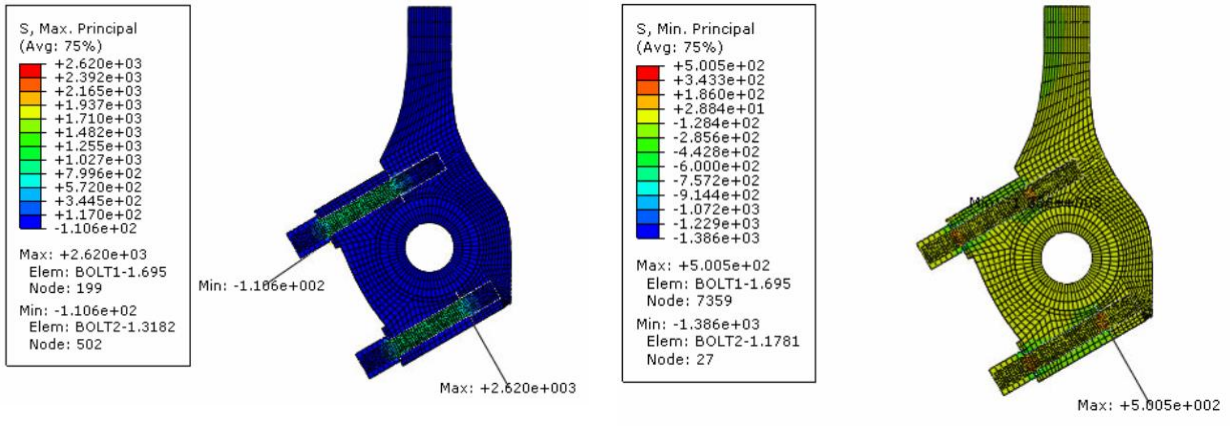

Figure 58: Realistic model, Max and min principal stress

Both max mises stress and principal stress is highest in bolt 2, as seen in Figure 57 and Figure 58. By inspecting these bolts further (see figure Figure 59 and Figure 60), it is clear that the highest principal stress is in the area where the thread starts. The stress around the thread edge is in the range from 2000 – 2600MPa. This is way above the yield limit for any steels meaning plastic deformation occurs. It is also way above the ultimate tensile strength for steels. The max principal stress in the bolt rod (green area) is around 820MPa.

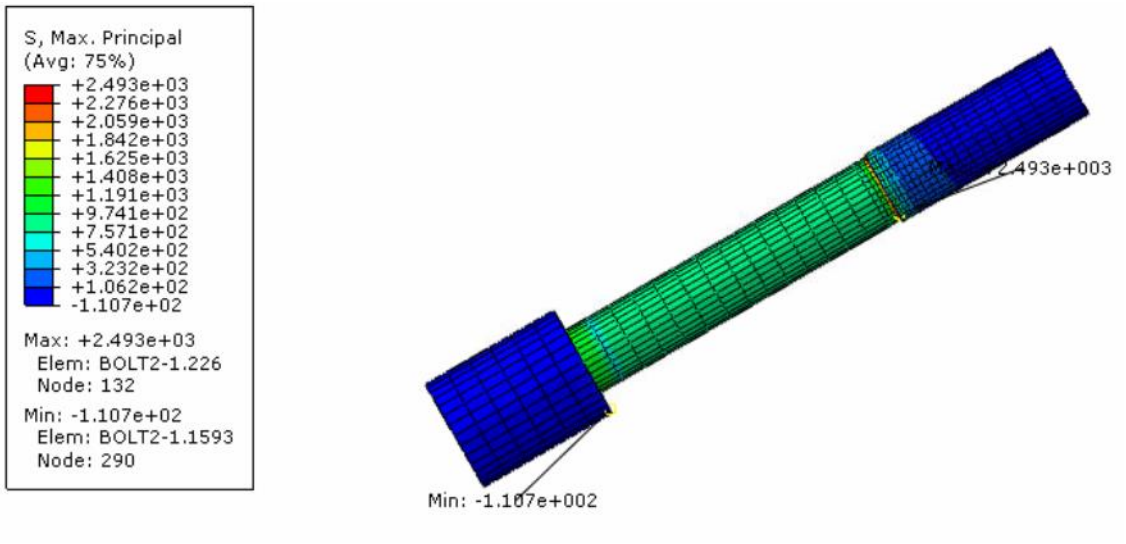

Figure 59: Max Principal stress bolt 1

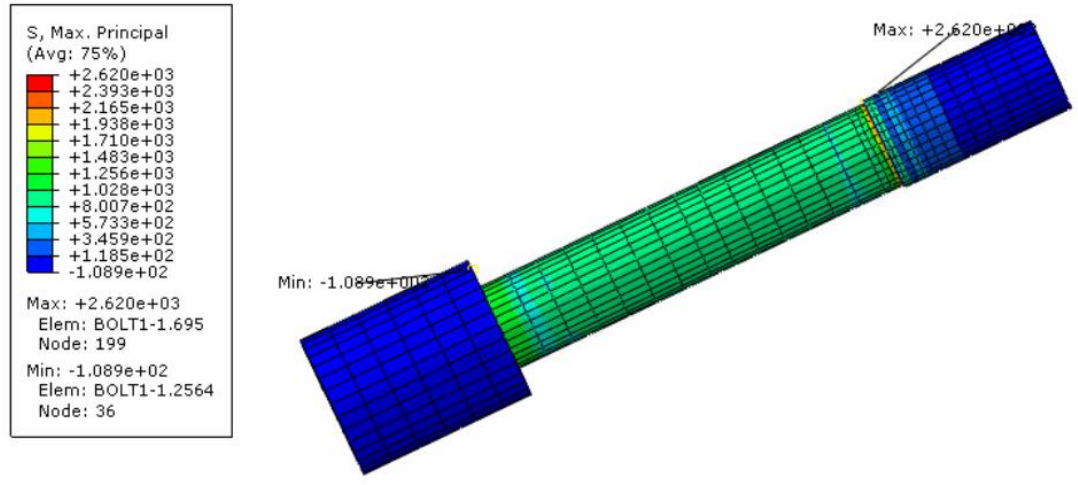

Figure 60: Max Principal stress bolt 2

4.4.1 Circumferential bolt stress analysis

Circumferential path around the high stressed thread section is defined for comparing the stress distribution for the 11 simulations at the top of the threads. This is illustrated in Figure 61. The results from the simulations is showed in Figure 62 and Figure 64.

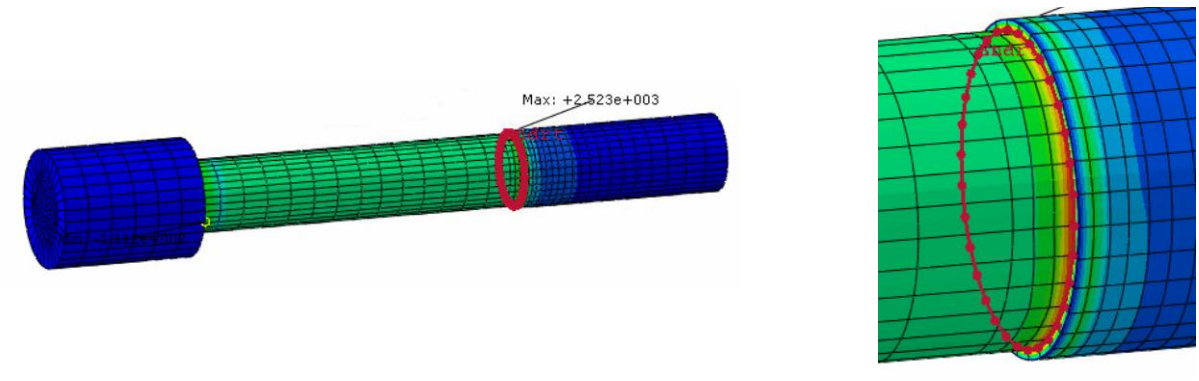

Figure 61: Circumferential path around first thread

4.4.1.1 Bolt 1 Results:

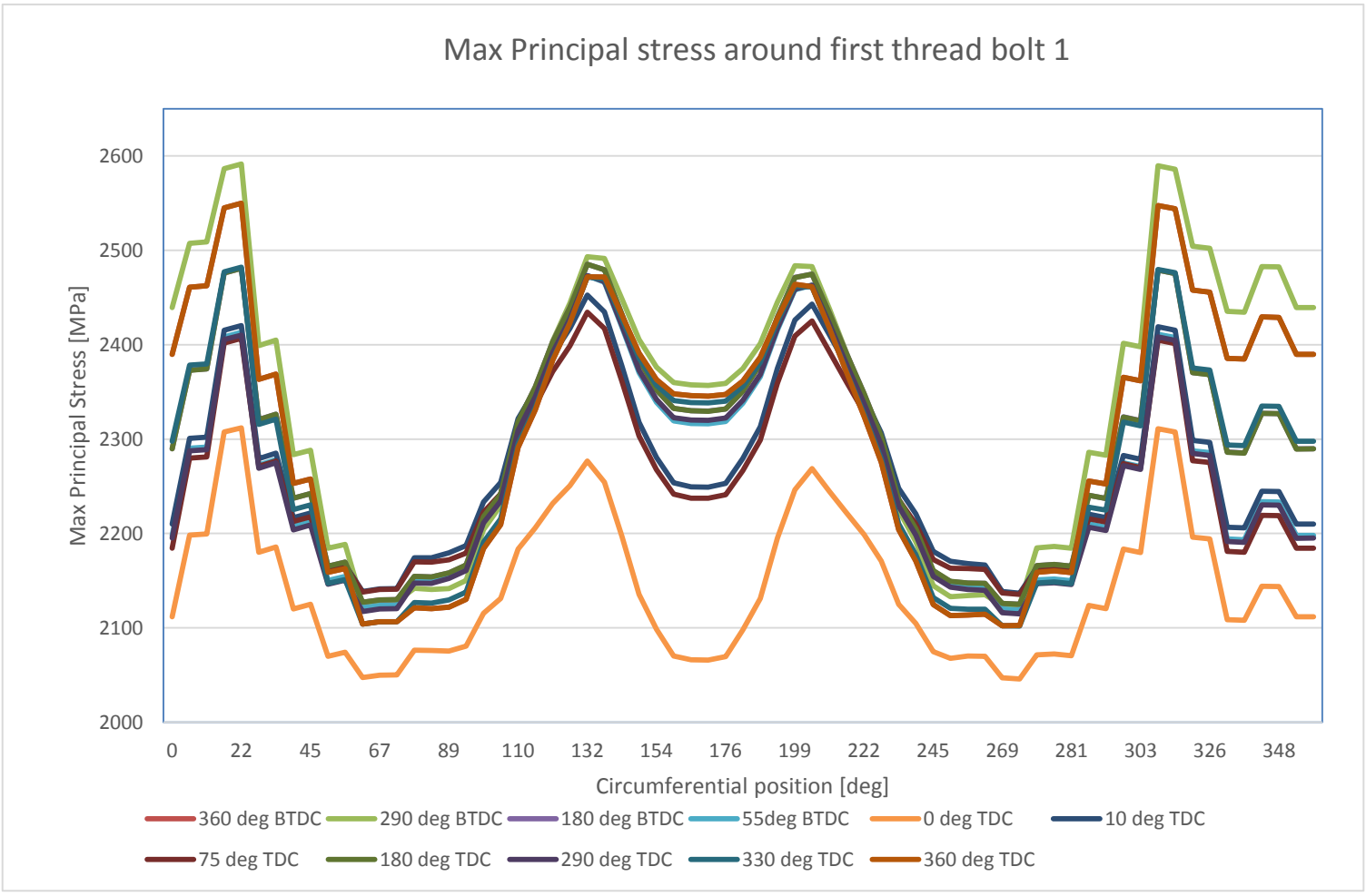

Figure 62: Max Principal stress around first thread bolt 1

Figure 62 shows the maximum principal stress around the thread section for bolt 1.

The highest change in stress is between “290 deg BTDC” simulation and “0 deg TDC” with change in max principal stress of 338.8 MPa. This is at point “348 deg” on the circumference around the thread.

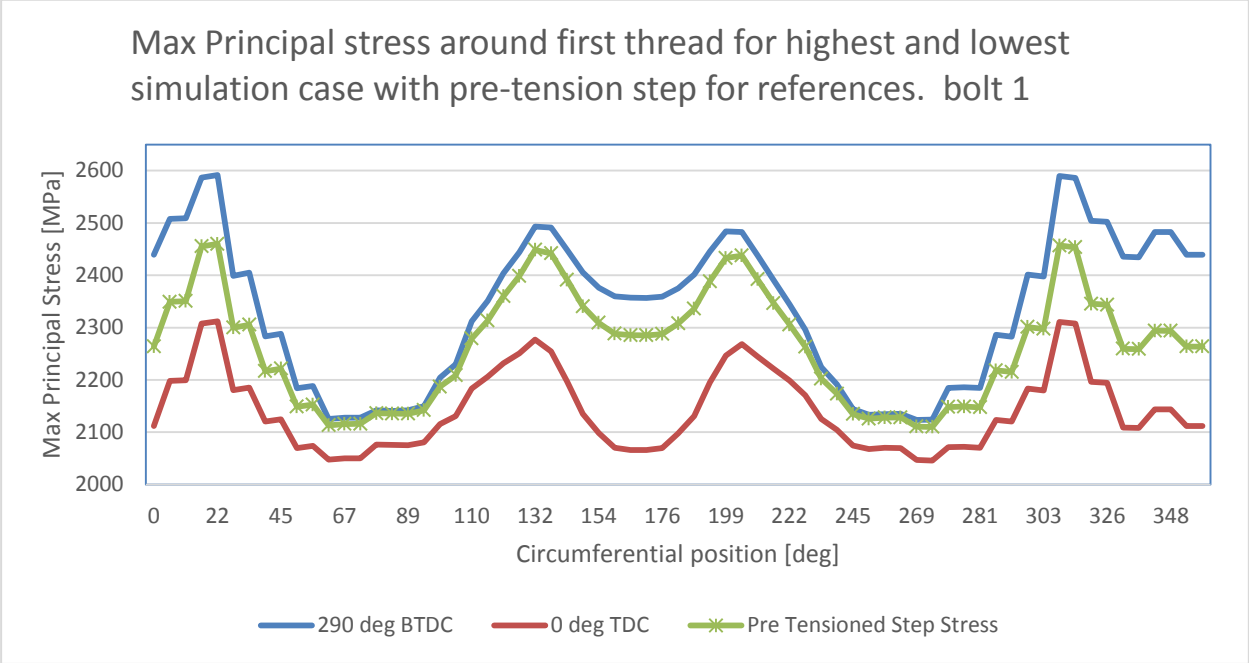

Figure 63: Max Principal stress high, low and pre tension, bolt 1

Figure 63 shows max principal stress for the circumference around the thread for bolt 1 in compare with pre-tension stress on the bolt. Note that the pre-tension stress is located between the highest and lowest simulation cases.

4.4.1.2 Bolt 2 results:

Figure 64 shows the maximum principal stress around the thread section for bolt 2. The highest change in stress is between “55 deg BTDC” simulation and “0 deg TDC” with change in max principal stress of 174.6 MPa. This is at point “231 deg” on the circumference around the thread.

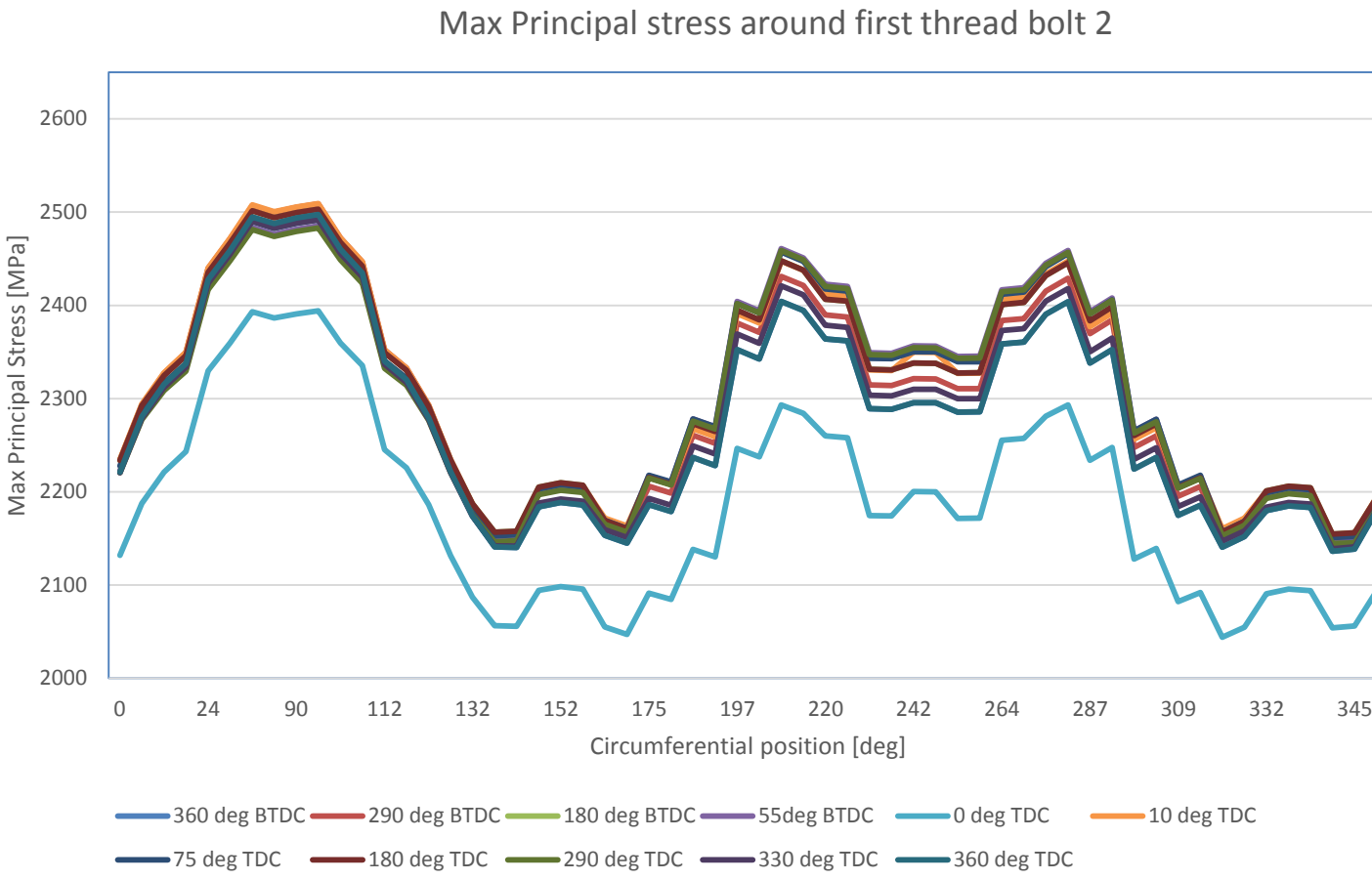

Figure 64: Max Principal stress around thread section bolt 2

Figure 65 shows max principal stress for the circumference around the thread for bolt 2 in compare with pre-tension stress on the bolt. Again the pre-tension stress is located between the highest and lowest stress simulation cases.

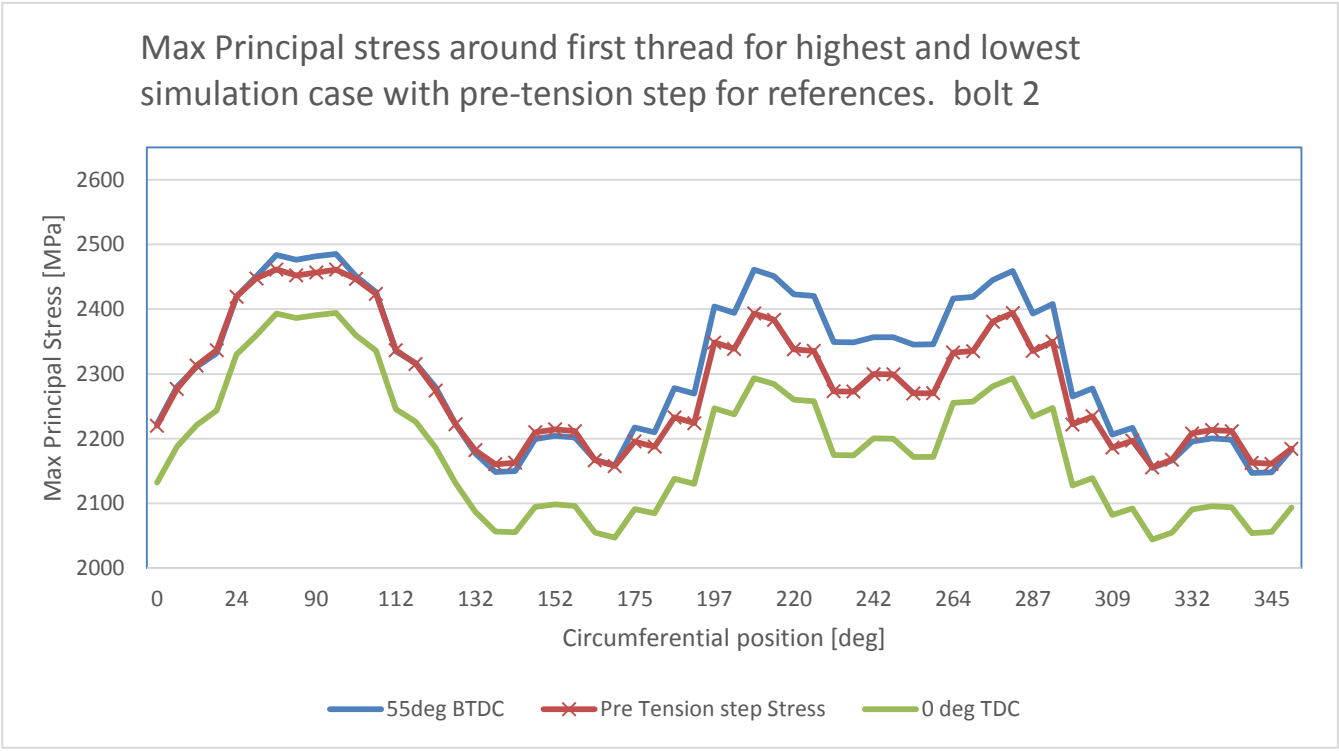

Figure 65: Max Principal stress high, low and pre tension, bolt 2

4.4.2 Longitudinal bolt stress analysis

This analysis is performed in the longitudinal direction along different paths of the threads for both bolts.

4.4.2.1 Bolt 1 results over notch path:

Figure 66, Figure 67 and Table 14 shows the max principal stress analysis over the notch for bolt 1. The path is running through the highest stressed point around the thread section for case "290deg BTDC". The results shows notch effect giving high max principal stresses up to approx. 2498 MPa. Lowest principal stress in this point during the "0 deg TDC" case gives 2153 MPa. This gives a cyclic difference of 344 MPa through the stroke. Note that the results at position 12 gives low stresses compared to surrounding.

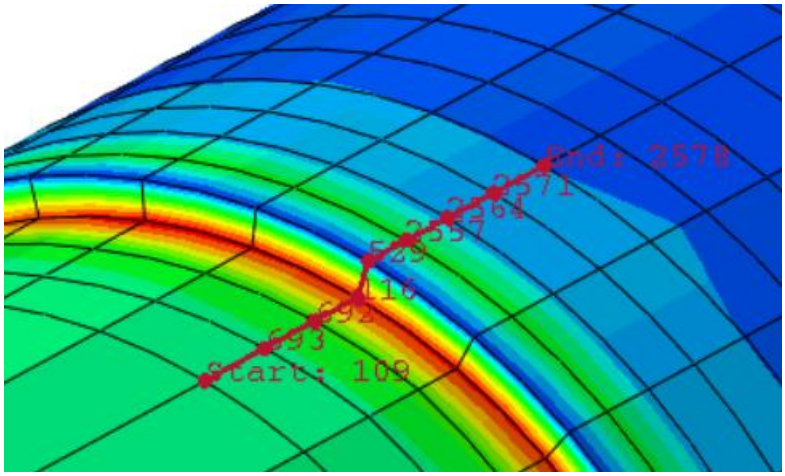

Figure 66: Path for longitudinal stress analysis bolt 1

Longitudinal stress bolt 1				
Position [mm]	**290 deg BTDC [MPa]**	**Pre Tensioned Step Stress [MPa]**	**0 deg TDC [MPa]**	**Delta Principal Stress [MPa]**
0.0	859	850	842	17
3.9	966	958	938	28
7.2	1 332	1 312	1 256	76
10.0	2 498	2 309	2 153	344
11.6	165	-35	7	158
14.1	1 176	1 120	988	188
16.9	429	409	362	67
19.9	412	328	346	65
23.2	348	309	303	45

Table 14: Longitudinal stress bolt 1

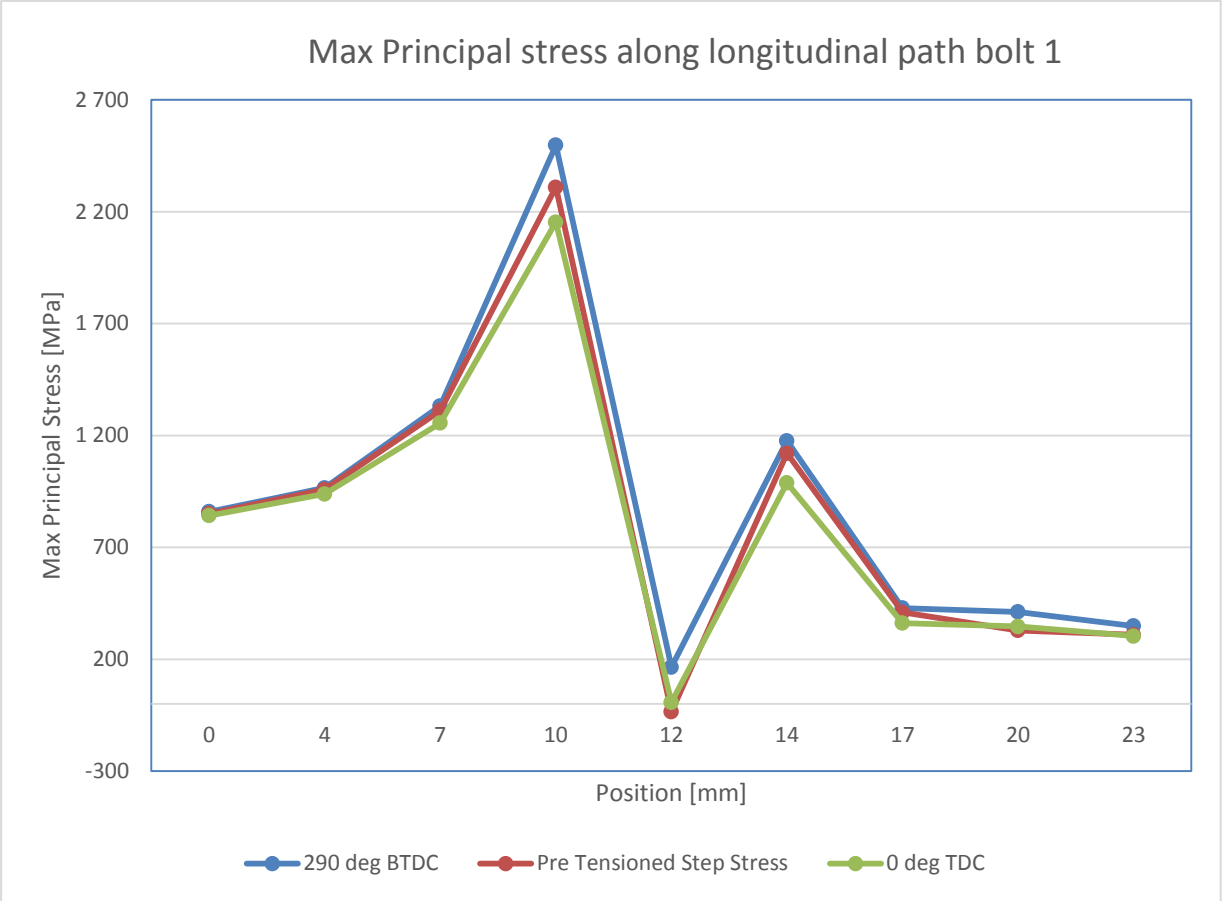

Figure 67: Max Principal stress along longitudinal path bolt 1

4.4.2.2 Bolt 1 results along thread:

The following analysis shows the stress along the thread section for bolt 1, see Figure 68, Figure 69 and Figure 70. The figures illustrates the load case with the highest local stress "290deg BTDC". These results shows high stress along the first 3, 4 mm along the path with peak stress at the 2 mm position. The stress rate decreases smoothly after 5 and 6 mm position until the end of the thread section.

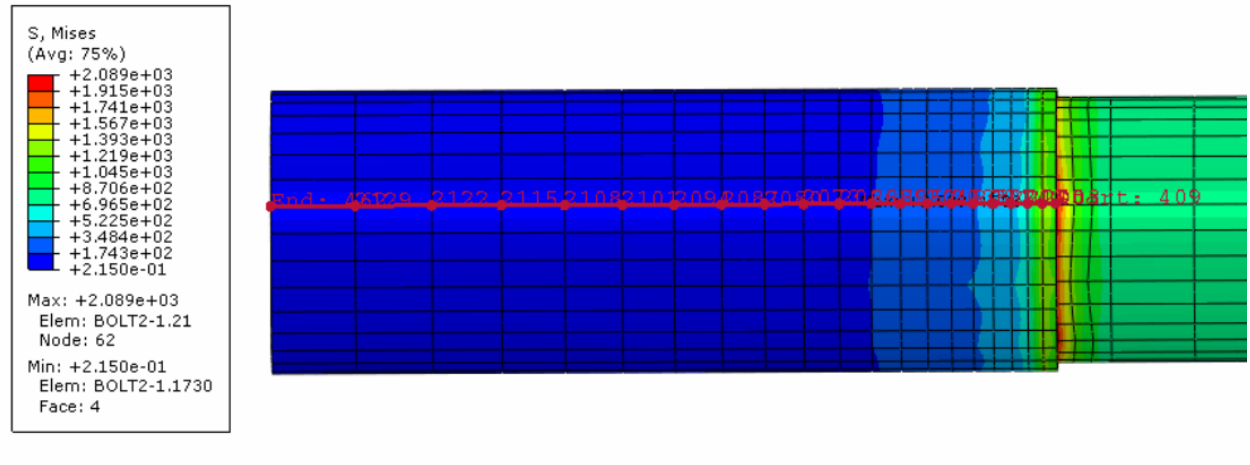

Figure 68: Path and mises stress along thread section bolt 1

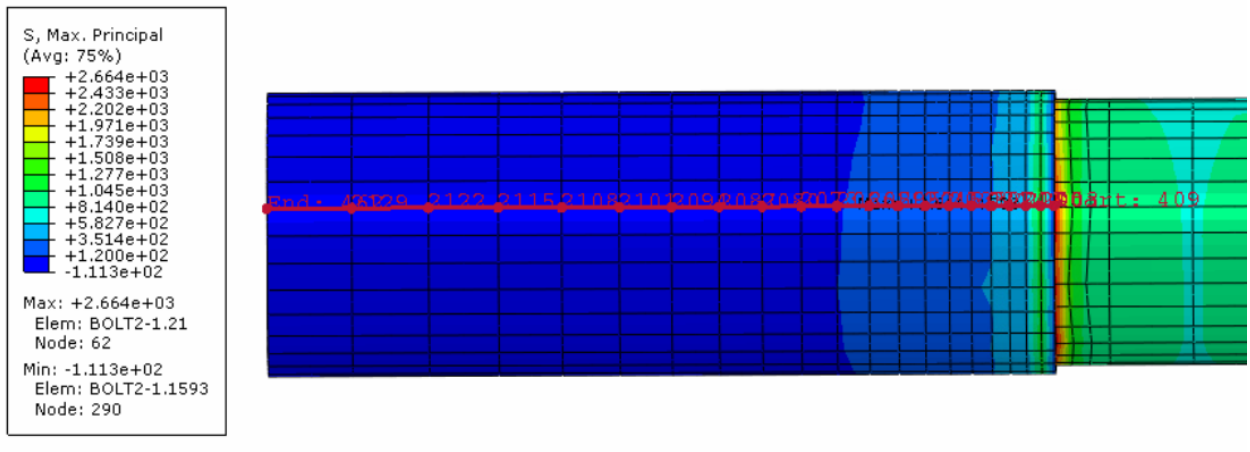

Figure 69: Path and max Principal stress along thread section bolt 1

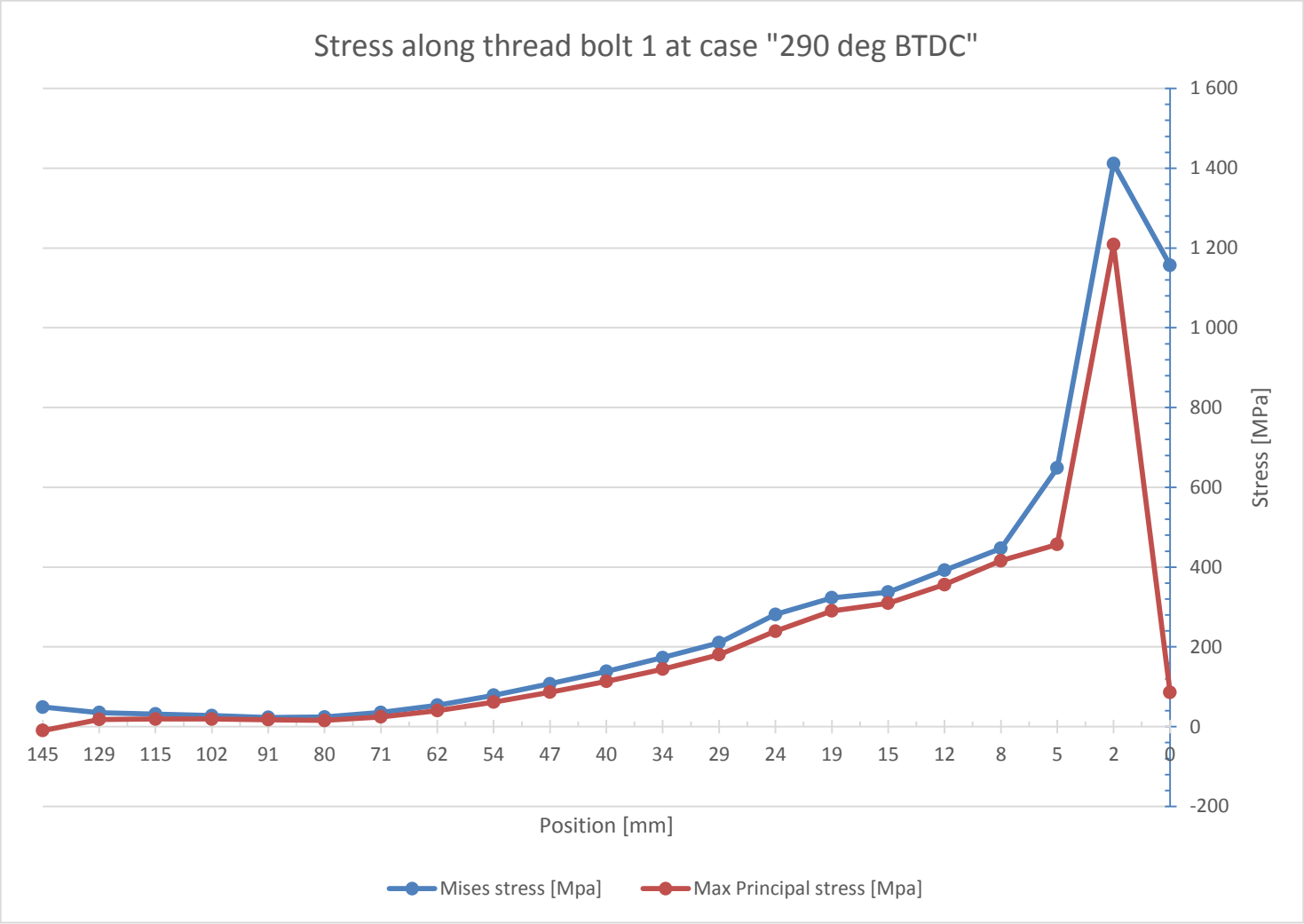

Figure 70: Stress along threads bolts 1

4.4.2.3 Bolt 2 results over notch path:

Table 15, Figure 71 and

Figure 72 shows the max principal stress analysis over the notch for bolt 2. The path is running through the highest stressed point around the thread section for case “55 deg BTDC”. The results shows notch effect giving high max principal stresses up to 2592 MPa at position 10.0mm. Lowest principal stress in this point during the “0 deg TDC” case gives 2491 MPa. This gives a cyclic difference of 100 MPa through the stroke. Note that the results at position 11.6 gives low stresses compared to surrounding stresses.

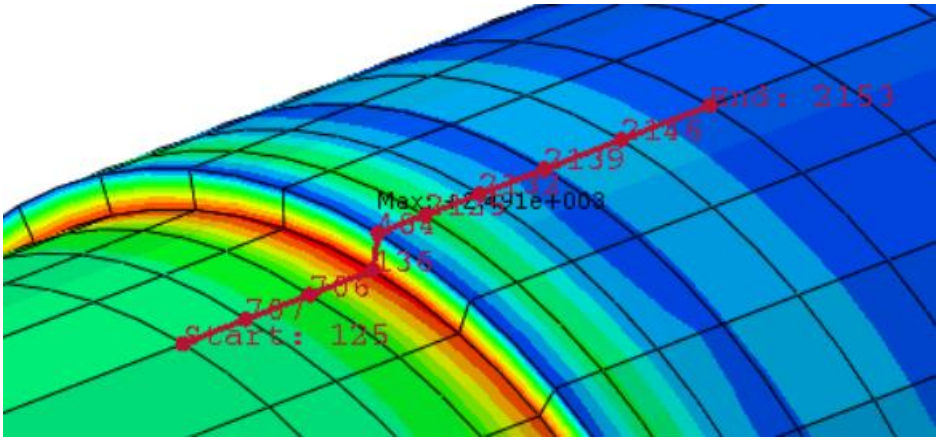

Figure 71: Longitudinal path bolt 2

Longitudinal max principal stress bolt 2				
Position [mm]	**55 deg BTDC [MPa]**	**Pre Tensioned Step Stress [MPa]**	**0 deg TDC [MPa]**	**Delta Principal Stress [MPa]**
0.0	821	837	830	-8
3.3	896	913	900	-5
6.7	1 053	1 071	1 049	5
10.0	2 592	2 580	2 491	100
11.6	149	35	121	28
14.1	1 114	1 098	1 063	51
17.0	377	369	373	3
20.5	300	294	309	-9
24.5	472	466	468	4
29.2	263	259	272	-9

Table 15 Longitudinal max principal stress bolt 2

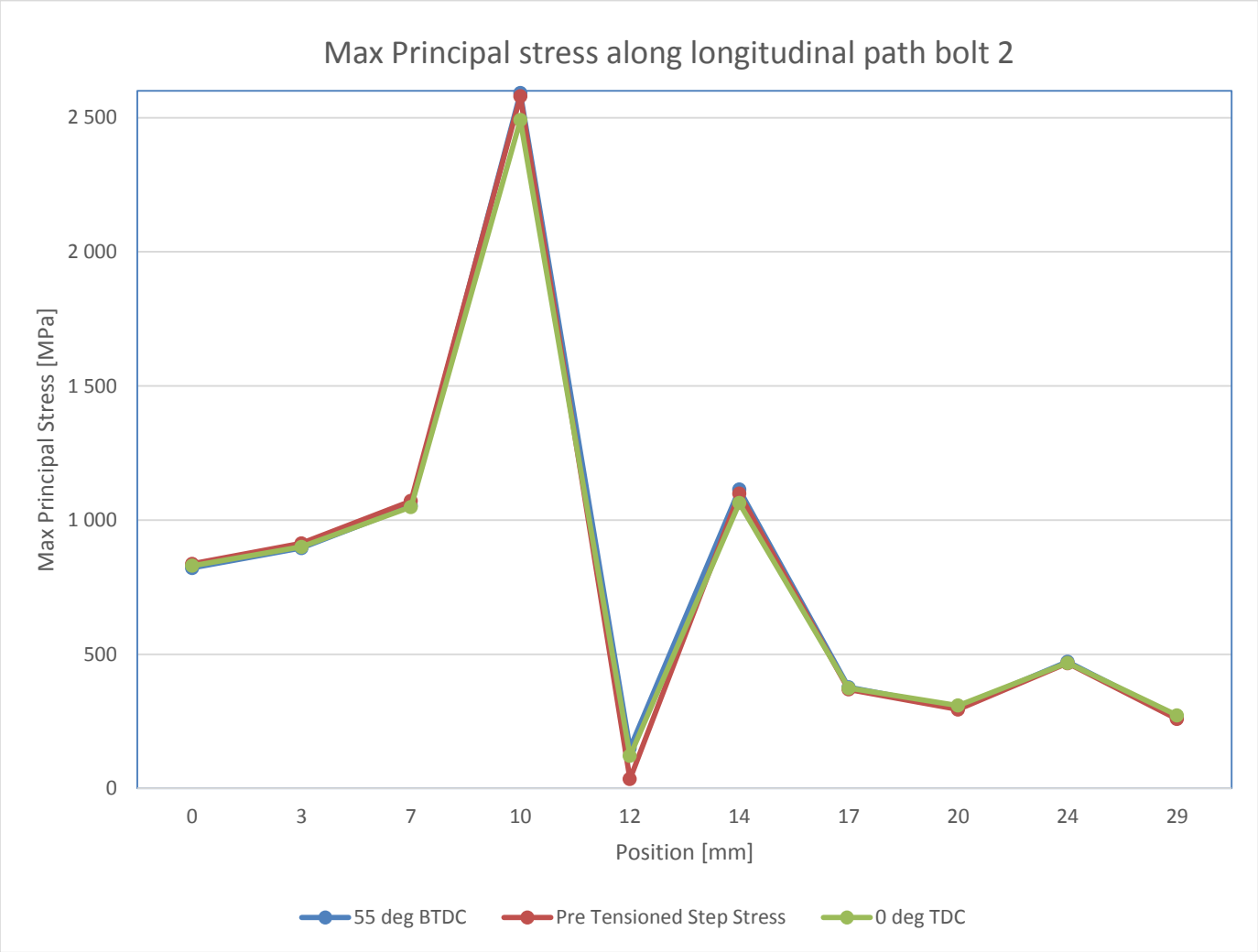

Figure 72: Max Principal stress along longitudinal path bolt 2

4.4.2.4 Bolt 2 results along thread:

The following analysis shows the stress along the thread section for bolt 2, see Figure 73, Figure 74 and Figure 75. The figures illustrates the load case with the highest local stress “55 deg BTDC”. These results shows stress peak at position 2 mm at 1080 MPa for max principal stress and 1200 MPa for mises stress. The stress decrease smoothly throughout the threads with a sudden increase at position 13 mm.

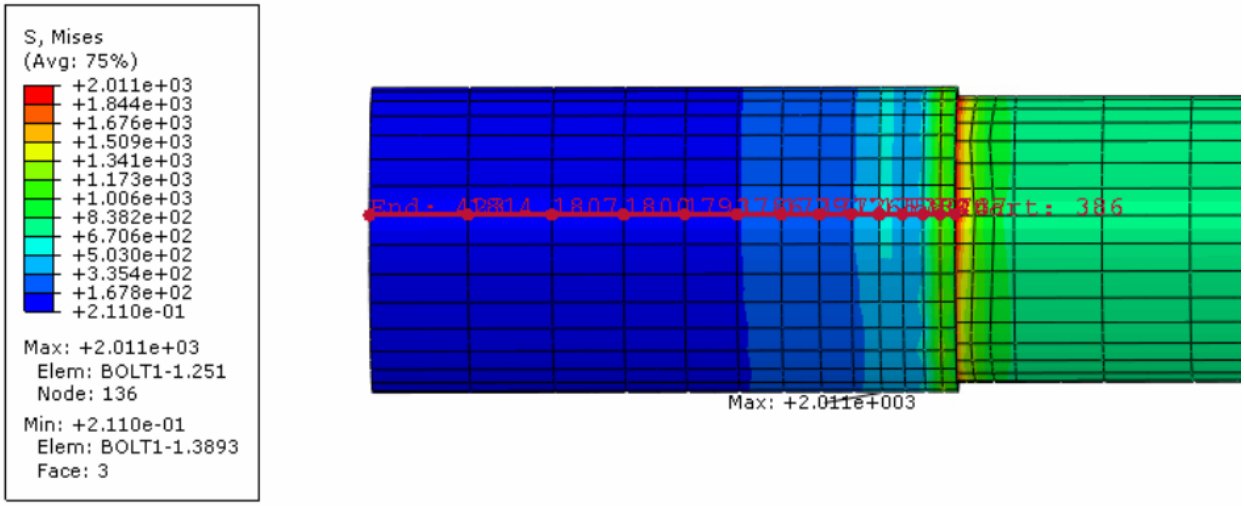

Figure 73: Path and mises stress along thread section bolt 2

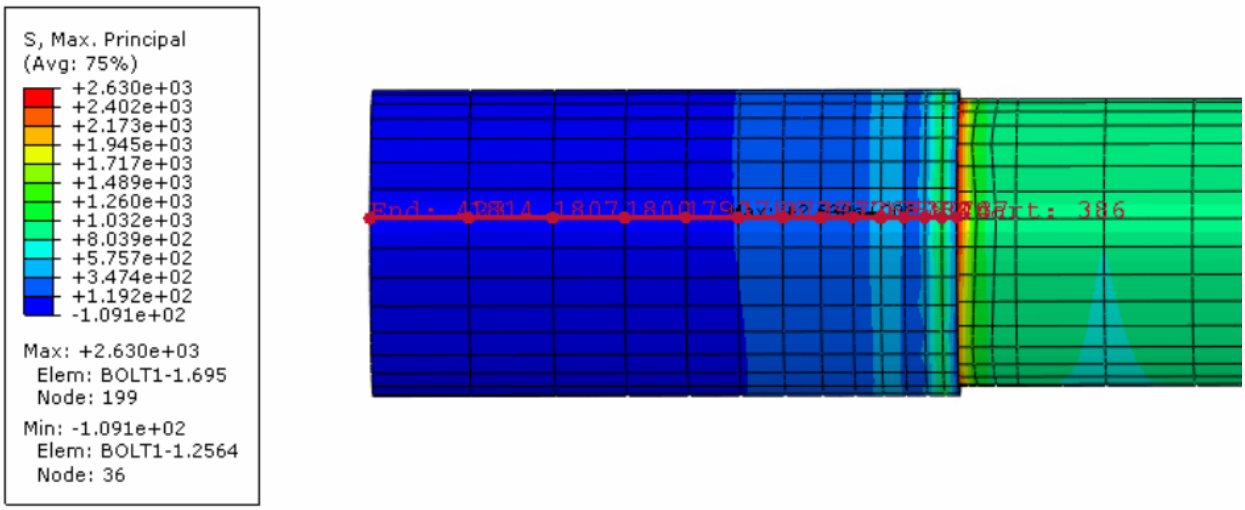

Figure 74: Path and max principal stress along thread section bolt 2

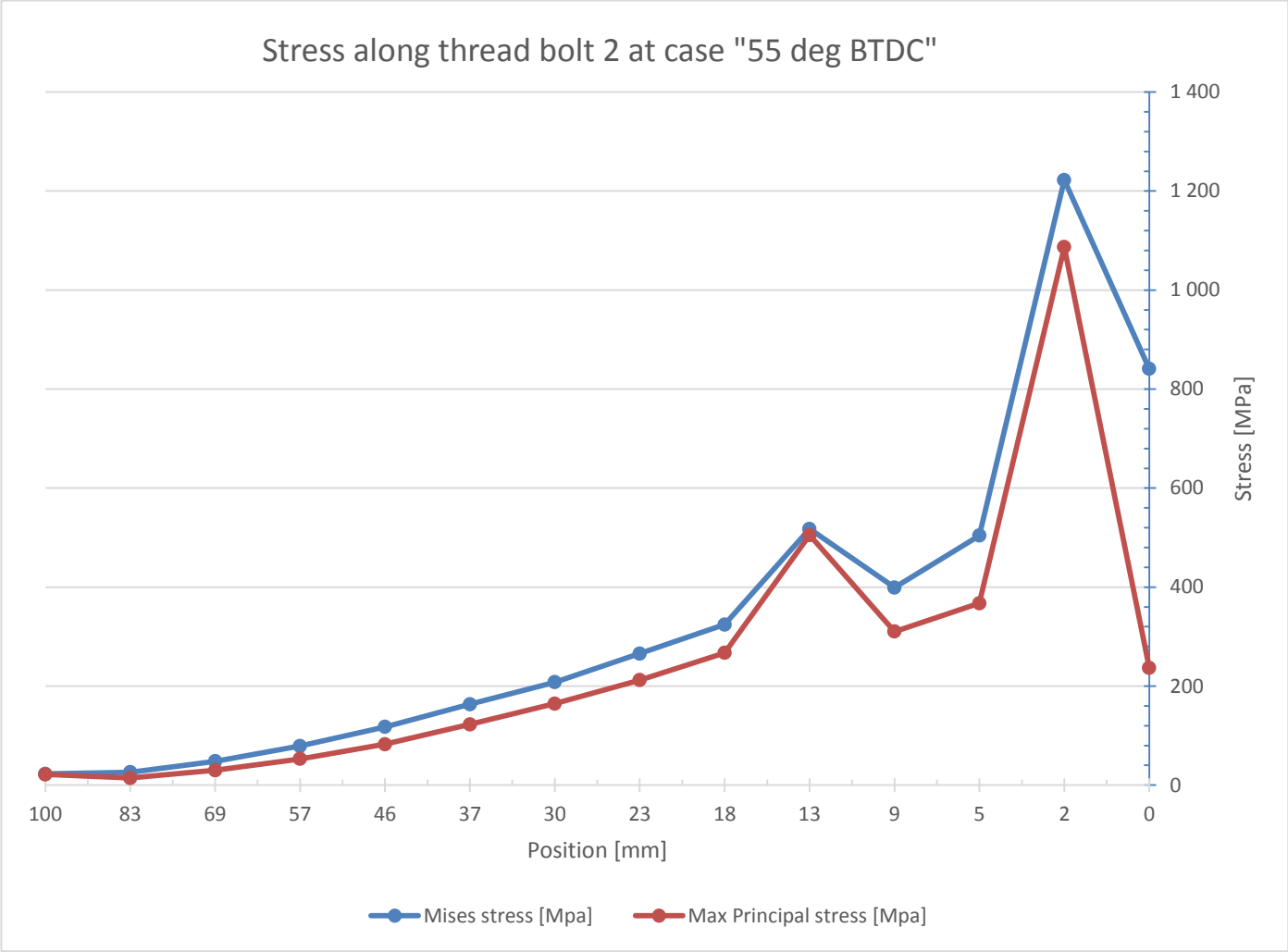

Figure 75: Stress along threads bolts 2

4.5 Activity 6: Verify Realistic Model Results

Pre-tension of bolts gives stress in the rod part of the bolts around 810-830 MPa depending on load case and bolt 1 and 2. Compared with simplified model results in Figure 54 giving max principal stress in the bolt rod of approx. 820 MPa, and Table 10 giving 824 MPa, this is within the same range.

Notch effect is observed in the first thread for both bolts. This gives max principal stresses up to 2500 MPa for bolt 1, and 2600 MPa for bolt 2. Simple hand calculations using the method from chapter 2.9 and geometry data for M52 bolt gives following results:

Notch effect results		
Input	d [mm]	48.8
	d [mm]	52.0
	σ ref [MPa]	820
	r [mm] (Assumed)	0.1
Calculations	D/d	1.0656
	r/d	0.0020
	Interpolated B	1.0006
	Interpolated a	-0.1794
	Kt	3.0379
	σ Max [MPa]	2 491

Table 16: Notch effect results for assumed r-value

Hand calculations in Table 16 gives stress in the area of 2500 MPa. This is within the same ballpark figure as the simulation results. Note that this result is with small assumed filet radius of 0.1 mm. This is used as the model bolt geometry does not have any filet radius.

However for an M52 bolt, the round fillet in the bottom of the thread is R=0.722mm according to DIN13. This gives results as showed in Table 17

Notch effect results (r=0.72)		
Input	d [mm]	48.8
	D [mm]	52.0
	σ ref [MPa]	820
	r [mm]	0.72
Calculations	D/d	1.0656

	r/d	0.0148
	Interpolated B	1.0006
	Interpolated a	-0.1794
	K_t	2.1309
	σ Max [MPa]	1 747

Table 17: M52 notch results (r=0.72)

Stress distribution along threads gives for the realistic model high stress at the first thread, as seen in Figure 70 and Figure 75. It looks that the first thread takes up most of the forces. Figure 9 by Leyers [16] shows a more evenly distributed load.

4.6 Fatigue calculations

The starting of cracking is most likely to start at the point with highest maximum principal stress [26]. This thesis shows highest change in max principal stress (338.8 MPa) at point 348 deg around the first thread in bolt 1. The results of stress analysis is illustrated in Table 18

Stress analysis		
Max stress [MPa]	σ_{max}	2498
Min stress [MPa]	σ_{min}	2153
Stress range [Mpa]	σ_r	345
Alternating stress [Mpa]	σ_a	173
Mean stress [Mpa]	σ_m	2326
Stress ratio	R	0.86
Amplitude ratio	A	0.07

Table 18: Stress analysis

Calculation on the endurance limit given at alternating stress for 12.9 grade steel using method described in chapter 2.6.3 gives the following results as described in Table 19.

Endurance Limit Calculations Results	
Mean load F_m [MPa]	820
Yield strength [MPa]	1098
RTAHT	0.75
Endurance Limit σ_a [MPa]	**44**

Table 19: Endurance limit results

Note that the results from bolt 1 is above the endurance limit, meaning it will fail before 10^8 Cycles.

Predicting the fatigue life using Goodman Miner rule and Basquin law predicts fatigue failure for uncracked components. For this thesis results is not possible because the mean stress is higher than the tensile strength, giving error. However, if the mean stress is assumed to be 820 MPa as it is for the rod area, still holding stress range of 345 MPa, calculations can be performed, by assuming other properties as well. The calculations uses data from Table 19 for zero value (R=0) predictions. Table 20 shows the results with stress range at 345 MPa, resulting in half a cycle before fatigue failure. This is low cycle fatigue, or simply over stressing the component to failure. The Basquin law is not valid for low cycle fatigue.

Fatigue lifetime calculations		
Mean stress [MPa]	σ_m	820
Stress range [MPa]	σ_r	345
Tensile strength [MPa]	σ_{ts}	1220
Zero Mean Stress equivalent [MPa]	$\Delta\sigma_{\sigma_o}$	1052.25
Number of cycles at zero	N_{f1}	10^8
Stress range at zero [MPa]	σ_{r1}	88
Constant (typically 0.07 and 0.13)	b (Assumed)	0.13
Number of cycles	**N_{f2}**	**0.51**
Engine speed (Typical generator set 50hz)	RPM	750
Power strokes pr. min (4T)	RPM	375
Minutes until break	min	0.00136
Hours until break	hours	2.2×10^{-5}

Table 20: Fatigue lifetime calculations

Table 21 shows a comparison with assumed stress range of 28 MPa, for references only. This is for highlighting how strong influence the stress range has on fatigue lifetime, as the stress range influence the zero mean stress equivalent.

Fatigue lifetime calculations		
Mean stress [MPa]	σ_m	820
Stress range [MPa]	σ_r	28
Tensile strength [MPa]	σ_{ts}	1220
Zero Mean Stress equivalent [MPa]	$\Delta\sigma_{\sigma_o}$	85.4
Number of cycles at zero	N_{f1}	10^8
Stress range at zero [MPa]	σ_{r1}	88
Constant (typically 0.07 and 0.13)	b (Assumed)	0.13
Number of cycles	**N_{f2}**	**125947856**
Engine speed (Typical generator set 50hz)	RPM	750

Power strokes pr. min (4T)	RPM	375
Minutes until break	min	335860
Hours until break	hours	5597
Years until break (Day/night power production)	years	0.638

Table 21: Comparison fatigue life at lower stress range

Typical engine parameters for a medium speed engine are combined in the calculation, for references only. This is to illustrate how the fatigue life would be in number of hours operational time, as number of cycles is not that easy to relate.

5 DISCUSSION

An important part in research is to discuss the validation of the results. Everything from the method for conducting the experiment, to how the data is interpreted may influence the result. The discussion should highlight weaknesses and strengths that may explain why the result is what it is. This, together with data from the results, will form the basis for the conclusion and improvements for future work.

5.1 Discussion on Methodology

In Abaqus there are many features which can be used for creating simulation models. Different methods can give similar results. However, different methods has strengths and weaknesses. It is not always straightforward to know which method is most suitable. For instance on contact mechanics when choosing discretization method, “nodal to surface” or “surface to surface”, both methods will solve, but surface to surface creates a more “averaged” result, which often is more correct [33].

3D model models used in this thesis has only representing geometry. Meaning it has weaknesses as the geometry is simplified. For instance on creating the “realistic model” which is based on a real connection rod, very few measures were available. Leading to the student having to interpret and guess most of the measures, of course this leads to errors, as the models are not identical.

Liberties are taken to reduce calculation time. This includes ignoring chamfers and round effects, which would lead to difficult partitioning, meshing and increased calculation time. Correct partitioning and good seeding of the mesh is important for good results; this could be improved and further optimized.

Meshing of the model might lead to deviations, as mesh refinement should be performed, especially over the notch area. Mesh sensitivity analysis has been conducted with the aim to find optimized meshing density.

Mesh Element type for this thesis is C3D20R elements having reduced integration, which is approx. 3.5 times faster compared to C3D20 elements. Due to limited computer power it was most reasonable to use reduced integration. Even with reduced integration, the computer used approx. 10-12 hours for each job limiting the progress of the thesis.

Simplifications has been used much throughout this thesis. One example is static analysis instead of dynamic analysis. The reason for this is mainly to lower the calculation cost. The forces and inertias, which the con-rod assembly is exposed to during load cycles, has been taken into account in the static analysis. However, the static analysis only simulates some cases, which might not show the peak or worst case loads scenarios.

The material properties for this model is defined for linear elastic behavior only. The results shows stress, which would exceed the yield and tensile limit even for high strength steels.

Interface between cap and connection rod is simplified by specifying rough behavior, which does not allow slippage. This was to done to avoid having to model serrations, which would be time consuming and not necessary important for the global results.

The interaction and contact mechanics could be improved as the friction factor was choosed to be 0.1 even though it could vary depending on the tribology.

The thread section is very simplified using tied nodes instead of modeling threads. This creates a stress distribution, which is not as realistic compared to other methods. In combination with no filet radiuses this leads to stress concentration areas with high SCF values.

Much time of the thesis has been spent pursuing methods and options, which did not give any result or ended in failed simulation attempts. Some of the reason for this is that the student did not have sufficient experience in the simulation software, and spent more time learning the tool than assumed. One important part of this thesis is the step-by-step guide in appendix A, which shows how the model was created, button to button. This document could prove valuable for future work.

5.2 Discussion on Results

Very high stress in areas, plastic deformation is most likely caused by simplified geometry, without any smooth changes in dimensions such as filets. This leads to a high stress concentration factor as the fillet radius is going towards zero. A local model of the first thread with refined mesh would give a more correct simulation of the stress concentration in the start of the thread.

The design of the realistic model might have the starting point ford the threads at an unfortunate place. This may lead to the stress from the bearing going straight through the notch area. Changing the start point of the threads could alter the results. Finding the optimum placing point for the first thread in the global model has not been analyzed. This could be investigated in future work.

Pre-tension force for the bolt can be discussed if is set correctly. The results shows that during the pre-tension step, the notch effect creates stress above tensile strength. However, there is documentation [22] which suggest higher pre-load force is good against fatigue as the stress range through the bolt might decrease. Again the amount needs to be optimized as overtightening clearly can lead to fracture. Optimization of the pre-tension force with regards to the notch effect is essential for obtaining good fatigue life. Future work should include adjusting the pre-tension force in a locally model with redefined mesh.

Change in stress around circumference path indicates that the bolts are subjected to bending. Bending is generally not optimal in bolts, as bolting material often has anisotropic properties with best strength properties in tension direction [2].

Longitudinal stress along threads is not distributed as evenly as compared to Figure 9 by Leyers [16]. In the global model the first thread, takes most of the load, giving high stress at this area. Further work could include investigating other approaches for fastening the threads to connection rod, using other features in Abaqus. Other bolt geometry like boring the lower thread part is also an interesting simulation case as this is a method used for distributing the load more evenly [8].

Unable to predict fatigue life due to stresses above tensile strength. Again, the next step would be to create a local model of the first thread applying the displacement from the global

model. This should be performed with a refined mesh, and updated geometry giving better SCF conditions at the notch. For the refined model there should also be possible to simulate the crack growth rate given by the paris law.

The fatigue calculations has clearly flaws regarding high level of assumptions on parameters. This in combination with results from the global model, with stresses above the tensile strength makes the need of further work on fatigue lifetime calculations necessary.

6 CONCLUSIONS

This thesis has confirmed that it is possible to create a global model, simulating the forces acting in the big-end section of a connection rod, during a power stroke.

In this simulation, it is showed that contact mechanics between parts is possible to simulate with reasonable results.

The realistic model shows that during loading of the big-end assembly, some areas especially in the bolts are exposed too much higher stress compared to other areas. These areas with high max principal stresses are more exposed to cracking and fatigue failure.

Analysis of the bolts shows that the most stressed areas is close to the first threads as this takes up most of the load in combination with notch effects. Circumferential analysis shows that the bolts are subjected to bending moment throughout the power stroke.

6.1 Future work

For enhancing the results on the topic, further work should be conducted, as this thesis only scratched the surface with regard to fatigue calculations.

A local model of the first thread section with enhanced redefined mesh should be created. This can use the displacements from the realistic model as input to the stress calculation. This would allow simulating more realistic notch effects, which could give better fatigue life predictions using empirical formulas. Furthermore, the simulation of crack growth from a point could be performed with the use of Paris law.

A better method for simulating correct stress distribution in the thread would also come in handy. When this is performed a comparison between coarse threaded vs. fine threaded bolts could be done. Other configurations, such as create boring in the thread end of the bolt could also be analyzed.

7 APPENDIX

7.1 APPENDIX A. STEP BY STEP HOW TO BUILD THE MODEL

Create part (Part module)

Create the connection rod with the following settings. The bearing is the same. But for the bolts, revolution is a better technique.

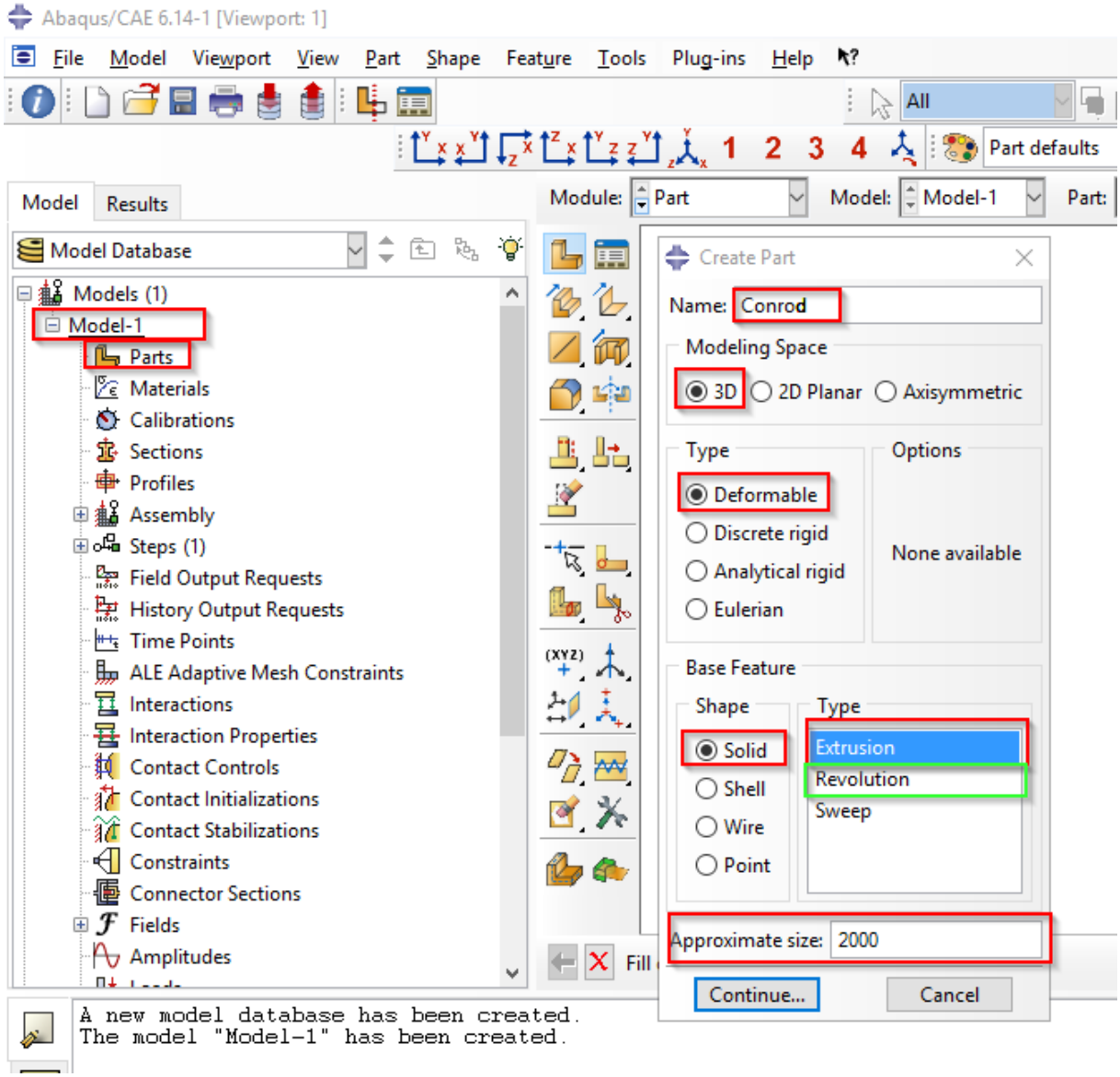

APPENDIX A 1: Part

Sketch the parts as desired. Technical drawings is in appendix. Make sure to save the parts as the works goes on, to your desired working directory.

Create materials (Property module)

Material specification for the connection rod:

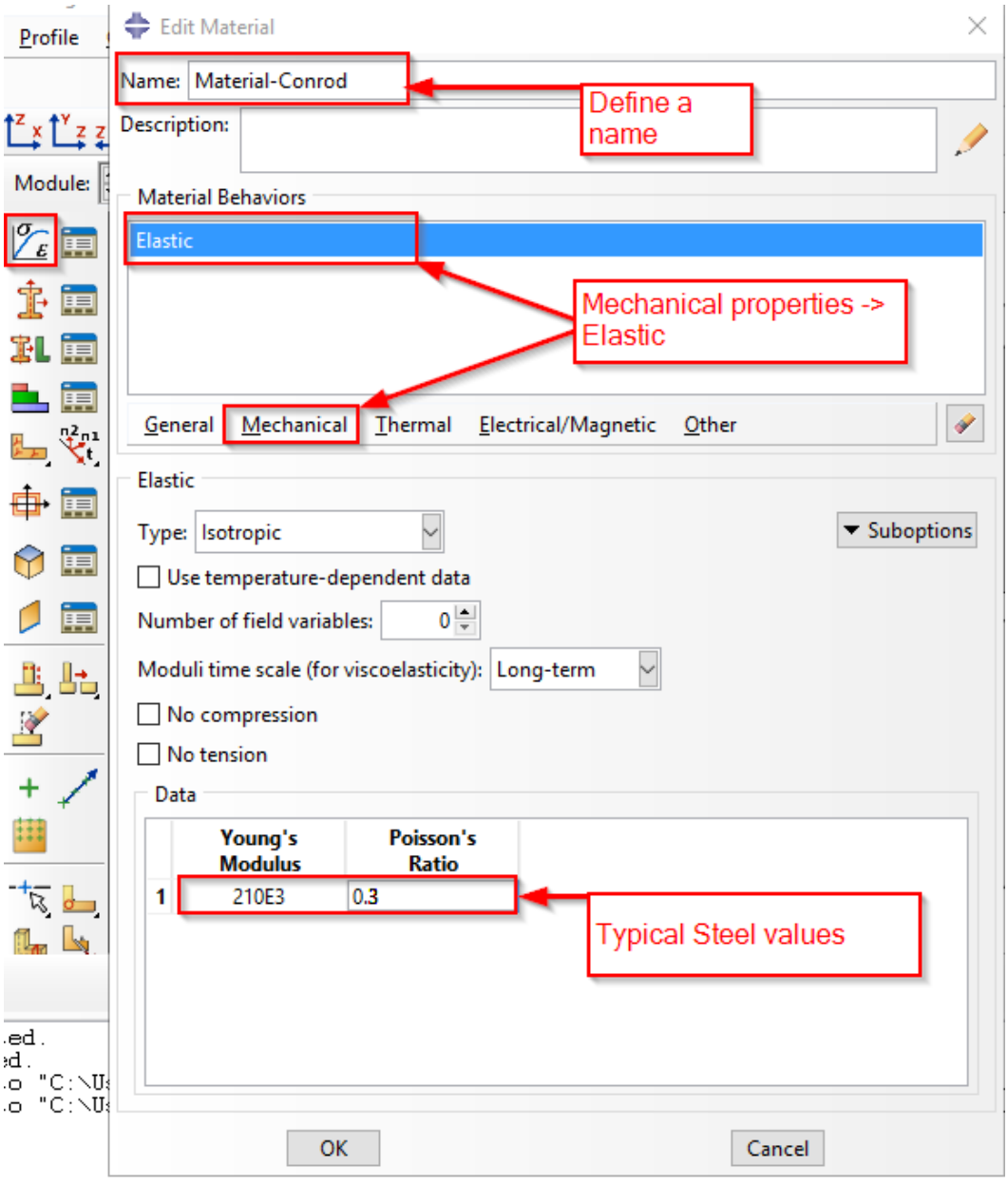

APPENDIX A 2 Material

Create material section

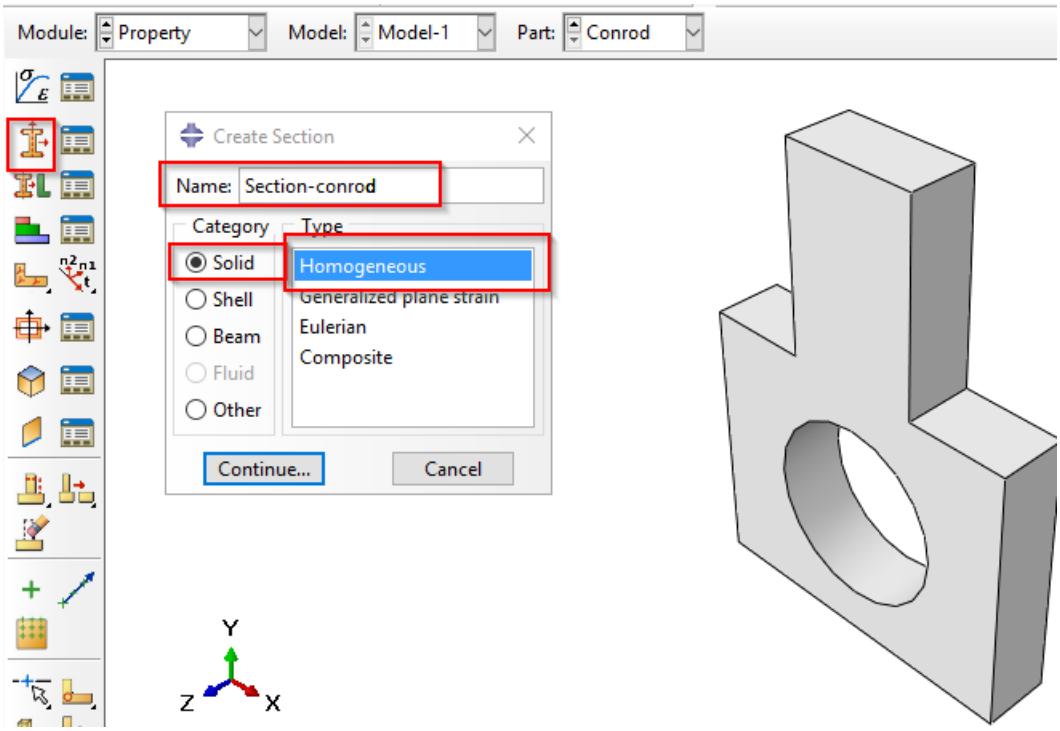

APPENDIX A 3: Section

In **edit section** choose **material-conrod.**

Assign the section or the parts, which should have the specified material properties.

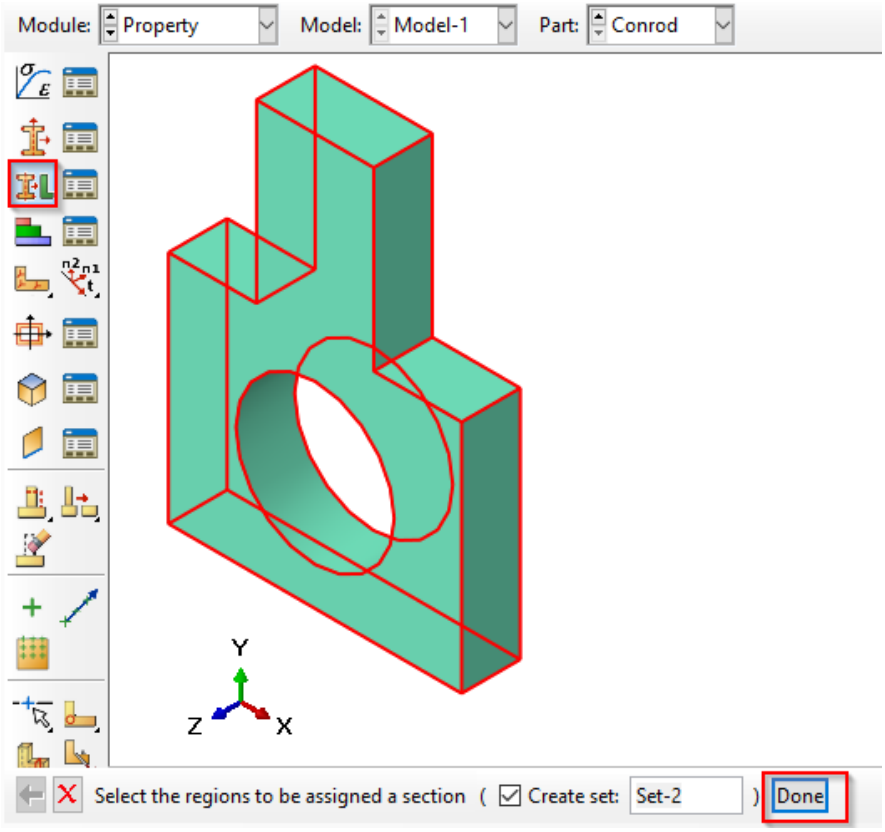

APPENDIX A 4: set section

Material Specification for the bearing:

The bearing is 3 times more stiff compared to the connection rod. Rigid elements was more unstable when processing, so workaround using stiff deformable material made the program solve more smoothly.

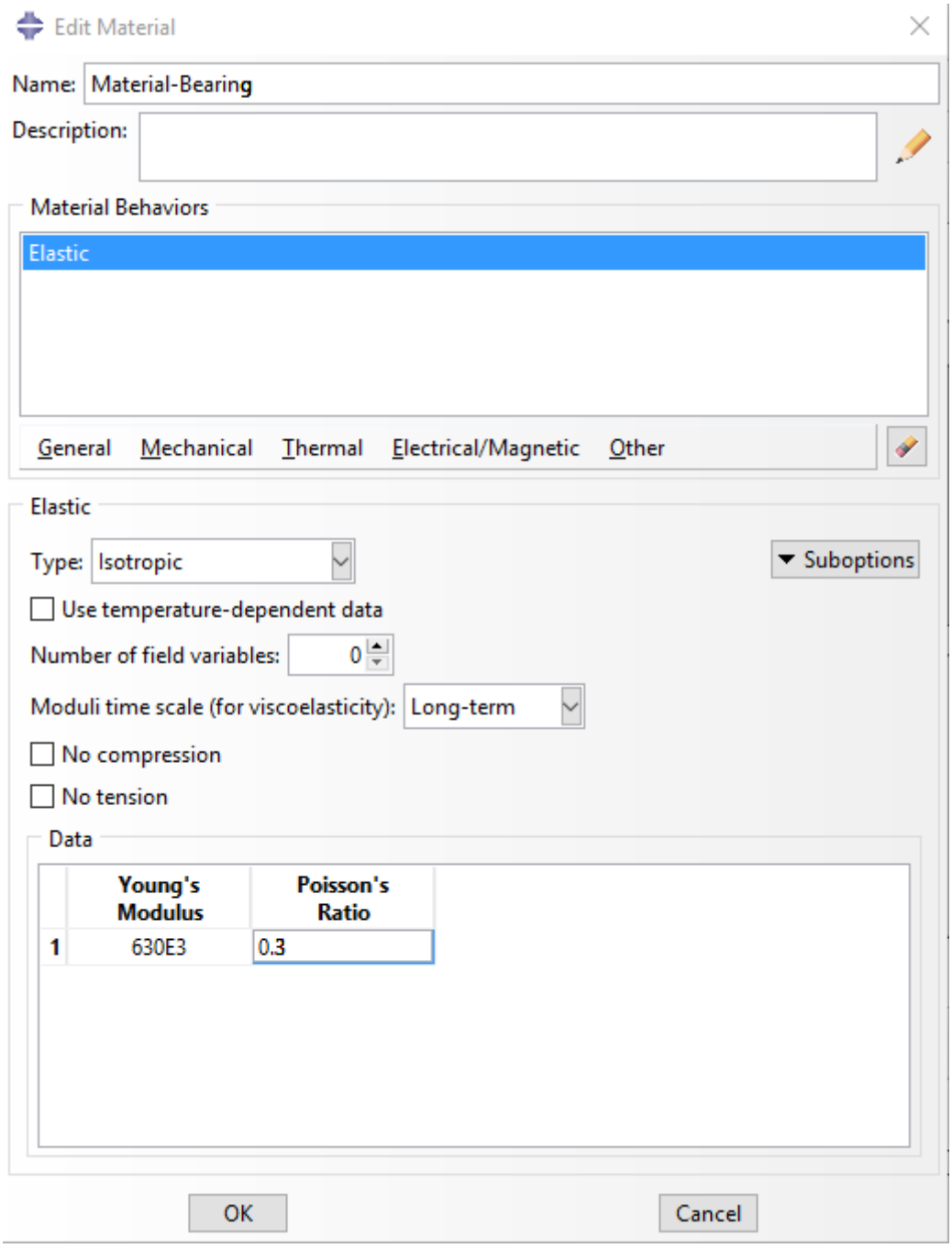

APPENDIX A 5: Bearing Material

The bearing also need to specify expansion because later when applying load, the clearance gap between the bearing and the conrod needs to be closed. After trying many methods the most stable proved to be expanding the bearing so that it closes the gap, apply the load, and then remove the expansion. The expansion is anisotropic and only expanding in radial direction.

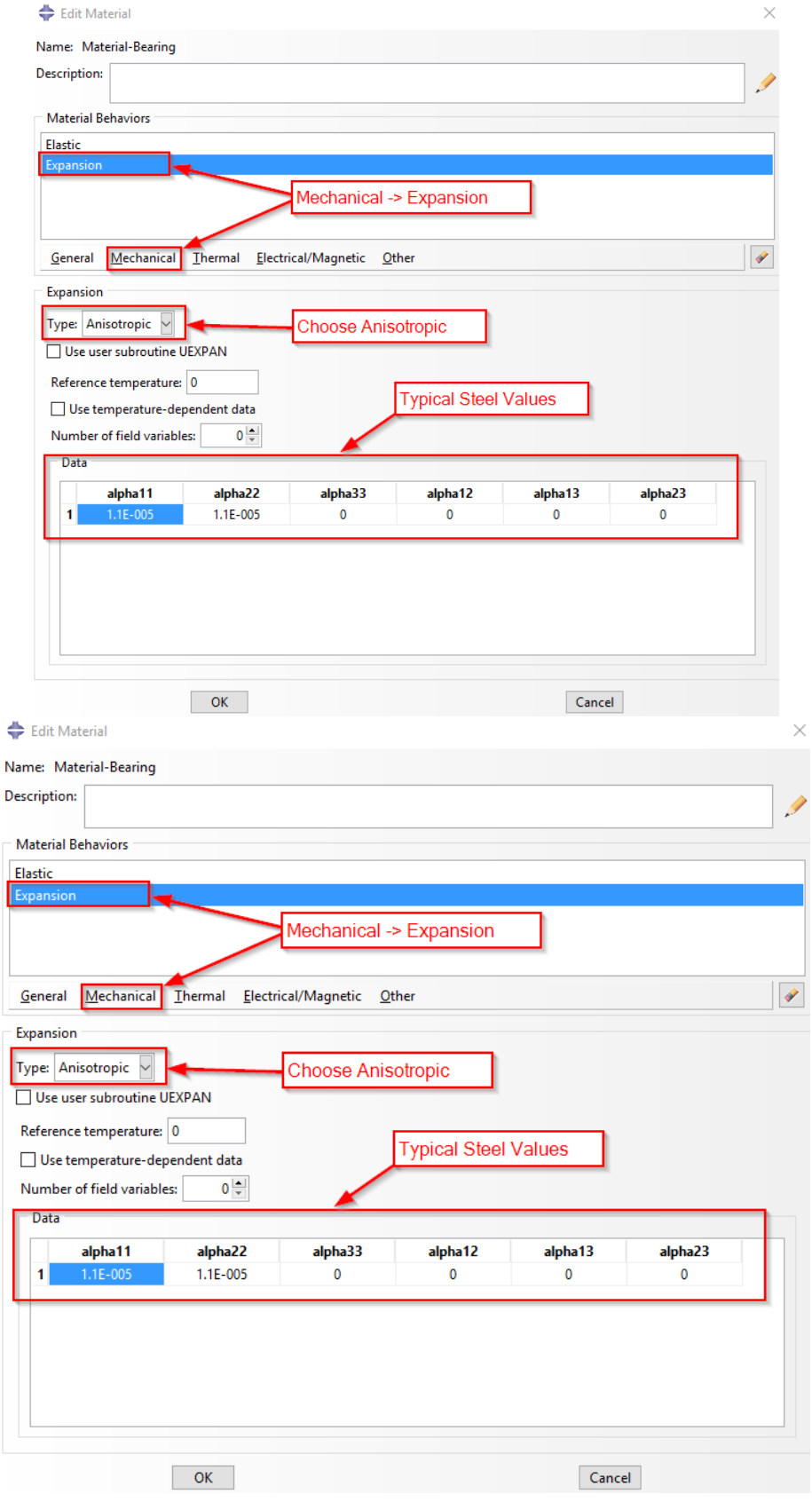

APPENDIX A 6: bearing material expansion

Assign section bearing (anisotropic material)

The section can be defined similar as for the connection rod. So follow the same steps for assigning the material properties to the bearing.

NOTE: Since the bearing has anisotropic material, direction of the material has to be assigned. First a datum cylindrical coordinate system has to be created for references.

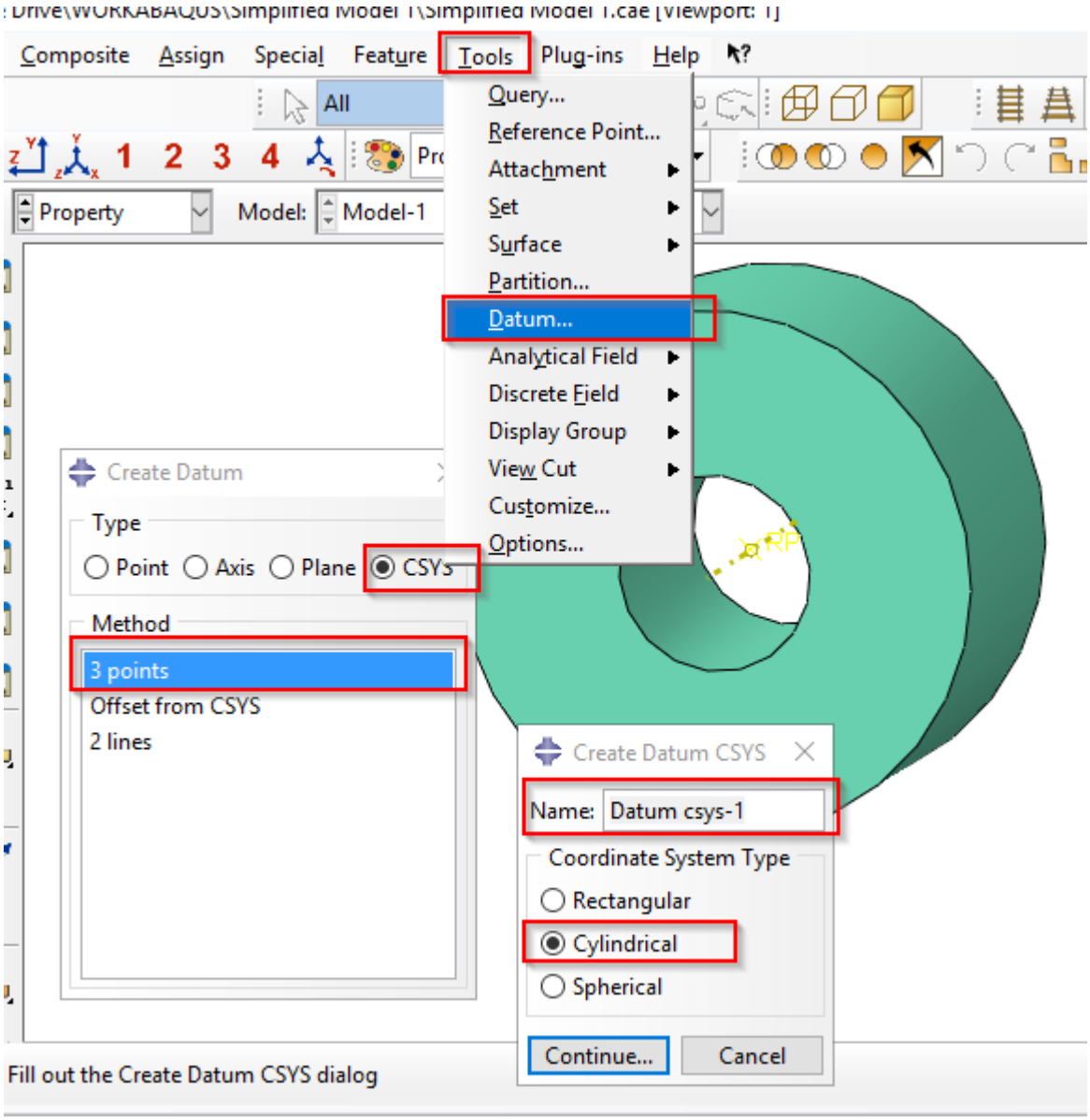

APPENDIX A 7: Datum

When Abaqus asks for points choose the defaults, and it will align with the assembly coordinate system.

For creating material orientation follow the instructions in the picture below. Depending on your cylindrical datum coordinate system orientation the rotational direction might be changed.

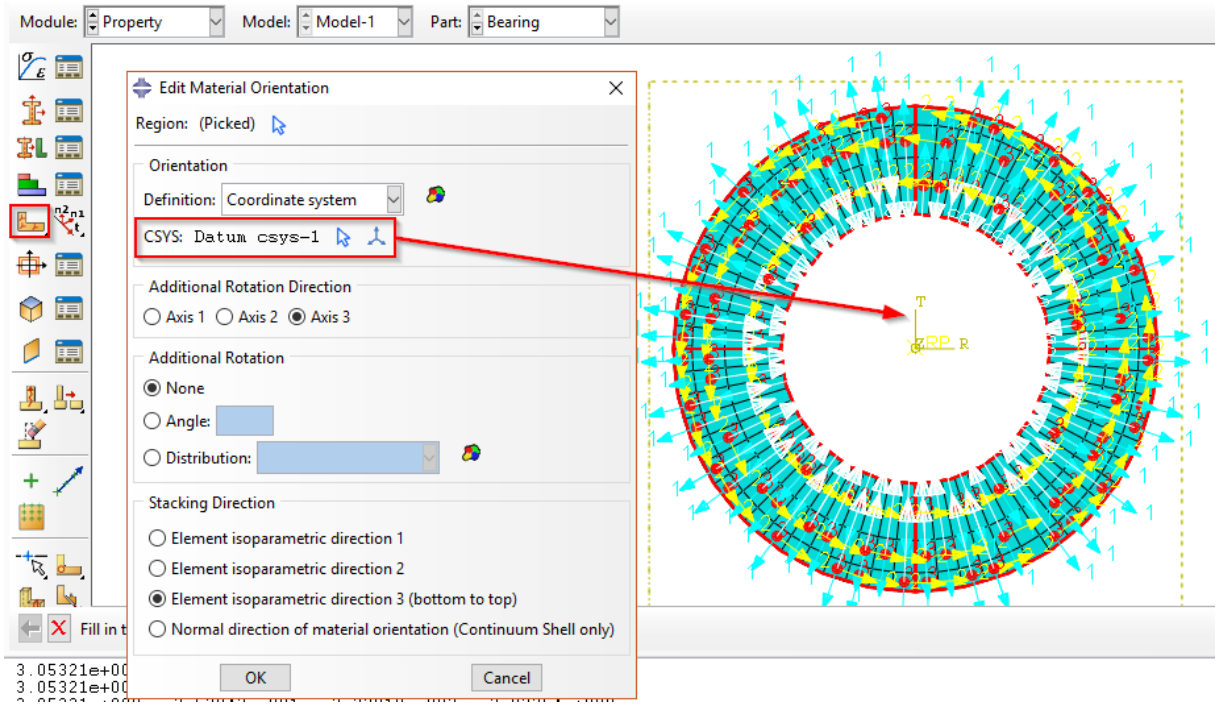

APPENDIX A 8: Material Orientation

Create Partitions

Before assembling the parts it is handy to partition the part first. This is because if you firs assemble the parts and then partition it, the names of the parts or surfaces might change and delete the sets and references creating problems for the model.

Go to **mesh module** and **object: parts**. Each part will have to be partitioned.

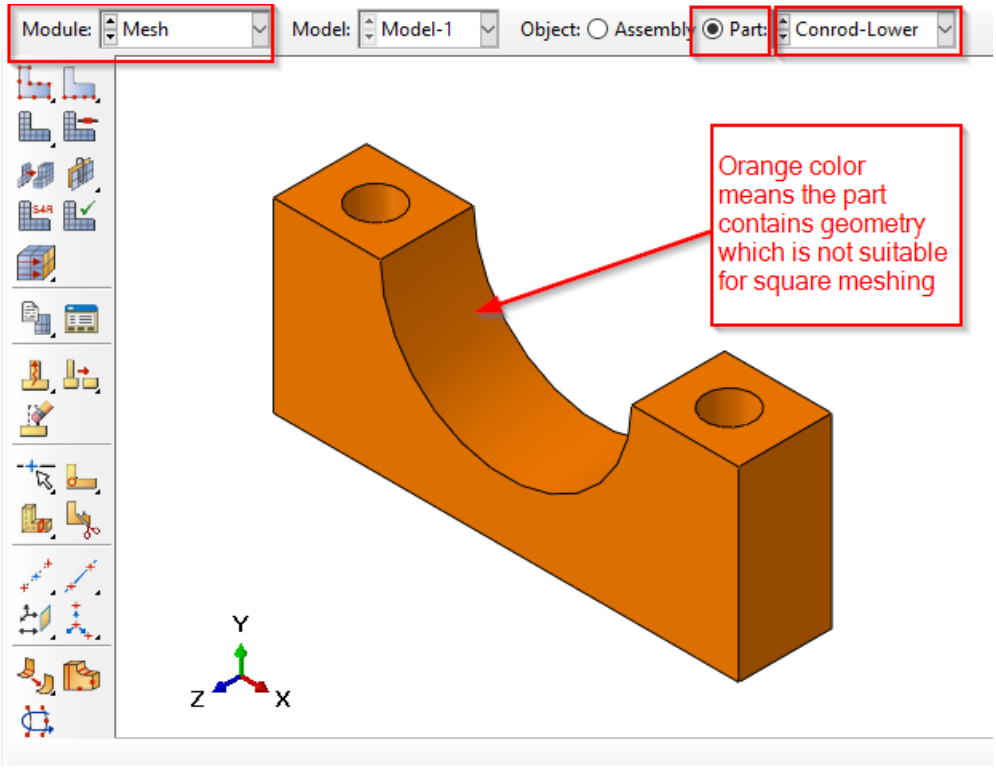

APPENDIX A 9: Partition 1

The geometry needs to be partitioned so that it exists of four-sided parts. Meaning that circles and half circles needs to be split.

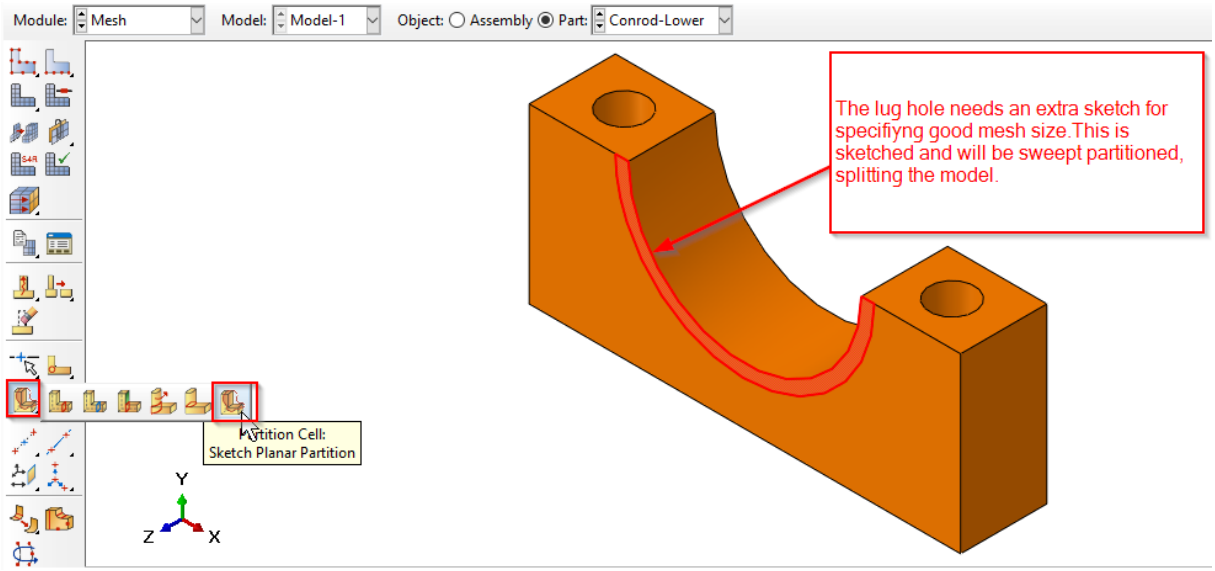

APPENDIX A 10: Partition 2

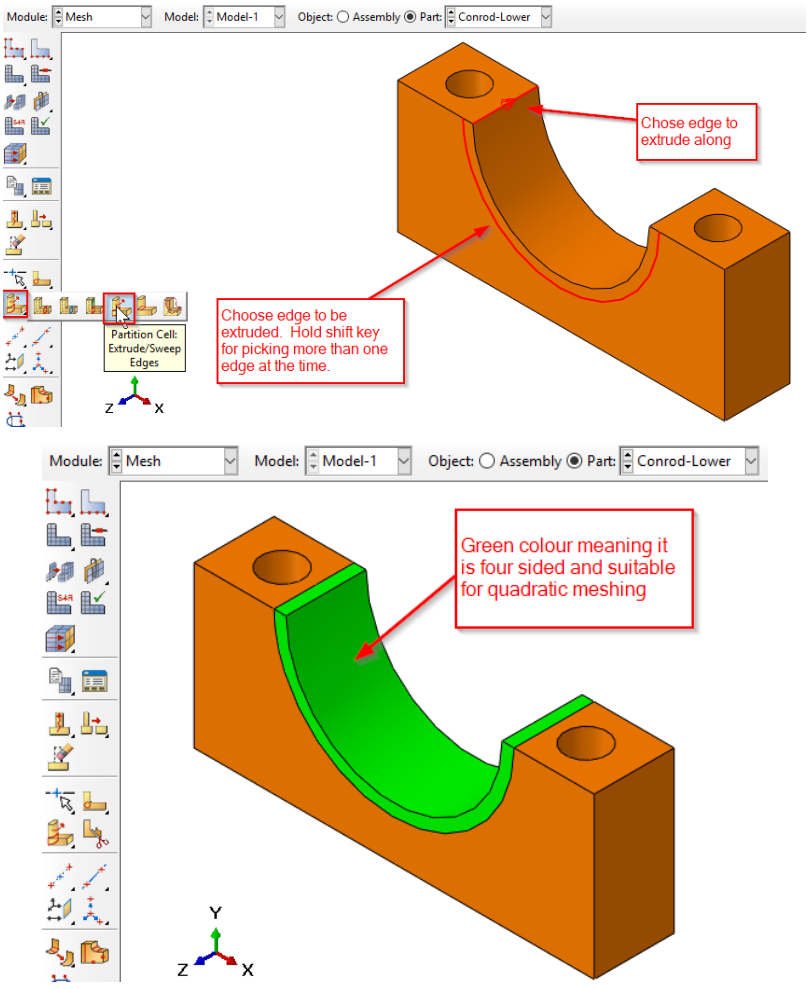

APPENDIX A 11: Partition 3

By defining cutting planes it is easy to partition the rest of the model. Putting in some extra partitioning will make sure that elements are align when meshed. For instance between the bearing and the lug, it is important to align the mesh so that it does not create issues during simulation.

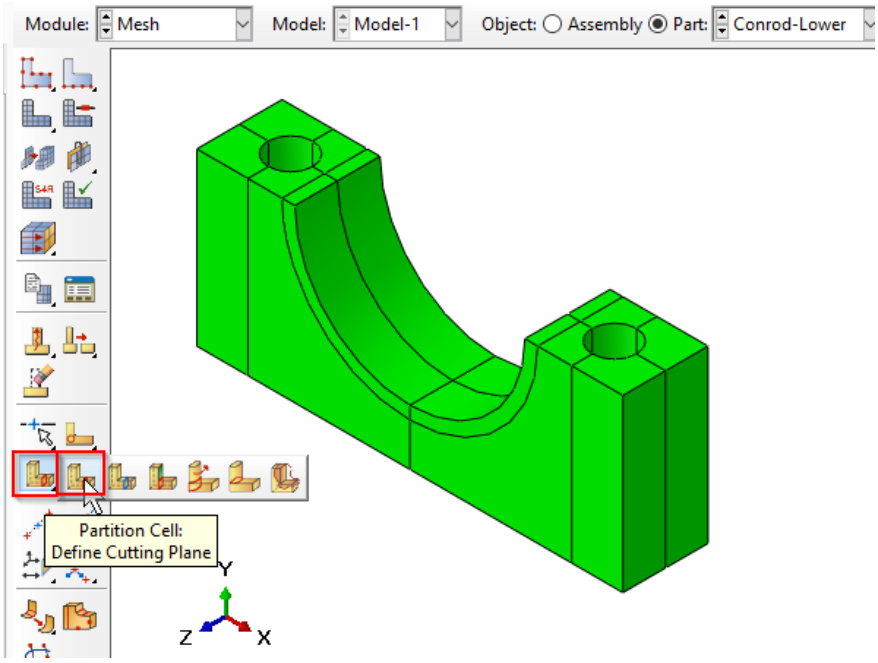

APPENDIX A 12: Partition 4

Create Assembly

Go to assembly module and insert the parts for the assembly. The parts needs to be constrained to each other

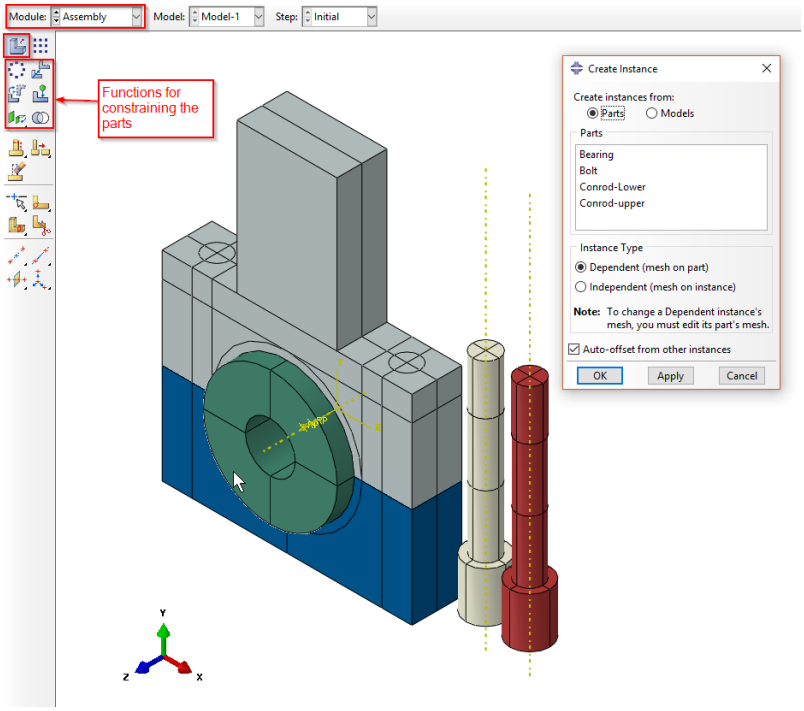

APPENDIX A 13: pre-Assembly

Model after assembly:

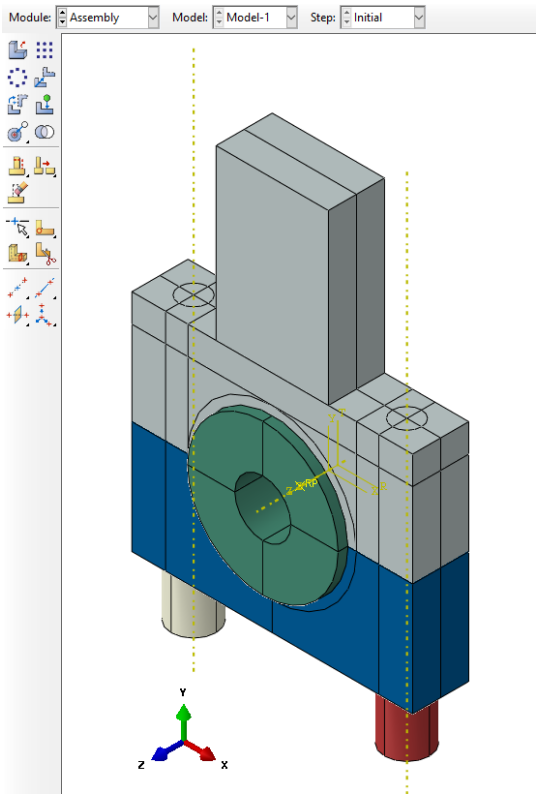

APPENDIX A 14: Assembly

Creating Mesh

This simulation uses C3D20R elements for all parts. This needs to be defined for the parts and can be done as follows:

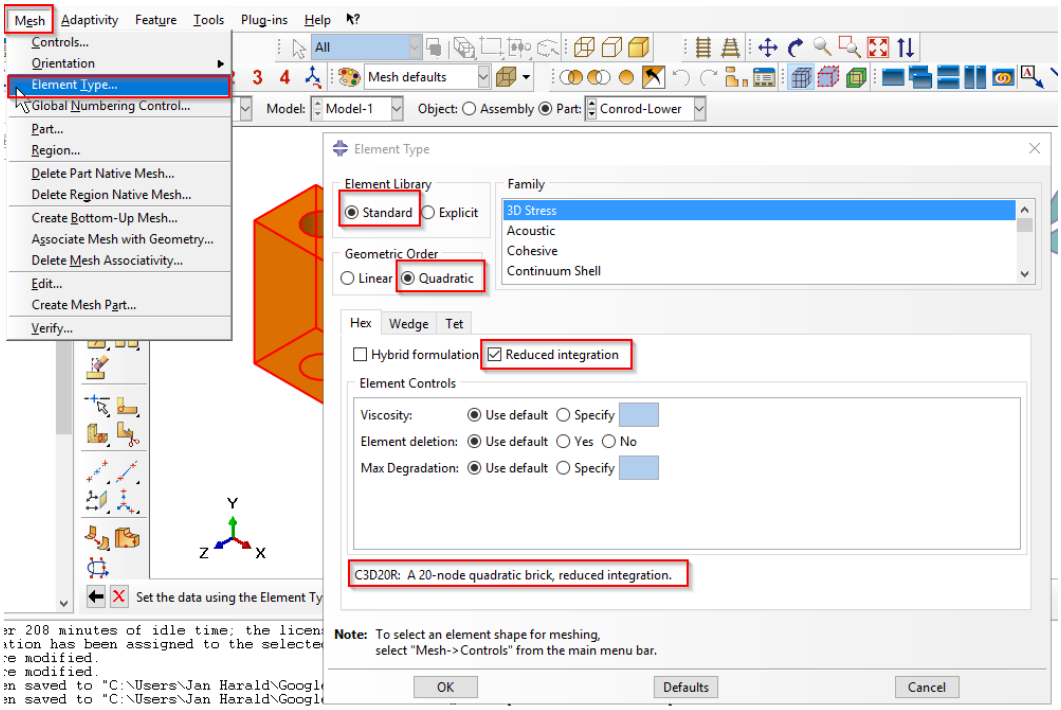

APPENDIX A 15: Create Mesh

Some edges and curves might need special attention for creating a good mesh structure.

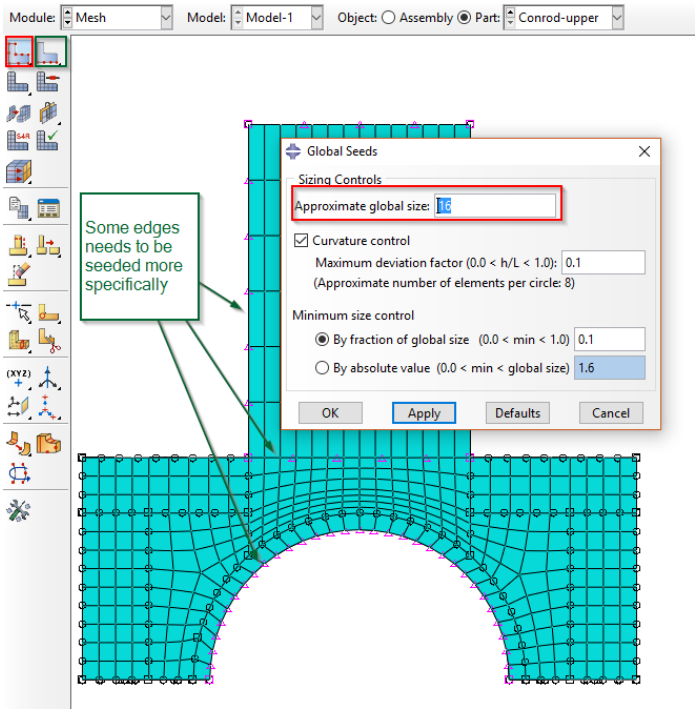

APPENDIX A 16: Global seeds

The parts needs to be partitioned as instructed in previous chapter. When creating mesh make sure to verify the mesh integrity. If this is not good enough adjustments in the partitioning needs to be performed.

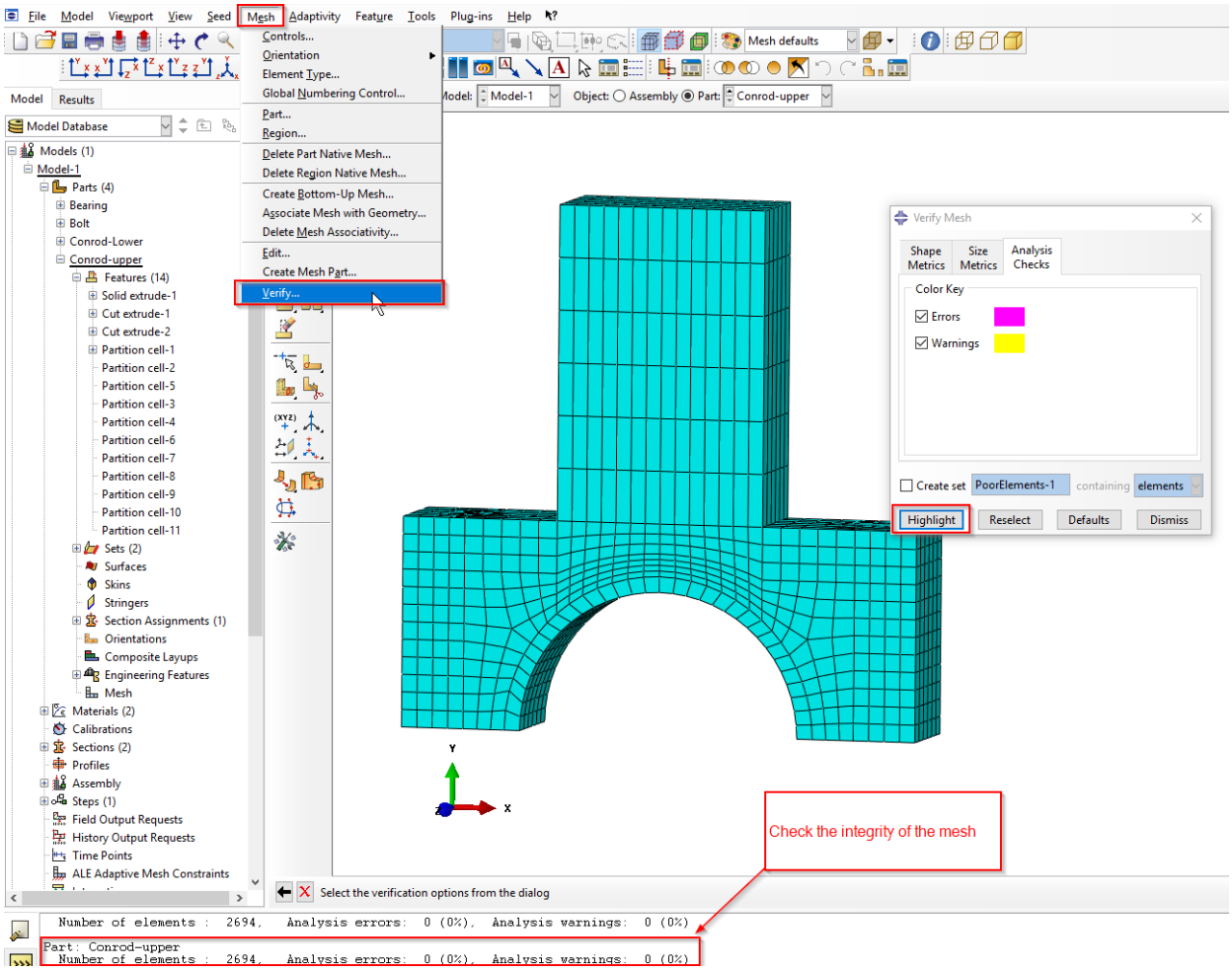

APPENDIX A 17: mesh verification

Create Step

The steps are used to tell abaqus what to be done at different time. Note that pre-tensioning of bolts has to be done in the first step. Intereactions such as contact mechanics can be inserted in the initial step.

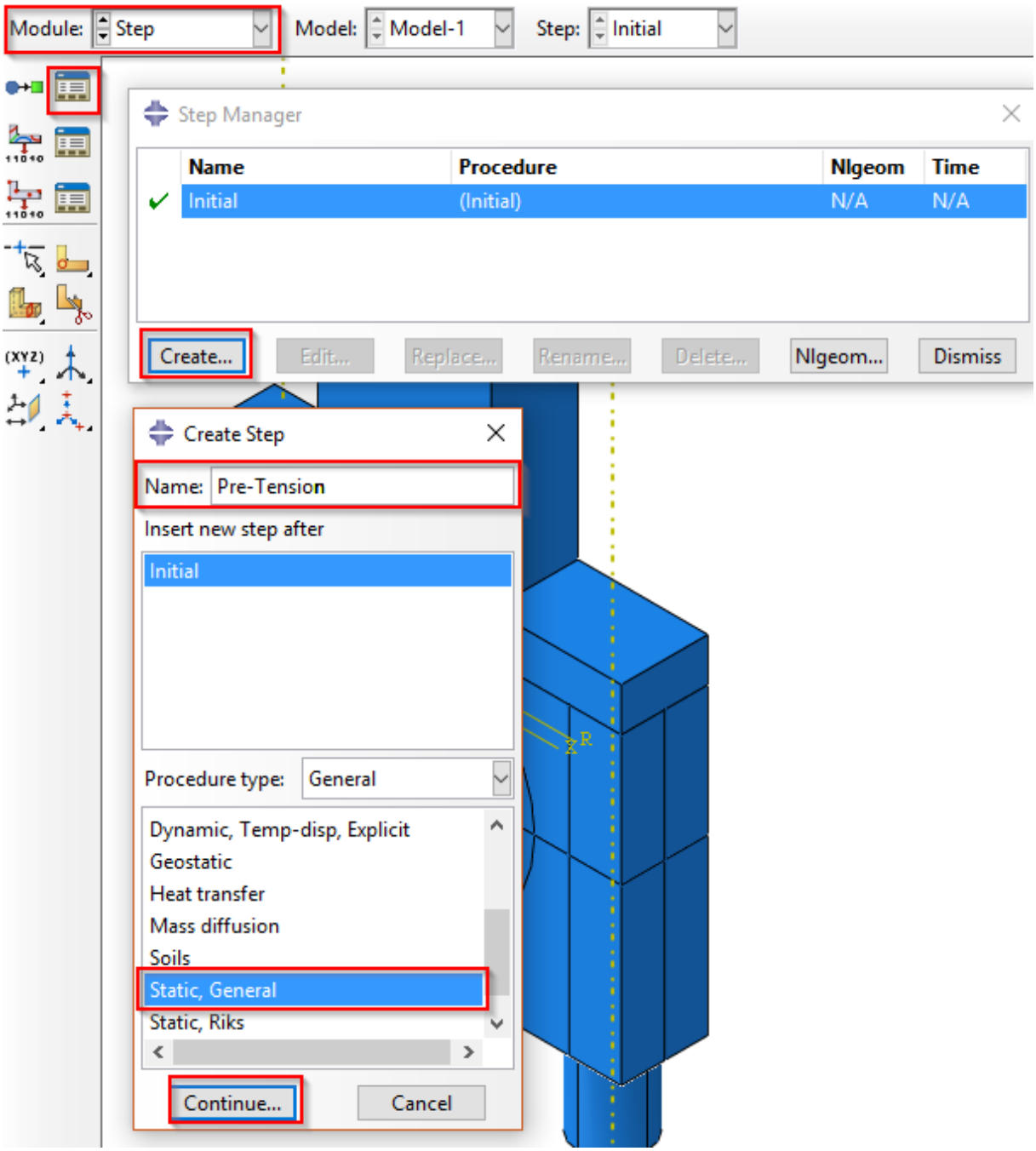

APPENDIX A 18: Steps

This thesis uses general procedure type, and static general step properties. Other types can be choosed depending on the simulation performed.

In **Edit step** choose **Nlgeom ON**. This feature allows for larger displacements, creates more stable simulations, but increases simulation time.

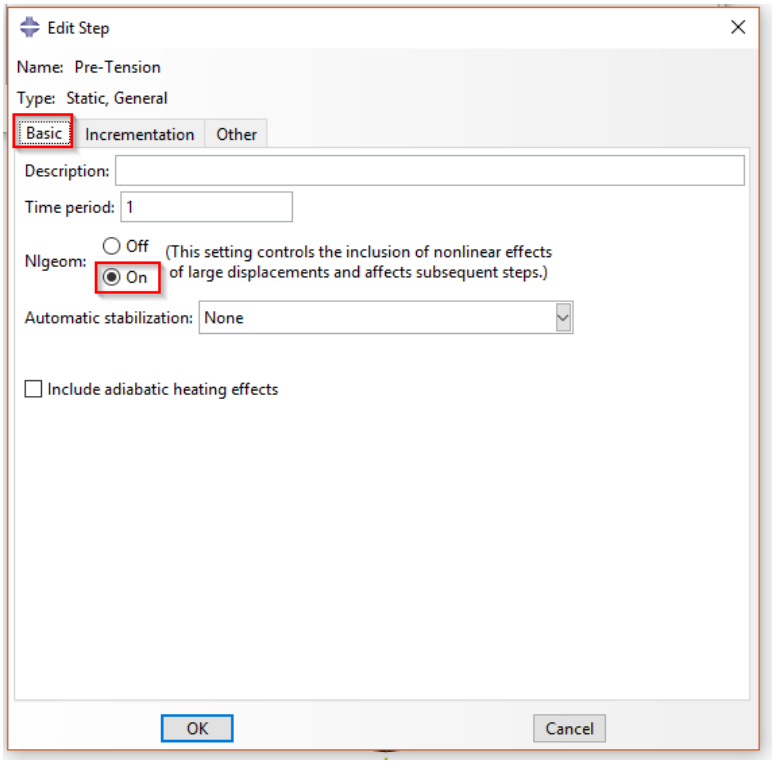

APPENDIX A 19: NIgeom on

In **incrementation tab** decrease the increment size to 0.1 or 0.01. This reduces the increment size, which might improve the stability of the simulation, but can increase simulation time.

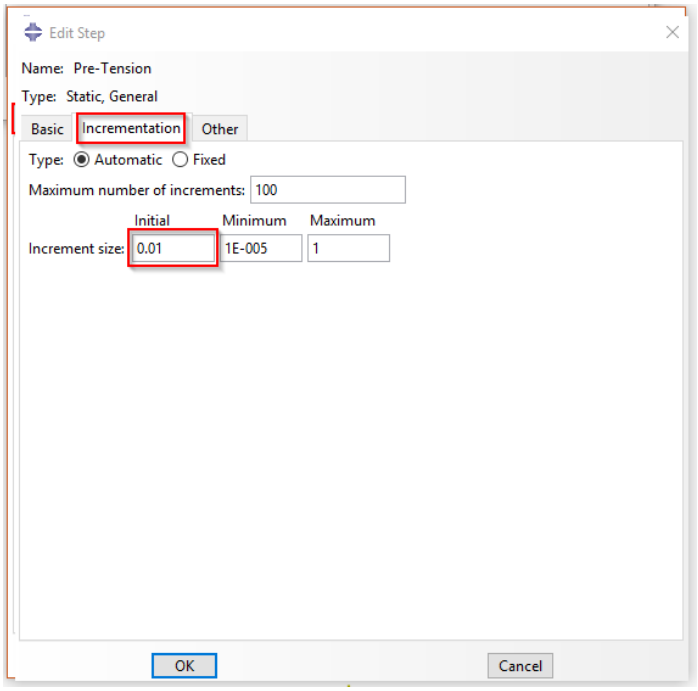

APPENDIX A 20: Increment size

Create Interaction/Contact mechanics

Go to interaction property manager and create the contact mechanics properties.

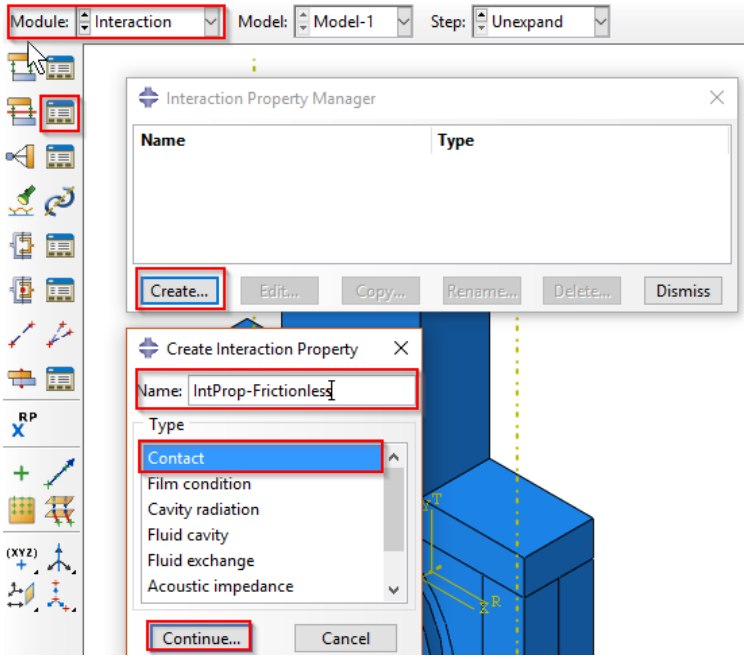

APPENDIX A 21: Interaction

When pressing **continue**, you continue to **Edit Contact Properties**, choose **Mechanical** and **Tangential Behaviour** -> **Frictionless** (for frictionless, between bearing and lug)

For **friction properties**, choose **Penalty** and specify the coefficient of friction.

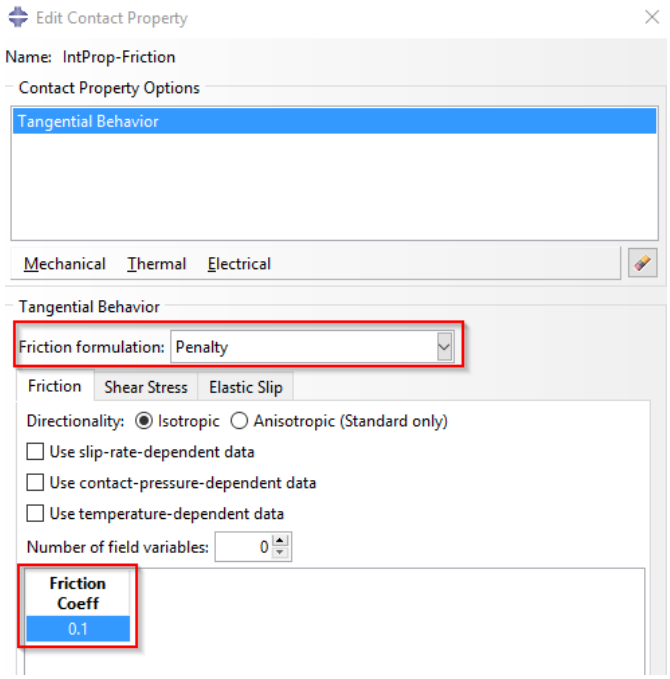

APPENDIX A 22: Friction

Specify contact mechanics for surfaces.

Abaqus has a built in tool for finding contact pairs. This saves the user much time when defining surfaces. All parts in contact is displayed in the table, and individual property values can be chosen for the different contact pairs.

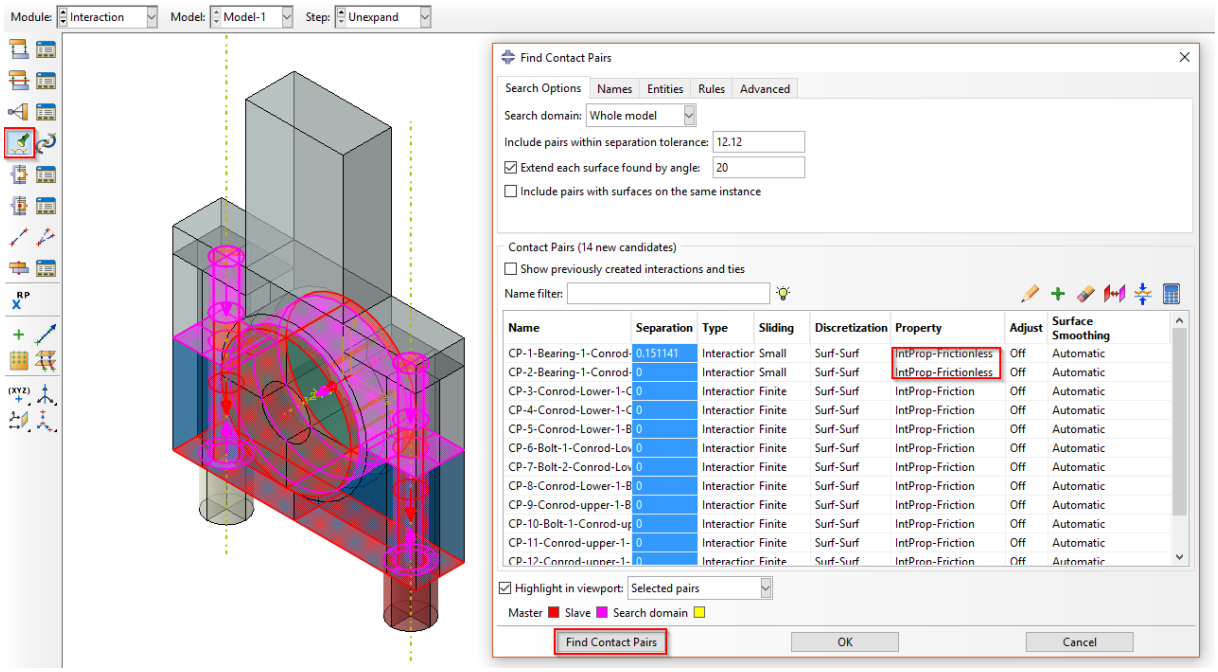

APPENDIX A 23: Global Pairs

NOTE:

- For the surfaces between upper and lower part of the connection rod, contact property is set to **Rough**. Meaning that no slip will occur when points are in contact. This is a simplification for simulating serrations
- For the surface in the thread region, contact properties can be turned off, because these surfaces are tied as a simplified simulation for threads

Tie thread region

For simulating the inside, threads locking the stud to the upper connection rod tie surfaces is used. This is a simplification for not spending time creating 3Dmodel of the treads, which is very time consuming and heavy to simulate for the computer.

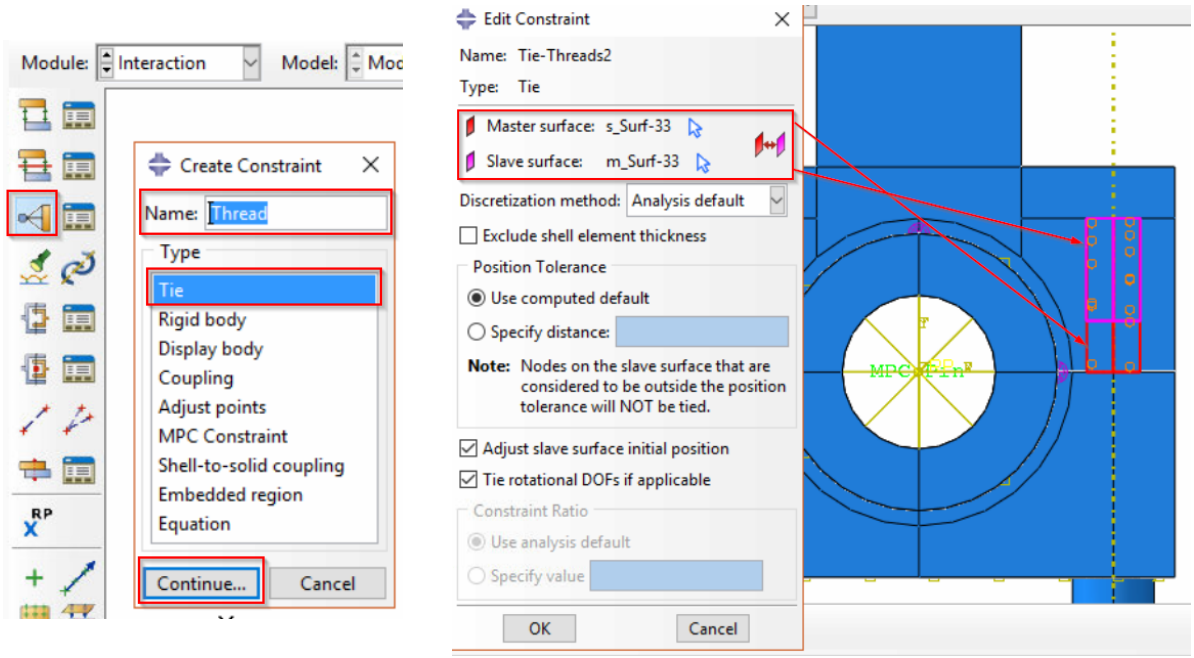

APPENDIX A 24: Tied Thread

MPC-Pin

Is a feature, which makes it possible to find a point and lock it to a surface. This comes in handy when for instance specifying a concentrated load over a surface. Make sure to have defined a reference point that can be defined as control point, and select the slave area. Use **MPC type pin**.

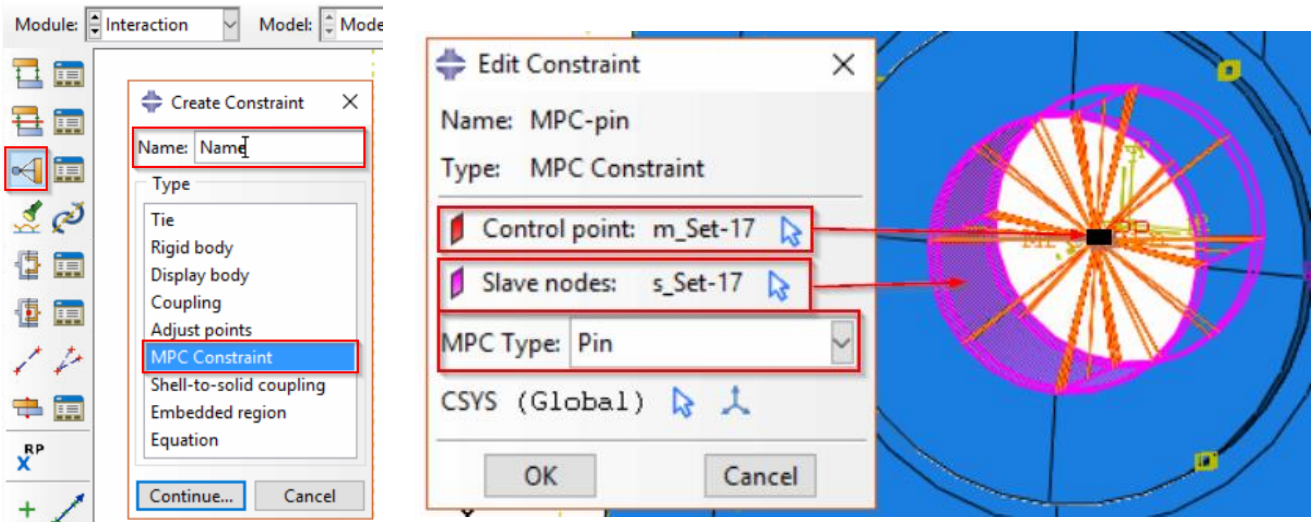

APPENDIX A 25: MPC-Pin

Create Strings

Strings needs to be added between the bearing and the lug. There is clearance here, and when applying load to the bearing, this moves and and will create discontinuities error in the simulation. A work around here is to add strings which holds the bearing in the lug. The spring constant is set to be very low typ. 0.1N/mm which will have no impact on the result

Go to **Assembly -> Engineering Features -> Springs/Dashpots**.

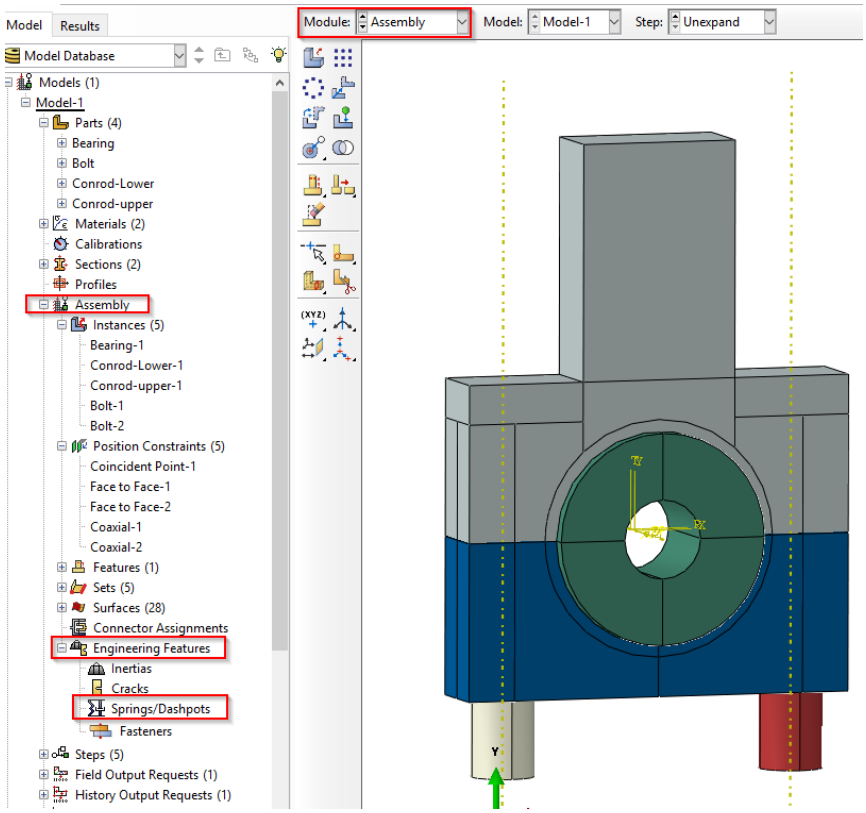

APPENDIX A 26: Springs

When applying strings, make sure that the nodes are on the same plane, so that the springs are as much in direct X or Y direction as possible. Creating extra partitions in the bearing might be necessary for having them in the same plane. Make sure to redefine sets and surfaces if new partitions are created.

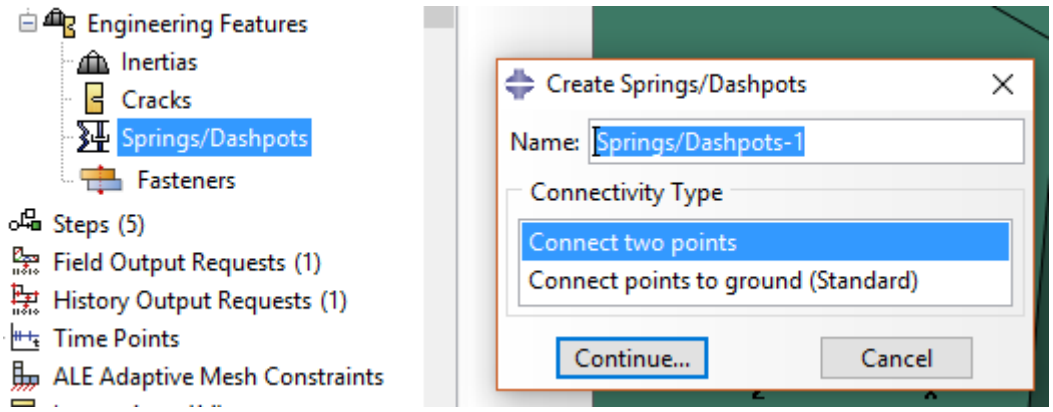

APPENDIX A 27: Springs 2

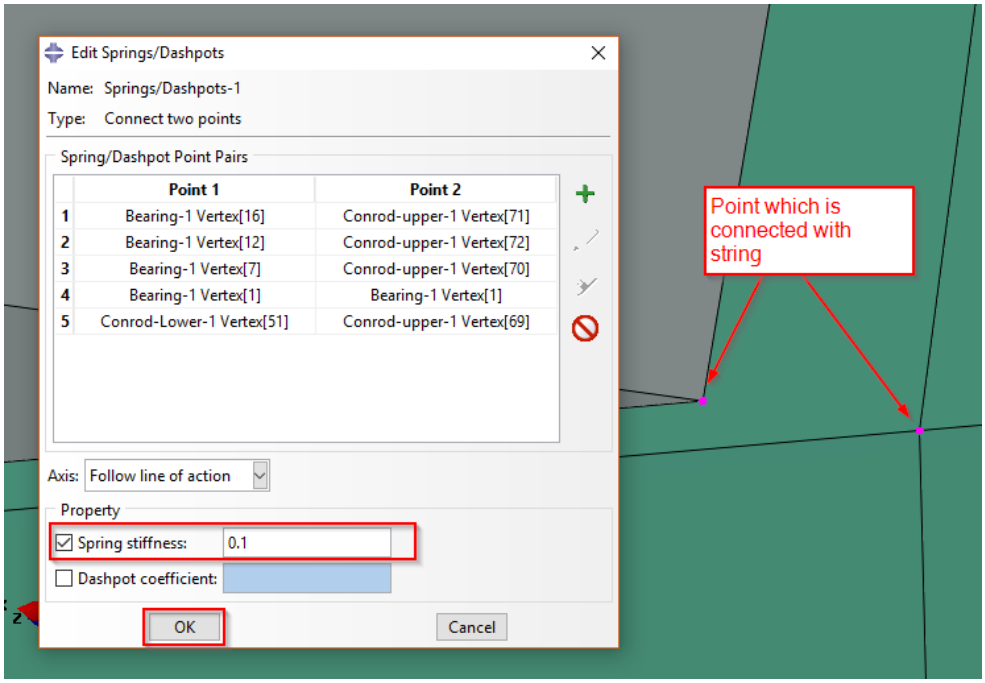

APPENDIX A 28: Connect springs

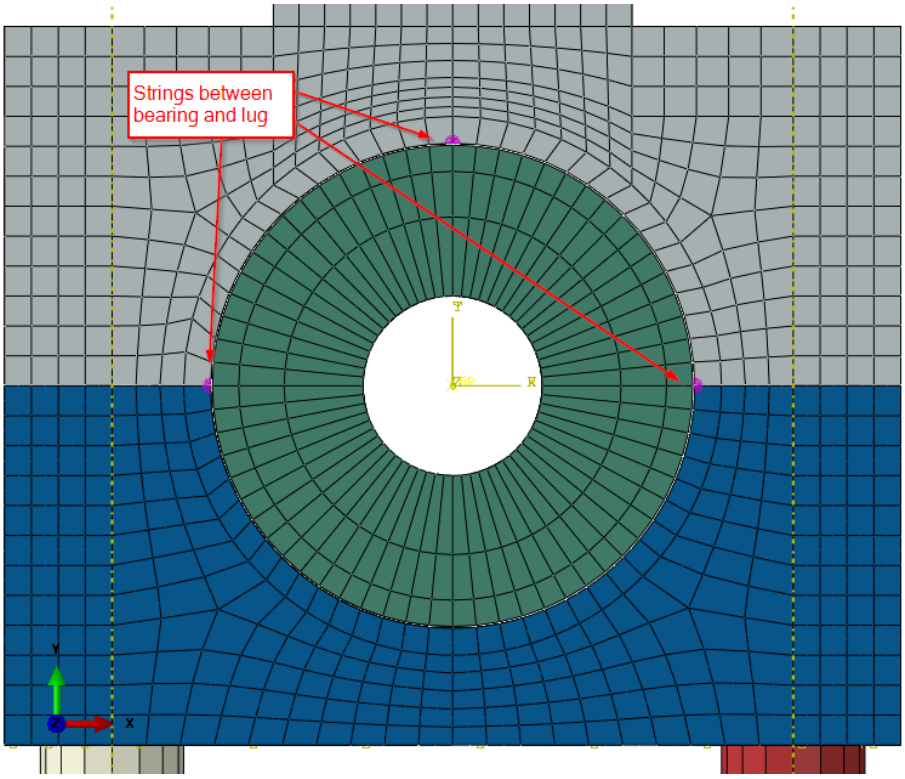

APPENDIX A 29: Springs 3

Create load cases and constraints

For performing the simulation, the model needs to be constrained and loads needs to be defined. Go to the **load module.**

Create pre-tension bolts

Abaqus has a built in feature for defining pre tension of bolts. Go to **Create load** and make sure that you are in the first step after initial step (bolt loads has to be defined in this step) follow the instructions from the pictures below:

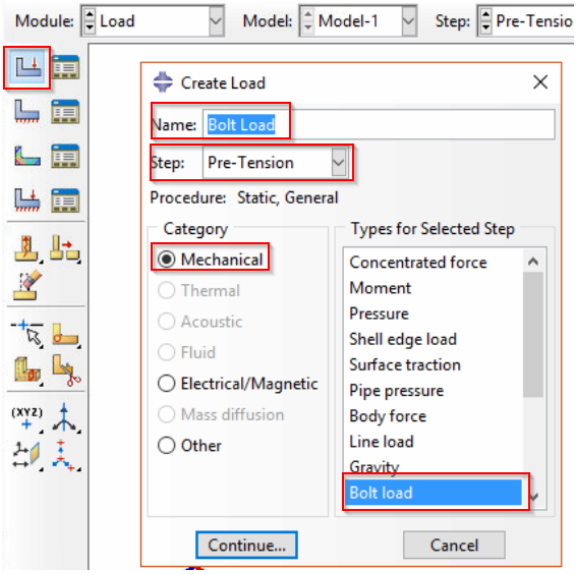

APPENDIX A 30: Load Case

Bolt area needs to be defined. Make sure that there is a partition around the middle of the bolt, which creates a cross section. Use **remove selected** button to remove the faces so that the cross section area is easy to pick. This function is also very handy for not showing parts and elements in the assembly. Choose the bolt axis, and select the pre tension magnitude.

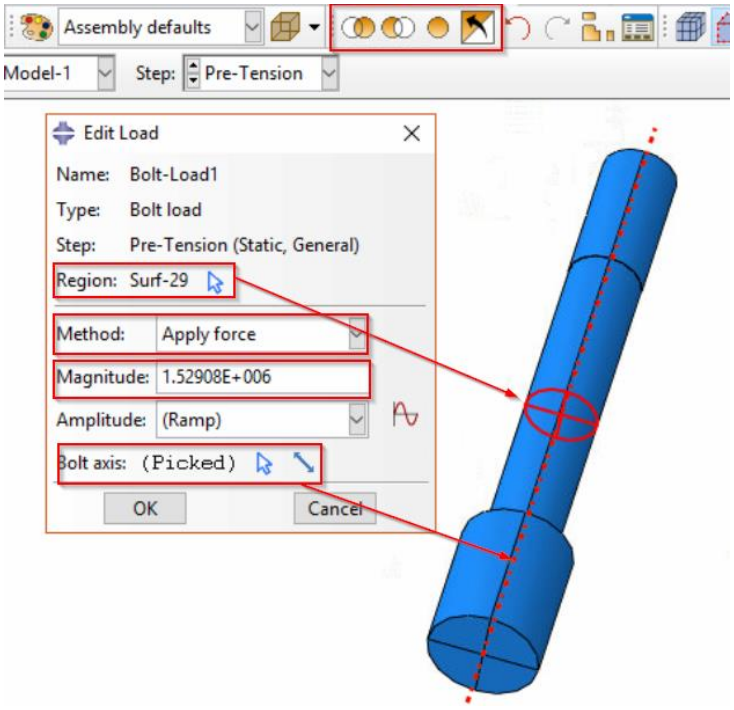

APPENDIX A 31: Bolt pre-tension

Create Bearing Load

The bearing load is the resultant force from the crankpin against the connection rod. This is defined as a concentrated force attacking the same reference point which was used in the MPC-pin interaction. This means that the force is distributed to the inside of the bearing, which again due to contact mechanics distributes a bearing load to the connection rod. The setup for the load is as described in the figure below. Note that the forces are placed in X-Y-Z direction. An excel sheet has been created to easily calculate the force vectors.

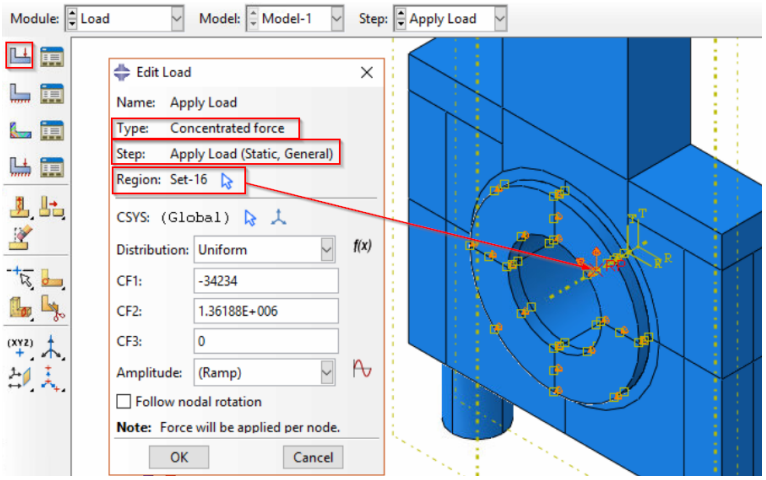

APPENDIX A 32: Bearing Load

Create Boundary Conditions

The connection rod is “welded” or encastred in the top. This is a simplification, as a real connection rod is pin connected between the piston and crank, and able to move.

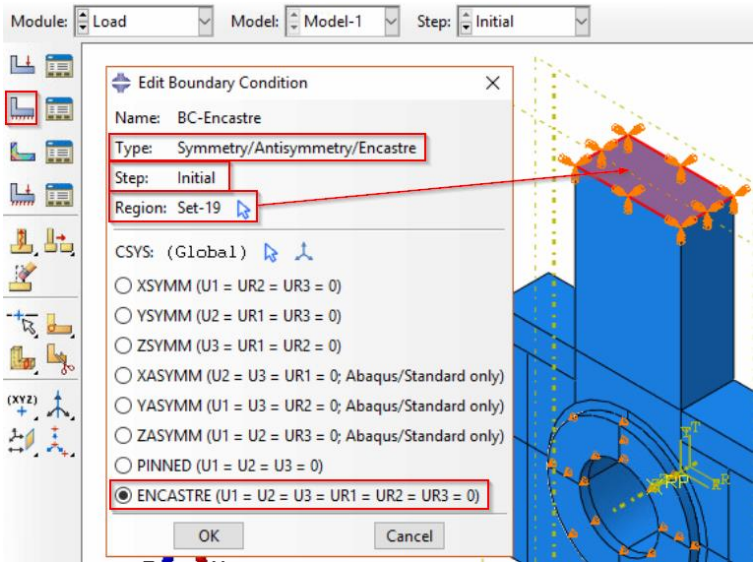

APPENDIX A 33: Constraints

The bearing is constrained in Z-direction so that it will not “fall out” of the assembly, as a real bearing is locked in place with keyways.

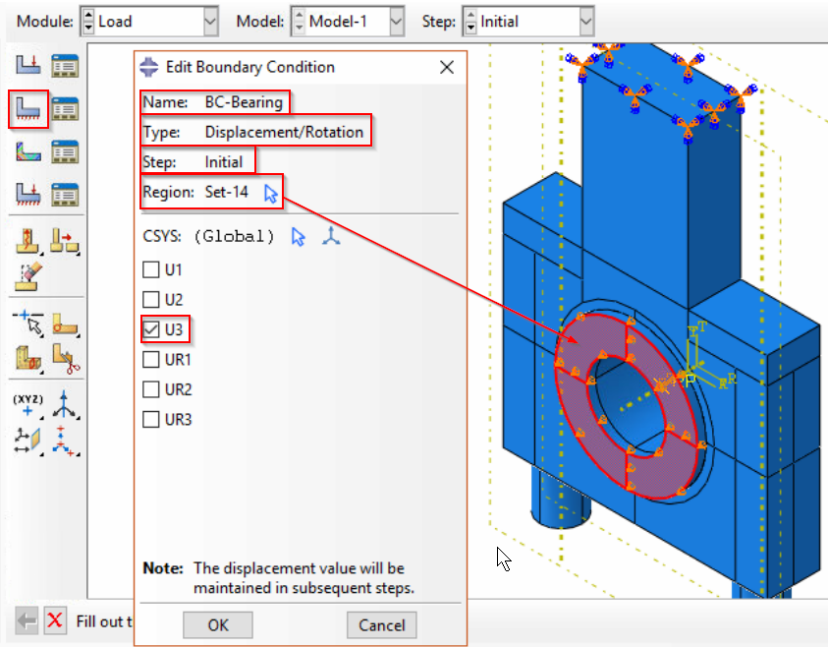

APPENDIX A 34: Constraints 2

Create Predefined Field

For making the bearing expand to close the clearance gap, predefined fields has to be created. Here the temperature of a specific part can be changed depending on the step. Depending on the coefficient of thermal expansion of the material and the clearance the delta temperature will change. This has to be calculated, so that the temperature can be increased, making the bearing expand in the expand step.

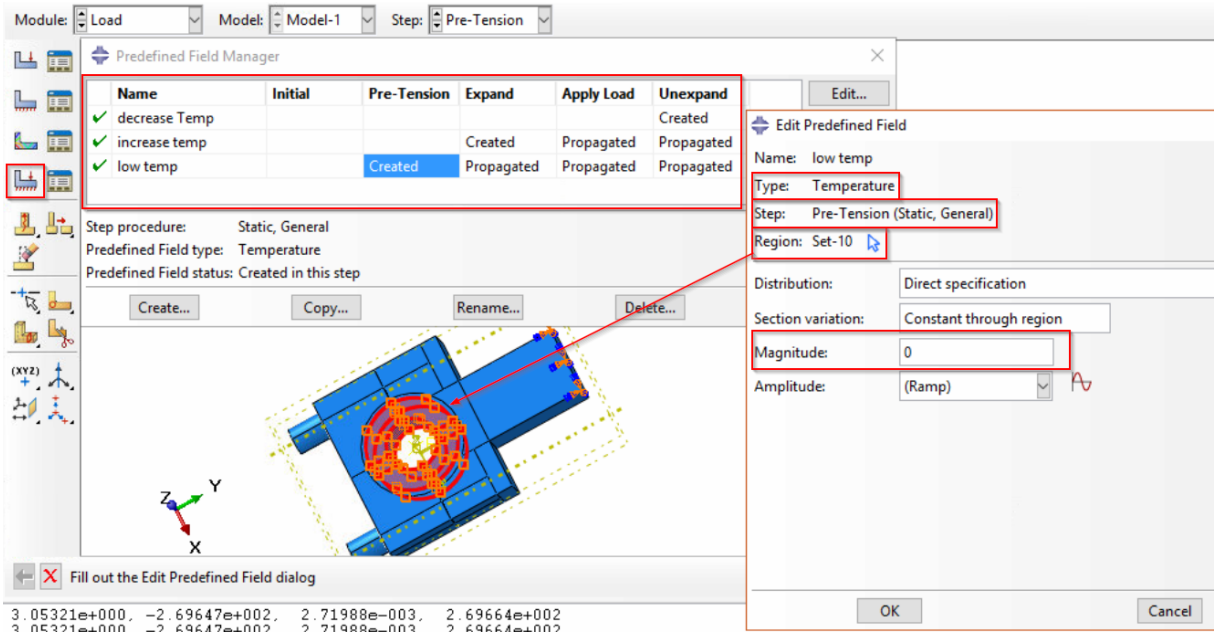

APPENDIX A 35: Predefined field

Create Job

For creating simulation jobs go to **job module** and **create job**.

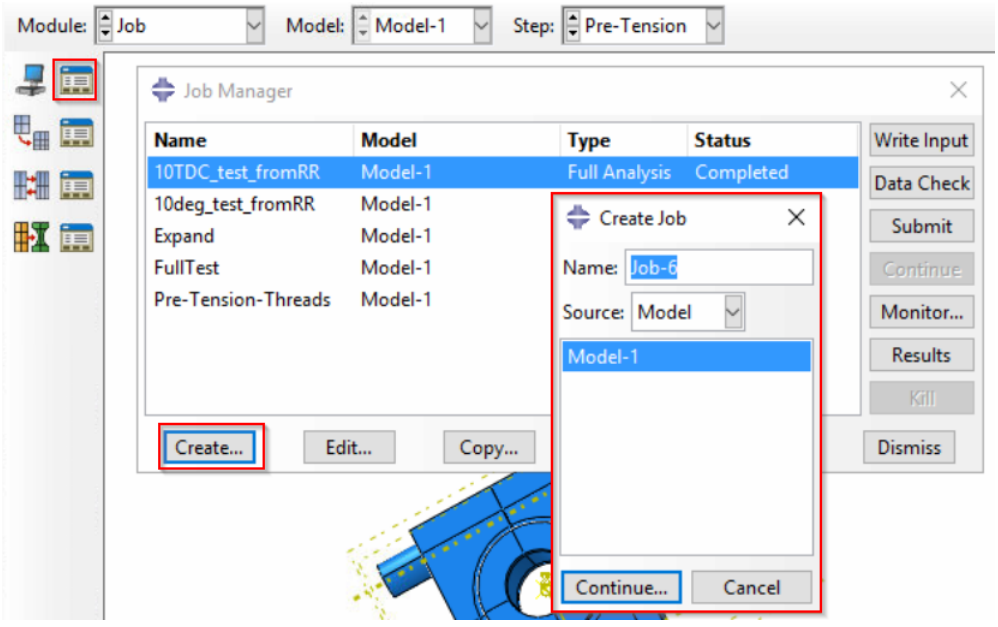

APPENDIX A 36: Create job

Use the default values in **edit job. Submit** the the job and follow the progress in **Monitor**

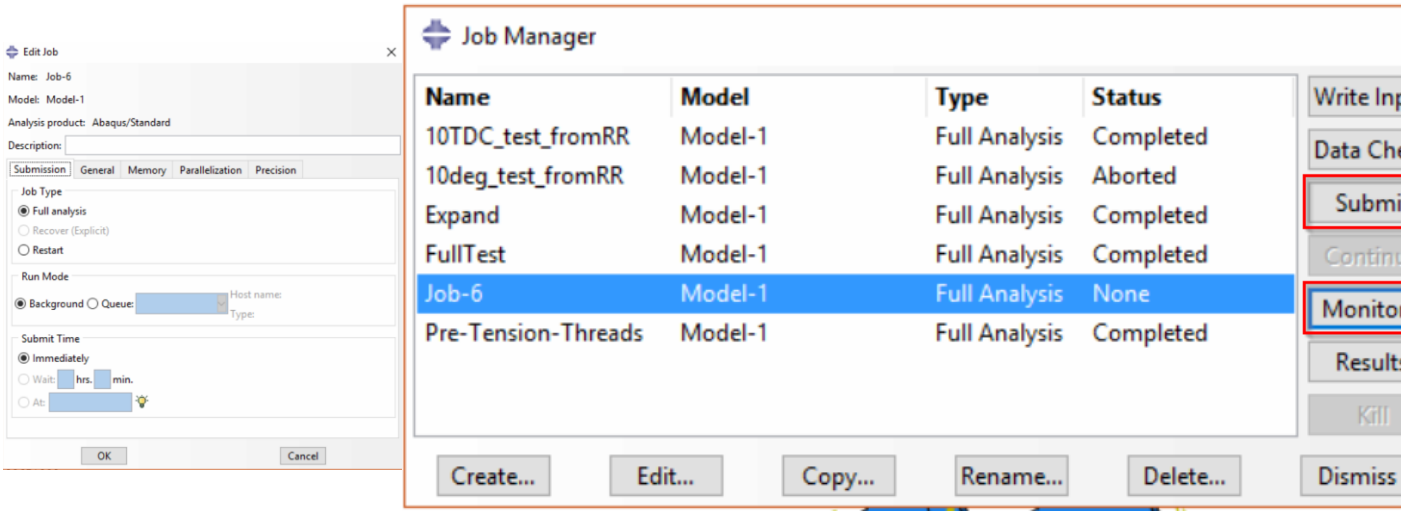

APPENDIX A 37: Submit Job/monitor

7.2 APPENDIX B: SIMPLIFIED MODEL ADDITIONAL RESULTS

Tresca stress

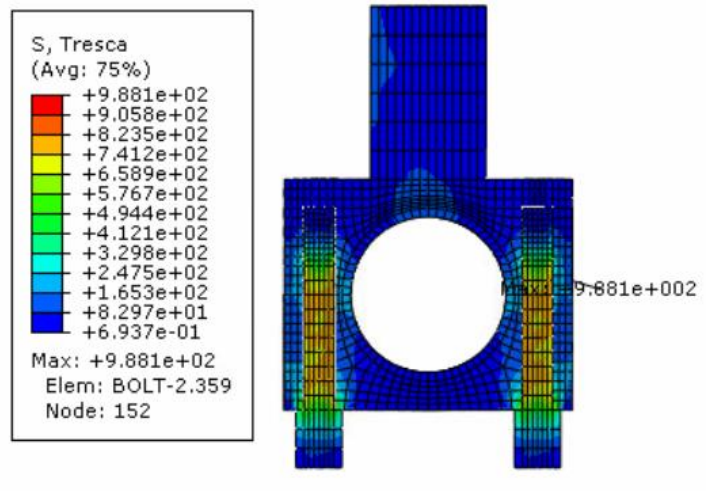

APPENDIX B 1: Tresca stress

Pressure Stress

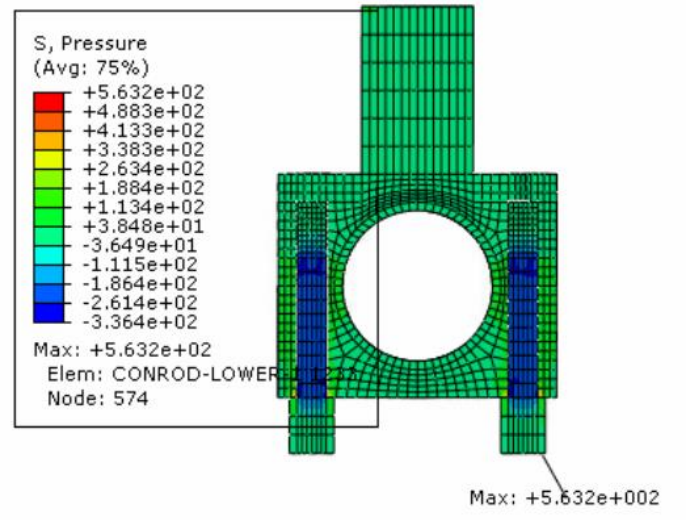

APPENDIX B 2: Pressure stress

Third Invariant Stress

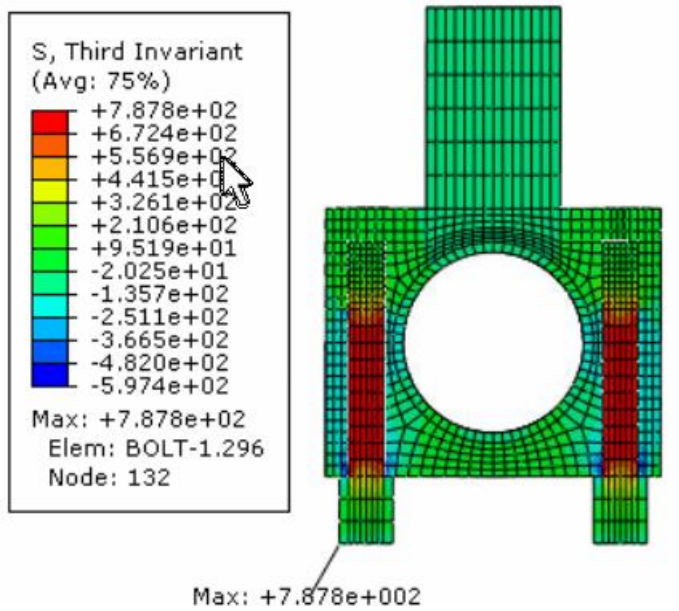

APPENDIX B 3: Third Invariant stress

Stress Components

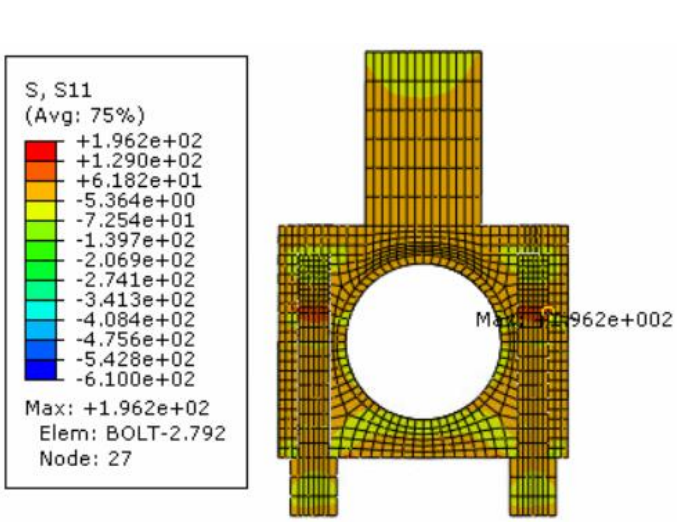

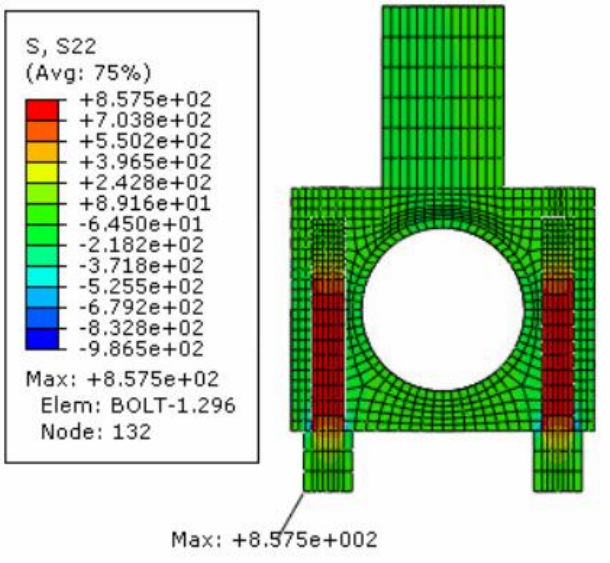

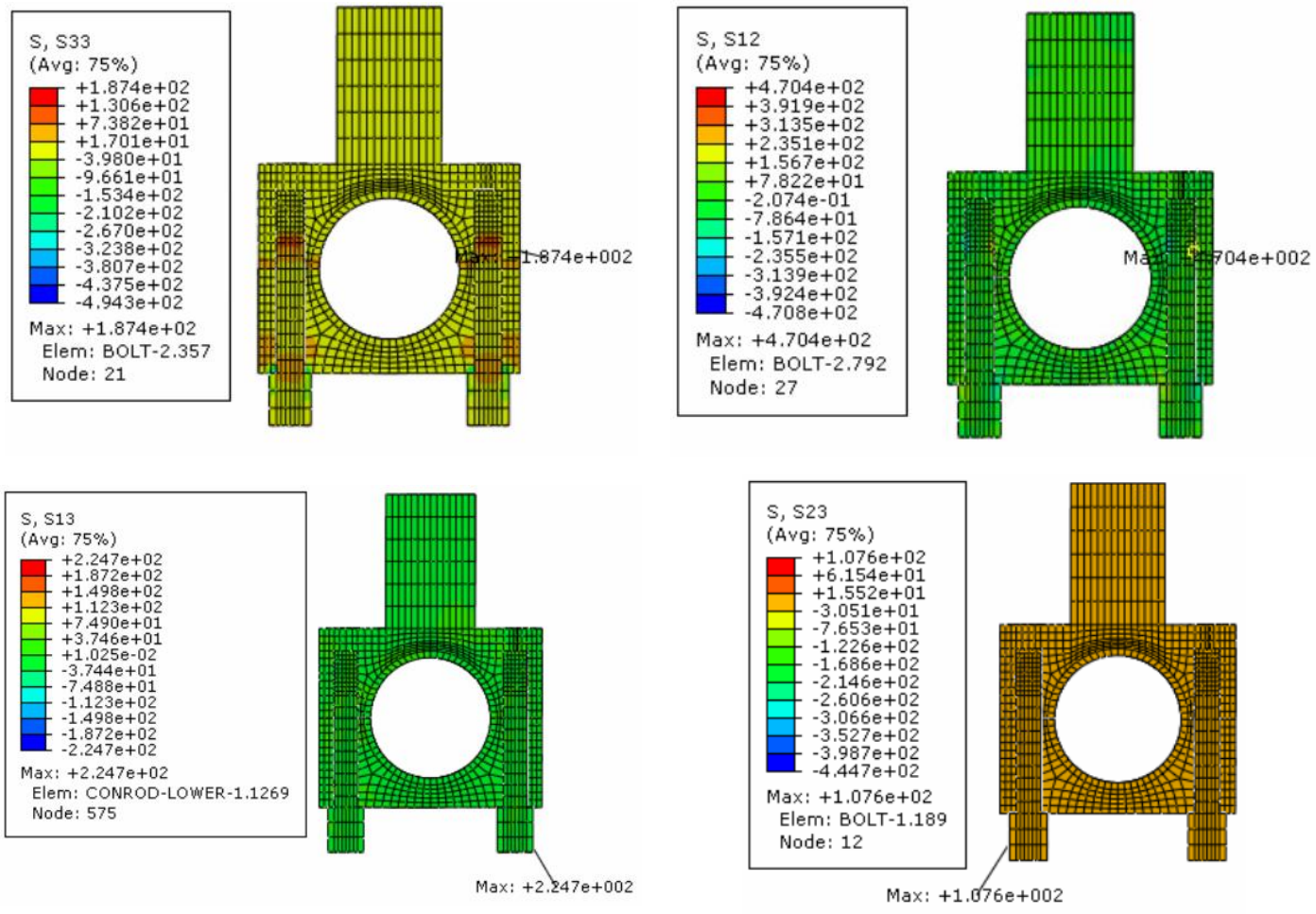

APPENDIX B 4: Stress components

7.3 APPENDIX C: REALISTIC MODEL ADDITIONAL RESULTS

Principal stresses

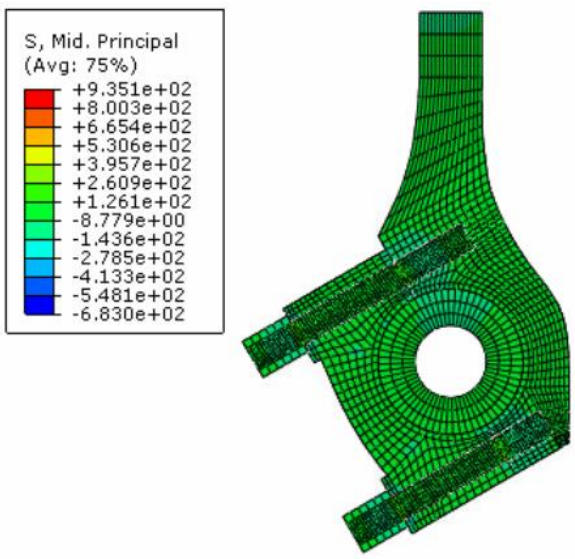

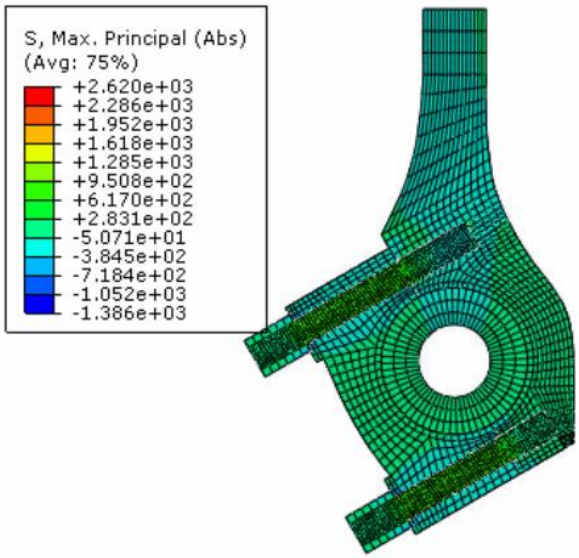

APPENDIX C 1: Principal stresses

Tresca and Pressure stresses

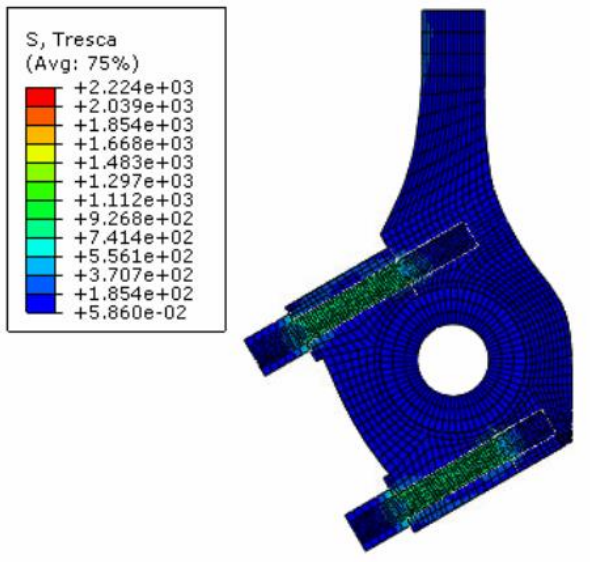

APPENDIX C 2: Tresca stress

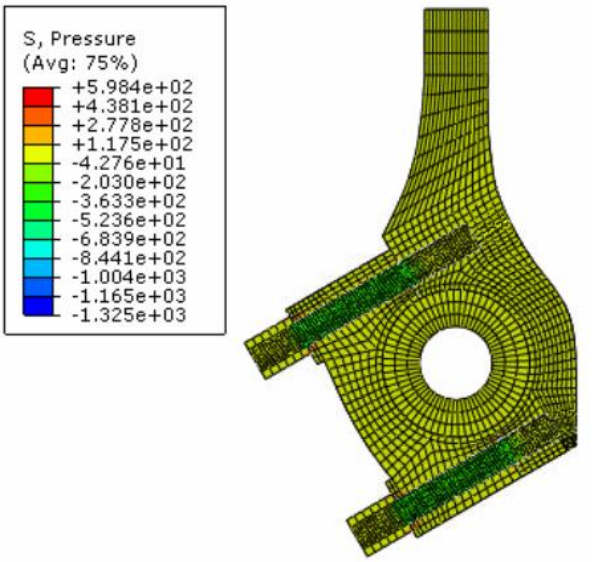

APPENDIX C 3: Pressure

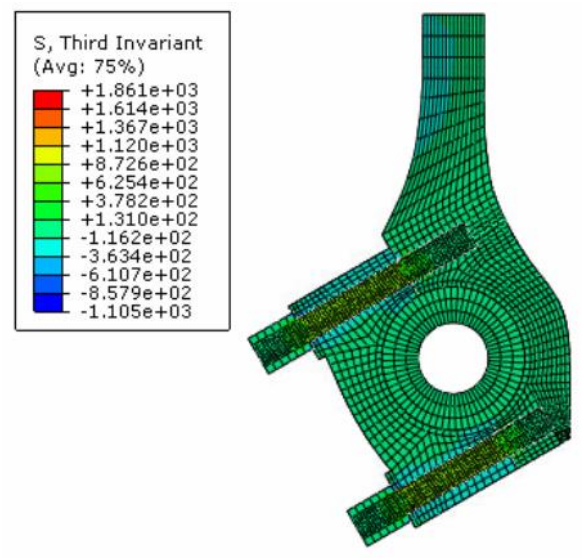

APPENDIX C 4: Third invariant

Stress components:

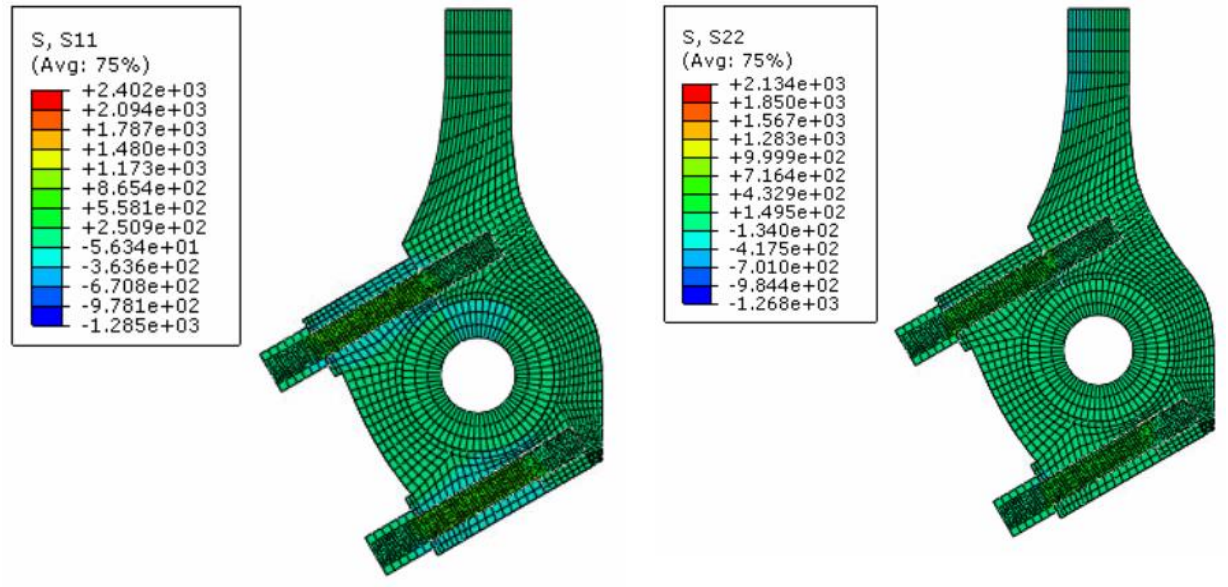

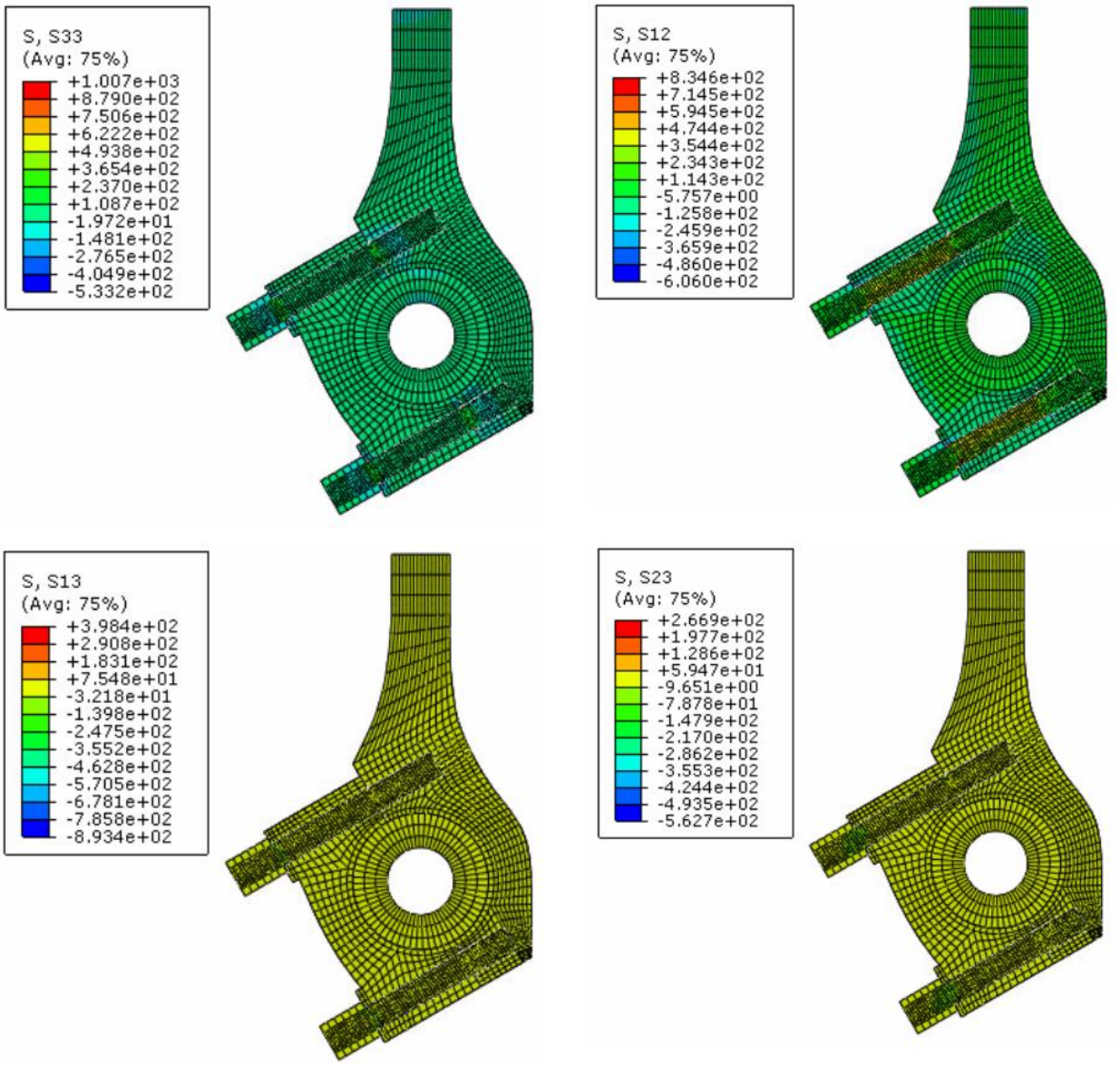

APPENDIX C 5: Stress components

7.4 APPENDIX D: CONNECTION ROD DRAWING

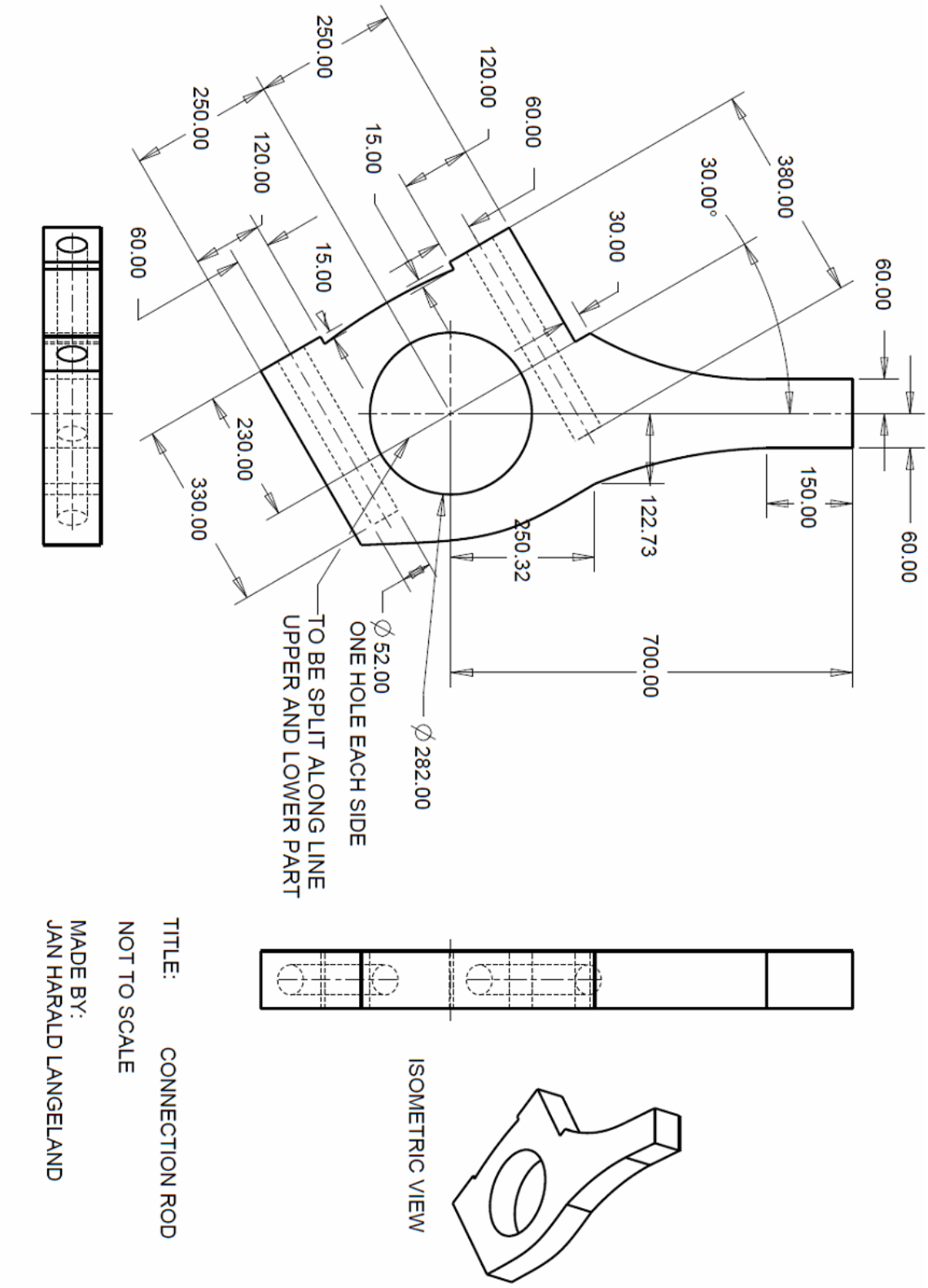

7.5 APPENDIX E: BOLT AND BEARING DRAWING

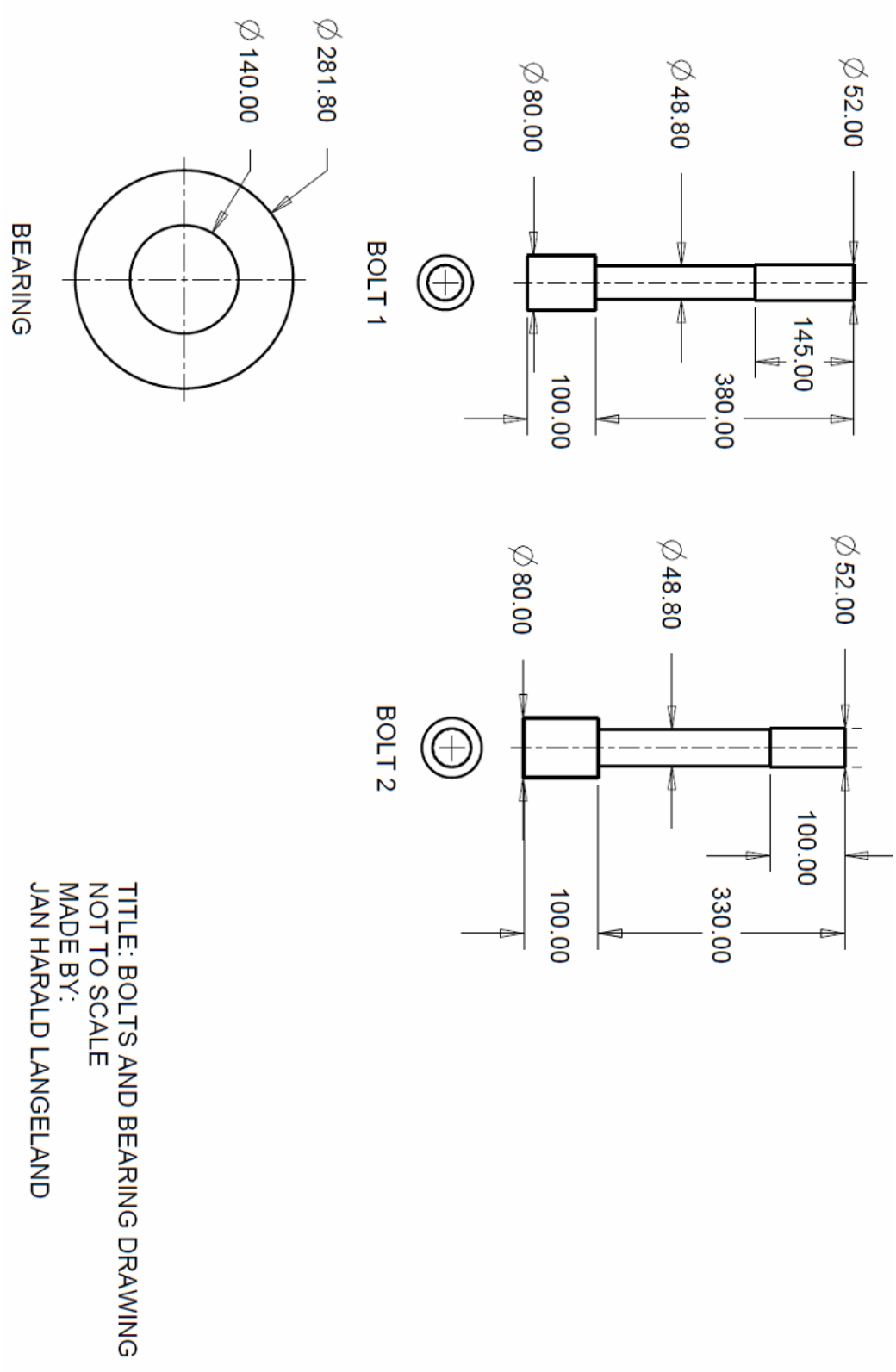

8 BIBLIOGRAPHY

[1] «Energy Information Administration,» US government, [Internett]. Available: https://www.eia.gov/forecasts/ieo/world.cfm. [Funnet 15 11 2016].

[2] K. Johansen, Konstruksjonsteknikk, Bergen: Fagbokforlaget, 2001.

[3] Bosch, «www.bosch-do-it.com,» Bosch, [Internett]. Available: https://www.bosch-do-it.com/gb/en/diy/knowledge/application-tips/screwdriving-and-drilling-in-wood-98726.jsp. [Funnet 13 01 2017].

[4] R. L. Hills, «Power from Steam: A history of the stationary steam engine,» i *Power from Steam: A history of the stationary steam engine*, Cambridge, Cambridge University Press, 1989.

[5] K. Kuiken, «Diesel-Engines II,» i *Diesel-Engines II*, Onnen The Netherlands, Target Global Energy Training, 2013.

[6] S. I. T. I. T. K. Tsuyoshi Kubota, «Development of Fracture Splitting,» Yamaha motor, 2005.

[7] «Roymech.co.uk,» [Internett]. Available: http://www.roymech.co.uk/Useful_Tables/Fatigue/Fatigue.html. [Funnet 09 12 2012].

[8] M. I. GmbH, «Cylinder components: Properties, applications, materials (ATZ/MTZ-Fachbuch),» i *Cylinder components: Properties, applications, materials*, Springer Vieweg, 2014.

[9] L. Lundby, «Forbrenningsmotorer 1,» i *Forbrenningsmotorer 1*, Trondheim, Universitetsforlaget, 1979.

[10] G. Lindsay, «Portlandbolt,» Portlandbolt, 09 02 2015. [Internett]. Available: http://www.portlandbolt.com/technical/faqs/rolled-vs-cut-threads-bolts/. [Funnet 20 05 2016].

[11] W. &. Bosch, Automotive Handbook 9th edition, Karlsruhe: Robert Bosch GmbH, 2014.

[12] Wheelabrator, «wheelabratorgroup.com,» Wheelabrator, [Internett]. Available: https://www.wheelabratorgroup.com/en-gb/my-application/application-by-process/what-is-shot-peening. [Funnet 21 05 2016].

[13] I. C. World, «industrialcoatingsworld.com,» Industrial Coating World, [Internett]. Available: http://industrialcoatingsworld.com/wear-resistant-coatings/hardening. [Funnet 25 04 2017].

[14] R. Stone, Introduction to Internal Combustion Engines 4th edition, Oxford: Palgrave

Macmillan, 2012.

[15] D. M. ISO-Thread, «www.scholz-mechanik.de,» [Internett]. Available: http://www.scholz-mechanik.de/servicedocs/GB233_Machine_Elements.pdf. [Funnet 03 04 2017].

[16] P. A. Leyers, «Scriptum im machinenelementen,» TH Stuttgart, ETH Zürich.

[17] S. a. Batchelor, Engineering Tribology, Elsvier Science Publisher B.V, 1993.

[18] W. D. R. D. G. Callister, Materials Science and Engineering, vol. Eight edition, Iowa: John Wiley & Sons, 2011.

[19] H. S. a. D. L. Micheal Ashby, Materials Engineering, Science, Processing and design, Cambridge: Elsevier, 2014.

[20] K. C. Marc Meyers, Mechanical behavior of materials, Cambridge: Cambridge University Press, 2009.

[21] A. International, «asminternational.org,» ASM International, [Internett]. Available: http://www.asminternational.org/documents/10192/1849770/05224G_Chapter14.pdf. [Funnet 07 12 2016].

[22] J. H. Bickford, Handbook of Bolts and Bolted Joints, New York: Marcel Dekker Inc. , 1998.

[23] «Aerospacengineering.net,» [Internett]. Available: http://aerospacengineering.net/?p=166. [Funnet 09 12 2016].

[24] M. S. Hans Albert Richard, Fatigue Crack Growth, Detect-Assess-Avoid, Springer International Publisher, 2016.

[25] Enventure, «enventure.com,» Eventure, 9 July 2015. [Internett]. Available: http://www.enventure.com/blog/stress-concentration-factor-an-important-parameter-for-the-safety-of-any-component/. [Funnet 30 05 2017].

[26] R. G. B. WARREN C. YOUNG, Roark’s Formulas for Stress and Strain Seventh Edition, New York: McGraw-Hill, 2002.

[27] SIMULIA, «www.3ds.com/,» [Internett]. Available: https://www.3ds.com/fileadmin/PRODUCTS/SIMULIA/PDF/brochures/simulia-abaqus-unified-fea-brochure.pdf. [Funnet 15 01 2017].

[28] D. Systèmes, Abaqus/CAE User's Guide, Providence: Dassault Systèmes Simulia Corp, 2014.

[29] D. Systèmes, Getting Started with Abaqus: Keywords Edition, Providence: Dassault Systèmes Simulia Corp., 2014.

[30] R. G. &. B. C. D. Flipo, «A parametric study of the elastic stress distribution in pin loaded lugs modelled in two and three dimensions and loaded in tension,» *JSA501 IMechE 2009,* 2009.

[31] A. L. GMBH, «Conrod analysis summary AVL 02.,» i *AVL list Gmbh*, 2002.

[32] J. Johannesen, Tekniske Tabeller, Cappelen, 2002.

[33] D. Systèmes, Abaqus Analysis User's Guide, Providence: Dassault Systèmes Simulia Corp., 2014.

[34] T. B. Jacob Fish, A first course in Finite Elements, Chichester: John Wiley & Sons Ltd., 2007.